



TECHNISCHE
UNIVERSITÄT
WIEN
Vienna | Austria



東京工業大学
Tokyo Institute of Technology

QUANTUM ADIABATIC COMPUTATION WITH DIABATIC METHODS

TWO-PARAMETER COUNTER DIABATIC DRIVING

A thesis presented for the title of
Master of Science (MSc)

within the studies of
Technical Physics (066 461)

submitted by
Luise Prielinger, BSc
Student no. 01426567

supervised by
Ass. Prof. Yuji Hasegawa
Prof. Hidetoshi Nishimori

executed at the Atominstitut, TU Vienna

in cooperation with
the Quantum Computing Unit, Tokyo Institute of Technology

Vienna, on 26. Mai 2021

(Signature author)

(Signature supervisor)

Abstract

Within the realm of solving hard optimization problems, adiabatic quantum computation has evolved into one of the leading approaches to reveal advantages over classical optimization methods.

The present work introduces an enhanced method, which goes beyond existing adiabatic quantum techniques. It builds upon a highly promising non-adiabatic method termed counter diabatic driving. The idea of counter diabatic driving is to control the external field to suppress naturally arising transitions between eigenstates. The objective is to speed up an originally adiabatic process by introducing an additional counter diabatic term (adiabatic gauge potential) to the driving protocol. Further, the introduced scheme is an application of a variational approach introduced by Sels and Polkovnikov, which is used to find an approximate counter diabatic term.

The present contribution introduces a second time-dependent control parameter to the solving operation. The additional control function widens the scope of the instantaneous system Hamiltonian, which leads to an enhanced search space to find an approximate counter diabatic term and broadens the gap between the lowest and next excited state during the transition. Both behaviours imply a higher probability to reach the final ground state of the problem Hamiltonian.

The introduced method is experimentally feasible and holds the potential to greatly benefit the performance of quantum annealing devices. The numerical results show significant improvement of state-of-the-art solving protocols on a wide range of commonly investigated and important quantum Ising spin models, such as the single-spin model (Landau-Zener), the two-spin model, the p -spin model, the Sherrington-Kirkpatrick model, the Coulomb glass model and the two-dimensional spin glass model.

Zusammenfassung

Die quanten-adiabatische Berechnung hat sich zu einem der führenden Ansätze zum Lösen von komplexen Optimierungsproblemen entwickelt und zeigt gegenüber klassischen Optimierungsmethoden vielerlei Vorteile. In der vorliegenden Arbeit wird eine erweiterte Methode vorgestellt, die über die bestehenden quanten-adiabatischen Verfahren hinausgeht.

Sie baut auf einer vielversprechenden diabatischen Methode auf, die als counter-diabatisches Verfahren bezeichnet wird. Die Idee des counter-diabatischen Lösens ist es, das externe Feld so zu steuern, dass natürlich auftretende Übergänge zwischen Eigenzuständen des quantenmechanischen Systems unterdrückt werden. Das Ziel ist es, einen ursprünglich adiabatischen Prozess zu beschleunigen, indem ein zusätzlicher counter-diabatischer Term (adiabatisches Eichpotential) in das Lösungsverfahren eingeführt wird. Um einen approximierten counter-diabatischen Term zu finden, wird ein Variationsansatz nach dem von Sels und Polkovnikov eingeführten Schema verwendet.

Die vorgestellte Methode führt einen zweiten zeitabhängigen Kontrollparameter in den Lösungsvorgang ein. Die zusätzliche Kontrollfunktion erweitert den initialen System-Hamiltonian insofern sie den Suchraum für einen counter-diabatischen Term erweitert und den Abstand zwischen dem niedrigsten und dem nächsten angeregten Zustand während des Übergangs vergrößert. Beides impliziert eine höhere Wahrscheinlichkeit, den Grundzustand des Problem-Hamiltonians zu erreichen.

Die Methode ist gut experimentell durchführbar und hat das Potenzial, die Leistung von sogenannten „quantum annealing devices“ erheblich zu verbessern. Die numerischen Ergebnisse zeigen eine signifikante Verbesserung von Lösungsprotokollen für eine Vielzahl von häufig untersuchten und wichtigen Quanten-Ising-Spin-Modellen, wie das Landau-Zener Modell, das Zwei-Spin-Modell, das p-Spin-Modell, das Sherrington-Kirkpatrick-Modell, das Coulomb-Glas-Modell und das zweidimensionale Spin-Glas-Modell.

Contents

Contents	1
1 Theoretical framework	2
1.1 Simulated annealing and quantum annealing	2
1.2 The transition from simple to complex	3
1.3 The Adiabatic Theorem	3
1.4 Counter-diabatic driving	5
1.4.1 Adiabatic gauge potentials	5
1.4.2 Approximate Adiabatic Gauge Potentials	7
2 Two-parameter method	9
2.1 Approximate gauge potentials $\mathcal{A}_\lambda, \mathcal{A}_\gamma$	9
2.1.1 Minimizing the distance operator $\mathcal{D}(\mathcal{X}, \mathcal{Y})$	10
2.2 Driver term constraints	11
2.3 Application to several quantum models	13
2.3.1 Landau-Zener formulation	13
2.3.2 Rotating frame	14
2.3.3 Two-spin model	16
2.3.4 Nearest Neighbour Model	17
2.3.5 p -spin Model	18
2.3.6 Sherrington-Kirkpatrick Model	18
2.3.7 Coulomb glass model	19
2.3.8 Two-dimensional spin glass	19
2.4 Numerical results	20
2.4.1 Landau-Zener formulation	21
2.4.2 Two-spin model	21
2.4.3 Nearest neighbour model	22
2.4.4 p -spin model	23
2.4.5 Sherrington-Kirkpatrick model	24
2.4.6 Coulomb glass model	27
2.4.7 Two-dimensional spin glass	29

3 Conclusion and outlook	32
Appendices	35
A Publication:	
Two-parameter counter-diabatic driving in quantum annealing	36
B Method Application	50
B.1 Landau-Zener Model	50
B.2 2 Spin Model	51
B.3 Nearest Neighbour Model	52
B.4 p-spin Model	55
Bibliography	61

Introduction

The cornerstones for quantum computation were set in the 1980s, when Feynman discussed the difficulties of describing quantum mechanics with classical physics: *Can a quantum system be probabilistically simulated by a classical universal computer? If you take the computer to be the classical kind [...] and there're no changes in any laws, and there's no hocus-pocus, the answer is certainly, No!* [1].

Two distinguished concepts have emerged from the fundamental idea of a quantum computer. First, the *quantum circuit model*, where logical quantum gates assemble to an executable quantum algorithm [2] and second, the concept of *adiabatic quantum computation* (AQC).

AQC is all about the controlled change of a quantum system. To understand this, let us envision a quantum system first to be in a configuration, which is easy to prepare. With time, the system transforms into another configuration. Due to the adiabatic theorem, the system is guaranteed to stay in its initial energy state, if and only if the described transition is sufficiently slow, i.e. *adiabatic* [3].

Without loss of generality, we assume that the final configuration represents the optimization problem we want to solve [4]. If we prepare the transformation such that it starts from the lowest energy eigenstate and if the state keeps this lowest energy value, the state at the end of the transformation is precisely the optimal solution we were looking for.

In other words, the idea of solving optimization problems with techniques based on AQC is to encode the problem formulation into the ground state of a Hamiltonian - the problem Hamiltonian. Starting from the well known configuration the system evolves into the problem configuration following the time-dependent Schrödinger equation. At the end of the transition the quantum system has fully reached the problem Hamiltonian whose ground state represents the optimal solution to the optimization problem [5].

The concept of AQC started out as a classical algorithm termed *quantum annealing*¹(QA). QA is often regarded as the quantum version of simulated annealing, which is a well established classical probabilistic optimization algorithm introduced by Kirkpatrick in 1983 [6]. In 1998 Kadowaki and Nishimori first introduced QA in a form which exploits quantum fluctuations to reach a global optimum, while SA is facilitated by thermal fluctuations to achieve the same goal. From a quantum computational viewpoint, QA can be understood as the *noisy* version of AQC, since QA allows diabatic (non-adiabatic) change, which is not the case for the latter [7]. Kadowaki and Nishimori were also the first to compare the performance of QA and SA and generated seminal findings for the still vibrant research field.

In this master's thesis a method is introduced that enhances AQC in the scope of closed quantum systems. Based on the procedure of single-parameter counter-diabatic driving (CD driving) by Demirplak and Rice in 2003 [8] the method leads to a larger ground-state fidelity than the traditional QA and the original CD driving approach.

The first Chapter gives a high level overview of the functionality of QA and its relation to the classical SA approach. Subsequently, we will discuss some important conclusions from both the adiabatic theorem and the adiabatic approximation. The chapter closes with an explanation of the CD driving method and the essential role of adiabatic gauge potentials in this method.

In Chapter 2 the developed method and its derivation are described. This part comprises the application of the method to several important quantum Ising spin models, including the simplest single-spin (Landau-Zener) model, the two-spin system, the p -spin model. and the two-dimensional spin glass problem. The chapter closes with the the analysis and discussion of the simulation results.

The third and last Chapter outlines the conclusions drawn from the previous Chapter and interesting potential tasks for future investigation.

This thesis comprises the work *Two-parameter counter diabatic driving in adiabatic quantum annealing* by Prielinger et al. which was recently published in the scientific journal *Physical Review Research*.

¹the word *quantum annealing* was first used for another algorithm introduced by Apolloni [5]. However, it is not QA in the present sense.

Chapter 1

Theoretical framework

Finding the optimal (or lowest energy) state of disordered and complex systems is a central problem in statistical physics and many other research fields. QA from an algorithmic perspective is a metaheuristic approach aiming to find the optimal solution to different types of NP-hard optimization problems.

QA was first compared to its classical counterpart SA by Nishimori and Kawakami in 1998 [9]. The intention was to use quantum fluctuations to find the global optimum of a complex function. As already mentioned in the Introduction, over the past two decades QA has proven to be an elegant alternative and in many cases an improvement to its classical counterpart SA [10–19].

This Chapter first gives an overview of the functionality of QA and its relation to the classical SA approach. Second, it presents some important conclusions from both the adiabatic theorem and the utilized adiabatic approximation. Third and last, it outlines the crucial aspects of the CD driving method and the essential role of adiabatic gauge potentials.

1.1 Simulated annealing and quantum annealing

Considering a physical system, the conventional goal is to find the global minimum of the system's cost (or energy) function, represented by the system's Hamiltonian $\mathcal{H}(\mathbf{x}, t)$.

The difficulty of finding the global minimum of a complex function with many local maxima and minima is to escape the latter and reach the desired global optimum.

In SA a physical system is considered in the classical sense. At the beginning of the solving process the system can go to higher energy states with a certain probability. With time, the probability to go to a higher energy state is continually decreased. Decreasing the probability is referred to as lowering the *temperature*. The process is therefore understood as *cooling* or *annealing*.

In QA thermal fluctuations are neglected and the system is viewed as a quantum mechanical one. In quantum mechanical terms the global optimum is referred to as the ground state of the quantum system. During the solving process the system follows the Schrödinger equation. Thereby the so-called transverse field plays a similar role as the temperature parameter in the classical SA, as it controls the rate of transition between the states [9].

QA was tested in the transverse Ising model. For this, Nishimori and Kadawaki compared the efficiency of QA directly with the performance of the classical SA. Thereby they solved the time-dependent Schrödinger equation and the classical master equation numerically for small-size systems with the same exchange interactions under the same annealing schedules. The transition rate in the QA approach appeared to be larger than the transition probability in the classical case. It was concluded that this leads to a more active search in wider regions of the phase space, leading to better convergence [9].

1.2 The transition from simple to complex

In mathematical terms the transition of the initial system configuration $\mathcal{H}_{\text{init}}$ to the problem Hamiltonian \mathcal{H}_p is expressed with the time dependent Hamiltonian $\mathcal{H}(t)$

$$\mathcal{H}(t) = [1 - \lambda(t)]\mathcal{H}_{\text{init}} + \lambda(t)\mathcal{H}_p \quad t \in [0, \tau] \quad (1.1)$$

with the control parameter $\lambda(t)$. This function causes the system to transform from its initial configuration at $\lambda(0) = 0$ to fully develop its problem configuration at $\lambda(\tau) = 1$.

1.3 The Adiabatic Theorem

Solving the Schrödinger equation for time-dependent Hamiltonians, is (to say the least) mathematically involved. Even for a two-level systems - also referred to as a *qubit*, a system with only two possible states - it is, in general, not possible to obtain a closed form solution given an arbitrary time-dependent Hamiltonian [21].

We know from the adiabatic theorem that if a system's Hamiltonian changes sufficiently slow, the system stays in its prepared eigenstate.

Driving the system faster leaves the ambiguity of the system being or not being *close enough* to its instantaneous ground state. Clarification of this subject is the very purpose of adiabatic approximation, which already received great scientific attention [22–26].

Since we are interested in slow and therefore hopefully small changes in a physical system, we start with perturbation theory: The time-dependent Schrödinger Equation in the interaction picture (where $\hbar = 1$) reads

$$id_t |\Psi(t)\rangle = \mathcal{H}(t) |\Psi(t)\rangle. \quad (1.2)$$

The eigenstates of the system $\mathcal{H}(t) |n(t)\rangle = E_n(t) |n(t)\rangle$ form a complete orthonormal basis and we write the general solution as follows

$$|\Psi(t)\rangle = \sum_n d_n(t) |n(t)\rangle e^{i\theta_n(t)} \quad (1.3)$$

where $\theta_n(t) = -\int_0^t E_n(t') dt'$ is called the dynamic phase factor.

The coefficients $d_n(t)$ can be further decomposed into coefficients $c_n(t)$ and the so-called Berry phase, which is referred to as geometric phase $\gamma_n(t)$.

$$d_n(t) = c_n(t) e^{i\gamma_n(t)} \quad (1.4)$$

$$\gamma_n(t) = -i \int_0^t \langle n(t') | \dot{n}(t') \rangle dt' \quad (1.5)$$

Inserting Eq.(1.5) into Eq.(1.3) gives

$$|\Psi(t)\rangle = \sum_n c_n(t) e^{i\gamma_n(t)} e^{i\theta_n(t)} |n(t)\rangle \quad (1.6)$$

Inserting the general solution Eq.(1.6) into the Schrödinger equation and overlapping the eigenstate with a different eigenstate $\langle m(t) |$, we obtain a differential equation for the coefficients

$$\dot{c}_n(t) = - \sum_{n \neq m} e^{i\gamma_{mn}(t)} e^{i\theta_{mn}(t)} \mathcal{M}_{mn}(t) c_m(t) \quad (1.7)$$

with the coupling terms

$$\mathcal{M}_{mn} = \langle m(t) | \dot{n}(t) \rangle = \frac{\langle m(t) | \dot{\mathcal{H}}(t) | n(t) \rangle}{E_m(t) - E_n(t)}. \quad (1.8)$$

We think of these coupling terms as drivers, which move the system away from its instantaneous eigenstate $|n(0)\rangle$. In other words, these terms cause transitions

between the energy levels of the original Hamiltonian [27]. We see that they depend on the rate of change of the system and are inversely proportional to the energy gap between the considered states. We can therefore conclude that the change of a systems energy state is small, if also the system's rate of change is small and if the difference between the energy eigenvalues is large.

$$|\mathcal{M}_{mn}|^2 \ll 1. \quad (1.9)$$

1.4 Counter-diabatic driving

Since the probability to stay in the instantaneous eigenstate is upper bounded by the adiabatic theorem, the main goal of AQC is to enhance the system's evolution in terms of speed and high ground-state fidelity. In other words, we want to suppress any transitions during the system's evolution.

A very elegant approach to suppress these unwanted transitions was introduced by Demirplak and S.Rice in 2003 [8]. The method has been termed in three different ways: *counter-diabatic driving*, *shortcuts to adiabaticity* and *transitionless driving* [8, 28, 29]. Here we proceed with the term *counter-diabatic driving*.

1.4.1 Adiabatic gauge potentials

The counter diabatic driving method can be understood with the concept of adiabatic gauge potentials. Assuming we consider a system $\mathcal{H}(\lambda)$, which depends on the function $\lambda(t)$, we define a unitary transformation $U(\lambda)$, which is implicitly time-dependent on the parameter $\lambda(t)$.

If a state $|\psi(t)\rangle$ is a solution to the Schrödinger equation $|\psi(t)\rangle = U |\tilde{\psi}(t)\rangle$, also $|\tilde{\psi}(t)\rangle$ is a solution to the time-dependent Schrödinger equation. Per convention the state $|\tilde{\psi}(t)\rangle$ is called a state in the *moving frame* and we write

$$id_t |\psi\rangle = \mathcal{H} |\psi\rangle \quad (1.10)$$

$$id_t (U |\tilde{\psi}\rangle) = \mathcal{H} (U |\tilde{\psi}\rangle) \quad (1.11)$$

$$i\partial_\lambda U \dot{\lambda} |\tilde{\psi}\rangle + iU d_t |\tilde{\psi}\rangle = \mathcal{H} U |\tilde{\psi}\rangle. \quad (1.12)$$

Applying U^\dagger from the left yields

$$iU^\dagger \partial_\lambda U \dot{\lambda} |\tilde{\psi}\rangle + i \underbrace{U^\dagger U}_{\mathbb{I}} d_t |\tilde{\psi}\rangle = U^\dagger \mathcal{H} U |\tilde{\psi}\rangle \quad (1.13)$$

Here $\tilde{\mathcal{H}} = U^\dagger \mathcal{H} U$ is the original Hamiltonian in the moving basis. We call

$$\mathcal{A}_\lambda = i\partial_\lambda \quad (1.14)$$

an adiabatic gauge potential and $\tilde{\mathcal{A}}_\lambda = iU^\dagger \partial_\lambda U$ an adiabatic gauge potential in the moving frame and rewrite Eq.(1.13) to

$$id_t |\tilde{\psi}\rangle = \tilde{\mathcal{H}} |\tilde{\psi}\rangle - \dot{\lambda} \tilde{\mathcal{A}}_\lambda |\tilde{\psi}\rangle \quad (1.15)$$

We can find the expected relation to the coupling terms Eq.(1.8) considering the orthonormal basis of the original Hamiltonian

$$\mathcal{M}_{mn}(\lambda) = \langle m(\lambda) | \dot{n}(\lambda) \rangle \quad (1.16)$$

$$= \dot{\lambda} \langle m(\lambda) | \partial_\lambda n(\lambda) \rangle \quad (1.17)$$

$$= -\dot{\lambda} i \langle m(\lambda) | \mathcal{A}_\lambda | n(\lambda) \rangle \quad (1.18)$$

and can equivalently write

$$\langle m(\lambda) | \mathcal{A}_\lambda | n(\lambda) \rangle = i \frac{\langle m(\lambda) | \partial_\lambda \mathcal{H} | n(\lambda) \rangle}{E_n - E_m} \quad (1.19)$$

We understand the term again as causing transitions between energy eigenstates. Since our main goal is to suppress these transitions we add it to Eq.(1.15) and the effective Hamiltonian $\tilde{\mathcal{H}}_{\text{eff}}$ in the moving frame reads

$$\tilde{\mathcal{H}}_{\text{eff}} = \tilde{\mathcal{H}} - \dot{\lambda} \tilde{\mathcal{A}}_\lambda + \dot{\lambda} \tilde{\mathcal{A}}_\lambda \quad (1.20)$$

The third term is therefore called the **counter-diabatic term** $\tilde{\mathcal{H}}_{CD}$.

$$\tilde{\mathcal{H}}_{CD} = \dot{\lambda} \tilde{\mathcal{A}}_\lambda \quad (1.21)$$

Since by definition $\tilde{\mathcal{H}}$ is the diagonalized version of \mathcal{H} , the system will always remain in its instantaneous ground state, if it is initially prepared as such.

Back in the stationary frame Eq.(1.20) reads

$$\mathcal{H}_{\text{eff}} = \mathcal{H} + \mathcal{H}_{CD} = \mathcal{H} + \dot{\lambda} \mathcal{A}_\lambda \quad (1.22)$$

and we could naively conclude that our work is done, since we driving the system according to the protocol Eq.(1.22) adds the appropriate counter-forces to suppress arising transitions.

Unfortunately finding an exact expression for \mathcal{A}_λ is not an easy matter. In fact, it is shown that in generic systems, there is no solution, since the exact analytic expression for \mathcal{A}_λ suffers from the problem of small denominators [30].

1.4.2 Approximate Adiabatic Gauge Potentials

Thus, our intention should not be to find an exact solution, but rather an approximate one, fairly preventing the system from dissipative transitions. Sels and Polkovnikov created a refined concept of finding approximate gauge potentials by utilizing the least action principle [30].

The relation Eq.(1.19) can be generalized to its matrix form

$$[\mathcal{A}_\lambda, \mathcal{H}] = i\partial_\lambda \mathcal{H} + iF_\lambda \quad (1.23)$$

where

$$F_\lambda = - \sum_n \partial_\lambda E_n |n\rangle \langle n| \quad (1.24)$$

is an operator which is diagonal in the energy eigenbasis [31]. We can comprehend this relation by differentiating the energy $E(\lambda)$ with respect to time

$$\frac{dE}{dt} = \frac{d}{dt} \langle \tilde{\psi} | \tilde{\mathcal{H}} | \tilde{\psi} \rangle = -i\dot{\lambda} \langle \tilde{\psi} | \tilde{\mathcal{A}}_\lambda \tilde{\mathcal{H}} | \tilde{\psi} \rangle + \dot{\lambda} \langle \tilde{\psi} | \partial_\lambda \tilde{\mathcal{H}} | \tilde{\psi} \rangle + i\dot{\lambda} \langle \tilde{\psi} | \tilde{\mathcal{H}} \tilde{\mathcal{A}}_\lambda | \tilde{\psi} \rangle \quad (1.25)$$

where we used $\partial_\lambda |\tilde{\psi}(\lambda)\rangle = \partial_\lambda (U^\dagger |\psi\rangle) = \partial_\lambda (U^\dagger U |\tilde{\psi}(\lambda)\rangle) = i\tilde{\mathcal{A}}_\lambda |\tilde{\psi}(\lambda)\rangle$ in the first and third term. Further we can write

$$\dot{\lambda} \partial_\lambda E = \dot{\lambda} \langle \tilde{\psi} | \partial_\lambda \tilde{\mathcal{H}} | \tilde{\psi} \rangle - \dot{\lambda} i \langle \tilde{\psi} | [\tilde{\mathcal{A}}_\lambda, \tilde{\mathcal{H}}] | \tilde{\psi} \rangle \quad (1.26)$$

$$\partial_\lambda E = \langle \tilde{\psi} | \partial_\lambda \tilde{\mathcal{H}} | \tilde{\psi} \rangle - i \langle \tilde{\psi} | [\tilde{\mathcal{A}}_\lambda, \tilde{\mathcal{H}}] | \tilde{\psi} \rangle. \quad (1.27)$$

Since the Hamiltonian $\tilde{\mathcal{H}}$ is diagonal in the instantaneous eigenbasis $|n(\lambda)\rangle$ and since the energy value is basis independent we can remove the tilde signs and obtain

$$\langle \psi | \partial_\lambda \sum_n E_n |n\rangle \langle n| \psi \rangle = \langle \psi | \partial_\lambda \mathcal{H} | \psi \rangle - i \langle \psi | [\mathcal{A}_\lambda, \mathcal{H}] | \psi \rangle \quad (1.28)$$

In absence of a basis this expression generalizes to Eq.(1.23).

Intuitively we can relate this to the fact that the off-diagonals of the systems change on the right hand side of equation Eq.(1.23) are responsible for the change in the basis states (left hand side). Hence, if there would be no change in the basis states \mathcal{A}_λ and \mathcal{H} would commute.

In the following we will see the variational ansatz to find an approximate gauge potential from the minimum action principle.

We define the Hermitian operator

$$G_\lambda(\mathcal{X}) := \partial_\lambda \mathcal{H} + i[X, \mathcal{H}] \quad (1.29)$$

and insert the gauge potential to Eq.(1.29), such that $G_\lambda(\mathcal{A}_\lambda) = -F_\lambda$. In order to find an approximate \mathcal{A}_λ , we minimize the distance between $G_\lambda(\mathcal{A}_\lambda)$ and $-F_\lambda$. Formulating the minimization task in the Frobenius norm yields

$$D^2(\mathcal{X}) = \text{Tr}[(G_\lambda(\mathcal{X}) + F_\lambda)^2] \quad (1.30)$$

$$\left. \frac{dD^2(\mathcal{X})}{d\mathcal{X}} \right|_{\mathcal{X}=\mathcal{A}_\lambda} = 0 \quad (1.31)$$

We will use this procedure as the basis and motivation for the introduction of the two-parameter method.

Chapter 2

Two-parameter method

Introducing a second time-dependent driving function $\gamma(t)$ to the counter-diabatic driving scheme naturally leads to an enhanced search space for finding approximate counter-diabatic terms, which suppress the arising dissipative transitions.

Moreover, considering the traditional annealing schedule

$$\mathcal{H} = (1 - \lambda)\mathcal{H}_{\text{init}}(\gamma) + \lambda\mathcal{H}_{\text{p}} \quad (2.1)$$

the driving function does only affect the first term $\mathcal{H}_{\text{init}}(\gamma)$. The additional driving function facilitates further control of the external transverse field. We choose $\gamma(t)$ such that the transverse field is intensified along the process. When intensifying the transverse field the spectrum of the eigenvalues gets broader, which means the gap between the ground state and excited state also widens, leading to a greater probability to stay at the lowest energy level.

Aside from the described assumptions, we choose $\gamma(t)$ more or less arbitrarily¹. The optimal choice therefore remains as an interesting task for future investigation. In the following chapters we will see that it already significantly improves the annealing process in all evaluated application.

2.1 Approximate gauge potentials $\mathcal{A}_\lambda, \mathcal{A}_\gamma$

The driving Hamiltonian $\mathcal{H}(\lambda, \gamma)$ depends on both driving functions. We again go to the moving frame with the help of a unitary transformation, which is parametrized by the driving functions $U(\lambda, \gamma)$. Then, as already anticipated, the

¹Both $\lambda(t)$ and $\gamma(t)$ have to satisfy some basic constraints outlined in Section 2.2

additional gauge potential \mathcal{A}_γ arises naturally from the Schrödinger equation

$$id_t |\psi\rangle = \mathcal{H} |\psi\rangle \quad (2.2)$$

$$id_t (U |\tilde{\psi}\rangle) = \mathcal{H} (U |\tilde{\psi}\rangle) \quad (2.3)$$

$$i\partial_\lambda U \dot{\lambda} |\tilde{\psi}\rangle + i\partial_\gamma U \dot{\gamma} |\tilde{\psi}\rangle + iU d_t |\tilde{\psi}\rangle = \mathcal{H} U |\tilde{\psi}\rangle \quad | U^\dagger. \quad (2.4)$$

$$iU^\dagger \partial_\lambda U \dot{\lambda} |\tilde{\psi}\rangle + iU^\dagger \partial_\gamma U \dot{\gamma} |\tilde{\psi}\rangle + i \underbrace{U^\dagger U}_{\mathbb{I}} d_t |\tilde{\psi}\rangle = U^\dagger \mathcal{H} U |\tilde{\psi}\rangle \quad (2.5)$$

and the diagonalized Hamiltonian $\tilde{\mathcal{H}}(\lambda, \gamma) = U^\dagger \mathcal{H}(\lambda, \gamma) U$ as well as its eigenstates depend now on the driving functions $\lambda(t)$ and $\gamma(t)$.

The gauge potentials in the moving frame read

$$\tilde{\mathcal{A}}_\lambda = U^\dagger i\partial_\lambda U \quad (2.6)$$

$$\tilde{\mathcal{A}}_\gamma = U^\dagger i\partial_\gamma U \quad (2.7)$$

We can therefore write the driver Hamiltonian $\tilde{\mathcal{H}}_{\text{eff}}^{\lambda, \gamma}$

$$\tilde{\mathcal{H}}_{\text{eff}}^{\lambda, \gamma} = \tilde{\mathcal{H}} - \dot{\lambda} \tilde{\mathcal{A}}_\lambda - \dot{\gamma} \tilde{\mathcal{A}}_\gamma. \quad (2.8)$$

When going back to the stationary frame, one has to add the terms in order to suppress the diabatic transitions

$$\mathcal{H}_{\text{eff}}^{\lambda, \gamma} = \mathcal{H} + \mathcal{H}_{CD}^{\lambda, \gamma} = \mathcal{H} + \dot{\lambda} \mathcal{A}_\lambda + \dot{\gamma} \mathcal{A}_\gamma. \quad (2.9)$$

Based on the previous chapter we determine the additional gauge potential \mathcal{A}_γ and construct the distance operator, which is to be minimized.

We introduce two Hermitian operators G_λ and G_γ as follows

$$G_\lambda(\mathcal{X}) = \partial_\lambda \mathcal{H} + i[\mathcal{X}, \mathcal{H}] \quad (2.10)$$

$$G_\gamma(\mathcal{Y}) = \partial_\gamma \mathcal{H} + i[\mathcal{Y}, \mathcal{H}] \quad (2.11)$$

where \mathcal{X} and \mathcal{Y} are themselves Hermitian operators.

2.1.1 Minimizing the distance operator $\mathcal{D}(\mathcal{X}, \mathcal{Y})$

To this end we construct two operators, such that $G_\lambda(\mathcal{A}_\lambda) = -F_\lambda$ and $G_\gamma(\mathcal{A}_\gamma) = -F_\gamma$. The distance operator in the Frobenius norm therefore reads

$$\mathcal{D}^2(\mathcal{X}, \mathcal{Y}) = \text{Tr}[(\partial_\lambda \mathcal{H} + i[\mathcal{X}, \mathcal{H}] + F_\lambda)^2] + \text{Tr}[(\partial_\gamma \mathcal{H} + i[\mathcal{Y}, \mathcal{H}] + F_\gamma)^2]. \quad (2.12)$$

We can simplify Eq.(2.12) as follows

$$\mathcal{D}^2(\mathcal{X}, \mathcal{Y}) = \text{Tr}[(G_\lambda(\mathcal{X}) + F_\lambda)^2] + \text{Tr}[(G_\gamma(\mathcal{Y}) + F_\gamma)^2] \quad (2.13)$$

$$= \text{Tr}[G_\lambda^2] + 2\text{Tr}[G_\lambda F_\lambda] + \text{Tr}[F_\lambda^2] + \text{Tr}[G_\gamma^2] + 2\text{Tr}[G_\gamma F_\gamma] + \text{Tr}[F_\gamma^2] \quad (2.14)$$

Following the reformulations Eq.(129) - (131) in [32] we find

$$Tr[G_\lambda F_\lambda] = Tr[\partial_\lambda \mathcal{H} F_\lambda] + iTr[[\mathcal{X}, \mathcal{H}] F_\lambda] \quad (2.15)$$

$$Tr[G_\lambda F_\lambda] = -Tr[F_\lambda^2] - \underbrace{iTr[[F_\lambda, \mathcal{H}] \mathcal{X}]}_{=0} \quad (2.16)$$

$$(2.17)$$

$$Tr[G_\gamma F_\gamma] = Tr[\partial_\gamma \mathcal{H} F_\gamma] + iTr[[\mathcal{Y}, \mathcal{H}] F_\gamma] \quad (2.18)$$

$$Tr[G_\gamma F_\gamma] = -Tr[F_\gamma^2] - \underbrace{iTr[[F_\gamma, \mathcal{H}] \mathcal{Y}]}_{=0} \quad (2.19)$$

and the simplified distance operator reads

$$\mathcal{D}^2(\mathcal{X}, \mathcal{Y}) = Tr[G_\lambda^2] - Tr[F_\lambda^2] + Tr[G_\gamma^2] - Tr[F_\gamma^2] \quad (2.20)$$

Since $Tr[F_\lambda^2]$ and $Tr[F_\gamma^2]$ do neither depend on \mathcal{X} nor on \mathcal{Y} , only the operator

$$\mathcal{S} = Tr[G_\lambda^2] + Tr[G_\gamma^2] \quad (2.21)$$

is to be minimized. Per convention \mathcal{S} is referred to as the action operator and the minimizations to be carried out read

$$\left. \frac{\partial S(\mathcal{X})}{\partial \mathcal{X}} \right|_{\mathcal{X}=\mathcal{A}_\lambda} = 0, \quad (2.22)$$

and

$$\left. \frac{\partial S(\mathcal{Y})}{\partial \mathcal{Y}} \right|_{\mathcal{Y}=\mathcal{A}_\gamma} = 0. \quad (2.23)$$

2.2 Driver term constraints

In accordance with Eq.(2.9) the annealing process starts with the simple initial Hamiltonian $\mathcal{H}_{\text{eff}}^{\lambda, \gamma}(t=0) = \mathcal{H}_{\text{init}}$. At the end of the procedure, the system should be found in the ground state of its problem Hamiltonian $\mathcal{H}_{\text{eff}}^{\lambda, \gamma}(t=\tau) = \mathcal{H}_p$.

$$\mathcal{H}_{\text{eff}}^{\lambda, \gamma} = (1 - \lambda)\mathcal{H}_{\text{init}}(\gamma) + \lambda\mathcal{H}_p + \mathcal{H}_{CD}^{\lambda, \gamma} \quad (2.24)$$

$$= (1 - \lambda)\mathcal{H}_{\text{init}}(\gamma) + \lambda\mathcal{H}_p + \dot{\lambda}\mathcal{A}_\lambda + \dot{\gamma}\mathcal{A}_\gamma \quad (2.25)$$

The desired final state of our system requires the familiar conditions

$$\lambda(t=0) = 0 \quad (2.26)$$

$$\lambda(t=\tau) = 1 \quad (2.27)$$

Since γ is a constant $\gamma = \gamma_{const}$ in the original one-parameter case, we choose

$$\gamma(t) > 0 \quad (2.28)$$

$$\gamma(t=0) = \gamma_{const} \quad (2.29)$$

in the two-parameter case, which facilitates reasonable comparison between the two driving protocols.

Since the last two terms in Eq.(2.25) only appear during the annealing process, we are presented with the constraints

$$\dot{\lambda}(t=0) = \dot{\lambda}(t=\tau) = 0 \quad (2.30)$$

$$\dot{\gamma}(t=0) = \dot{\gamma}(t=\tau) = 0 \quad (2.31)$$

Both $\lambda(t)$ and $\gamma(t)$ have to be continuously differentiable functions at all times $t \in [0, \tau]$. We follow [32] and conventionally choose

$$\lambda(t) = \sin^2\left(\frac{\pi}{2} \sin^2\left(\frac{\pi t}{2\tau}\right)\right) \quad (2.32)$$

According to literature this is a convenient², but not as a necessary choice [33].

As previously described, we define $\gamma(t)$ in such a way that the transverse field is intensified along the process.

$$\gamma(t) := \gamma_{const} + \sin^2\left(\frac{\pi}{2} \sin^2\left(\frac{\pi t}{2\tau}\right)\right) \quad \gamma_{const} \in \mathbb{R}^+ \quad (2.33)$$

Figure 2.1 outlines the driving coefficients of the initial system Hamiltonian for the one-parameter and the two-parameter protocols. In the Ising spin model γ represents the ratio between the interactive forces between the qubits and the strength of the transverse field. The product form $\gamma(1 - \lambda)$ therefore accounts for the strength of the transverse field acting on the initial Hamiltonian \mathcal{H}_{init} .

Intensification mentioned just above in Eq.(2.33) means multiplying by a larger factor. As a consequence, the spectrum of the eigenvalues gets broader. This in turn means the gap between the ground state and the first excited state is expected to widen. Thus the system is less likely to go from the ground to the first excited state.

²The requirements would also be satisfied e.g. by the function

$$\lambda(t) = \sin^3\left(\frac{\pi t}{2\tau}\right)$$

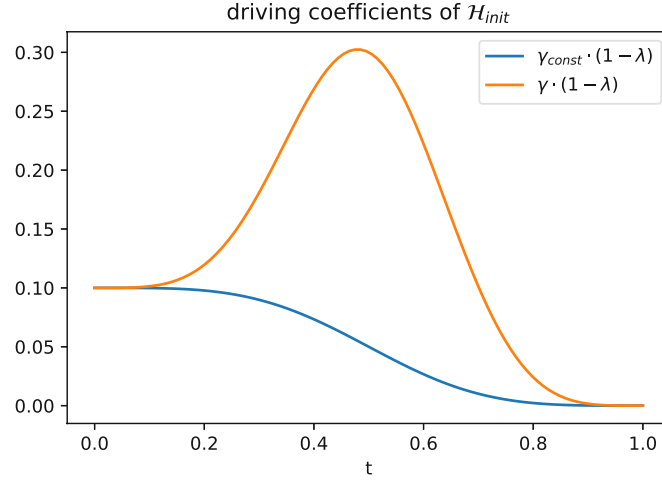


Figure 2.1: Different driving schedules for the one parameter (blue) and two parameter case (orange), with $\gamma_{const} = 0.1$

2.3 Application to several quantum models

In this section, the driving schedules for a wide range of different, and very common quantum Ising spin models are presented.

2.3.1 Landau-Zener formulation

We start with the simplest form of a quantum model: a single spin³ in the Landau-Zener formulation. The Hamiltonian of the one-body system reads

$$\mathcal{H} = (1 - \lambda)(-\gamma)\sigma^x - \lambda h\sigma^z \quad (2.34)$$

where we have our driving parameters $\lambda(t)$ and $\gamma(t)$. The x and z components of the Pauli matrices are denoted by σ^x and σ^z .

We add the counter-diabatic term and make the following ansatz for the gauge potentials

$$\mathcal{X} = \alpha\sigma^y, \quad (2.35)$$

$$\mathcal{Y} = \beta\sigma^y. \quad (2.36)$$

³In the quantum community it is common to use the term *spin* or *qubit* for a two-state quantum system. In literature we also often read the word *site* in this context, which relates to the index or position of a two-state quantum system.

where $\alpha(t)$ and $\beta(t)$ are the time dependent parameters of the counter diabatic term. The effective driving Hamiltonian therefore reads

$$\mathcal{H}_{eff}^{\lambda,\gamma} = \mathcal{H} + (\dot{\lambda}\alpha + \dot{\gamma}\beta)\sigma^y \quad (2.37)$$

As outlined in the method section (Chapter 2), our goal is to minimize the action \mathcal{S} Eq.(2.21)

$$\mathcal{S} = Tr[G_\lambda^2] + Tr[G_\gamma^2] \quad (2.38)$$

and find the optimal formulation for $\alpha(t)$ and $\beta(t)$.

The complete derivation is outlined in the Appendix section B.1.

After successfully minimizing the action operator, we are presented with the two parameter functions

$$\alpha = -\frac{1}{2} \frac{h\gamma}{\lambda^2 h^2 + (1-\lambda)^2 \gamma^2}, \quad (2.39)$$

$$\beta = \frac{1}{2} \frac{(1-\lambda)\lambda h}{\lambda^2 h^2 + (1-\lambda)^2 \gamma^2}. \quad (2.40)$$

As expected, we obtain the same generator α as in the familiar counter diabatic case, where $\gamma = \gamma_{const}$. In addition we now have an optimal driving schedule for the term

$$\dot{\gamma}\mathcal{A}_\gamma = \dot{\gamma}\beta\sigma^y \quad (2.41)$$

2.3.2 Rotating frame

In this section we take a short digression to elaborate on the rotating frame. Our goal is to rewrite the driver Hamiltonian \mathcal{H}_{eff} only in terms of σ^x and σ^z components. Since it is desirable to drive a quantum system with real (measurable) control, a formulation without σ^y terms is more feasible for the realization in the laboratory.

In order to do so, we apply the unitary transformation $U_{rot} = e^{i\theta\sigma^z/2}$, which accounts for a rotation around the z -axis and write the associated Schrödinger equation

$$i\frac{d}{dt} |\tilde{\psi}\rangle = \tilde{\mathcal{H}}_{eff} |\tilde{\psi}\rangle - \frac{\dot{\theta}}{2} \sigma^z |\tilde{\psi}\rangle \quad (2.42)$$

where $\tilde{\mathcal{H}}_{\text{eff}} = U_{\text{rot}} \mathcal{H}_{\text{eff}} U_{\text{rot}}^\dagger$ and $|\tilde{\psi}\rangle = U_{\text{rot}} |\psi\rangle$ denote the driver Hamiltonian and the system state in the rotating frame, respectively. We determine the obtained effective Hamiltonian in the rotating frame

$$\tilde{\mathcal{H}}_{\text{eff,rot}} = \tilde{\mathcal{H}}_{\text{eff}} - \frac{\dot{\theta}}{2} \sigma^z. \quad (2.43)$$

In the following we derive the formulation on the example of the simple Landau-Zener model for both the one-parameter and the two-parameter cases. The procedure can be applied to all other more complicated quantum spin models in the same manner.

The driver Hamiltonian from the previous section in the one-parameter counter diabolic case reads

$$\mathcal{H}_{\text{eff}}^\lambda = (1 - \lambda)(-\gamma)\sigma^x - \lambda h \sigma^z + \dot{\lambda} \alpha \sigma^y. \quad (2.44)$$

We follow the notation of Sels and Polkovnicov [30] (supporting information) and write the same Hamiltonian in the form

$$\mathcal{H}_{\text{eff}}^\lambda = X \sigma^x - \lambda h \sigma^z + Y \sigma^y \quad (2.45)$$

with the parameters $X = (1 - \lambda)(-\gamma)$ and $Y = \dot{\lambda} \alpha$. The first step is to rewrite the driver Hamiltonian

$$\tilde{\mathcal{H}}_{\text{eff}}^\lambda = U_{\text{rot}} \mathcal{H}_{\text{eff}}^\lambda U_{\text{rot}}^\dagger \quad (2.46)$$

$$= U_{\text{rot}} (X \sigma^x - \lambda h \sigma^z + Y \sigma^y) U_{\text{rot}}^\dagger. \quad (2.47)$$

We use the relations

$$U_{\text{rot}} \sigma^x U_{\text{rot}}^\dagger = \cos \theta \sigma^x - \sin \theta \sigma^y, \quad (2.48)$$

$$U_{\text{rot}} \sigma^y U_{\text{rot}}^\dagger = \cos \theta \sigma^y + \sin \theta \sigma^x, \quad (2.49)$$

$$U_{\text{rot}} \sigma^z U_{\text{rot}}^\dagger = \sigma^z \quad (2.50)$$

and obtain

$$\tilde{\mathcal{H}}_{\text{eff}}^\lambda = (X \cos \theta + Y \sin \theta) \sigma^x + (-X \sin \theta + Y \cos \theta) \sigma^y - \lambda h \sigma^z. \quad (2.51)$$

In order to eliminate the σ^z term, we choose $\tan \theta = \frac{X}{Y}$ and the first term of the effective Hamiltonian in the rotating frame becomes

$$\tilde{\mathcal{H}}_{\text{eff}}^\lambda = \sqrt{X^2 + Y^2} - \lambda h \sigma^z. \quad (2.52)$$

The second term of equation (2.43) is obtained by differentiating $\tan \theta$ with respect to time

$$\frac{d}{dt} \tan \theta = \frac{1}{\cos^2 \theta} \dot{\theta} = \frac{\dot{Y}X - \dot{X}Y}{X^2} \quad (2.53)$$

which further results in

$$\dot{\theta} = \frac{X^2}{X^2 + Y^2} \frac{\dot{Y}X - \dot{X}Y}{X^2} = \frac{\dot{Y}X - \dot{X}Y}{X^2 + Y^2}. \quad (2.54)$$

We can finally write the fully reformulated Hamiltonian in the rotation frame

$$\tilde{\mathcal{H}}_{\text{eff,rot}}^{\lambda} = \tilde{\mathcal{H}}_{\text{eff}}^{\lambda} - \frac{\dot{\theta}}{2} \sigma^z \quad (2.55)$$

$$= \sqrt{X^2 + Y^2} - \lambda h \sigma^z + \frac{1}{2} \frac{\dot{Y}X - \dot{X}Y}{X^2 + Y^2} \sigma^z. \quad (2.56)$$

In the two-parameter case the effective Hamiltonian reads

$$\mathcal{H}_{\text{eff}}^{\lambda,\gamma} = X \sigma^x - \lambda h \sigma^z + Y \sigma^y \quad (2.57)$$

with the parameters $X = (1 - \lambda)(-\gamma)$ and $Y = \dot{\lambda}\alpha + \dot{\gamma}\beta$. With the prescribed procedure one can show that the effective Hamiltonian in the rotating frame has the very same form (with the only difference in the parameter Y and the time-dependence of $\gamma(t)$)

$$\tilde{\mathcal{H}}_{\text{eff,rot}}^{\lambda,\gamma} = \tilde{\mathcal{H}}_{\text{eff}}^{\lambda,\gamma} - \frac{\dot{\theta}}{2} \sigma^z \quad (2.58)$$

$$= \sqrt{X^2 + Y^2} - \lambda h \sigma^z + \frac{1}{2} \frac{\dot{Y}X - \dot{X}Y}{X^2 + Y^2} \sigma^z. \quad (2.59)$$

Driving the system with the described effective Hamiltonians does of course not effect the final fidelity.

2.3.3 Two-spin model

The traditional Ising Hamiltonian of the two body system reads

$$\mathcal{H} = (1 - \lambda) \sum_{i=1}^2 -\gamma_i \sigma_i^x - \lambda \left(\sum_{i=1}^2 h_i \sigma_i^z + J \sigma_1^z \sigma_2^z \right) \quad (2.60)$$

where J accounts for the interaction between the two spins.

We again minimize the familiar action operator $\mathcal{S} = \text{Tr}[G_\lambda^2] + \text{Tr}[G_\gamma^2]$ with respect to the two gauge potentials

$$\mathcal{X} = \sum_{i=1}^2 \alpha_i \sigma_i^y, \quad (2.61)$$

$$\mathcal{Y} = \sum_{i=1}^2 \beta_i \sigma_i^y. \quad (2.62)$$

and obtain the driving schedules

$$\alpha_i = -\frac{1}{2} \frac{\gamma_i h_i}{\lambda^2 h_i^2 + (1-\lambda)^2 \gamma_i^2 + \lambda^2 J^2}, \quad (2.63)$$

$$\beta_i = \frac{1}{2} \frac{(1-\lambda) \lambda h_i}{\lambda^2 h_i^2 + (1-\lambda)^2 \gamma_i^2 + \lambda^2 J^2}. \quad (2.64)$$

Please refer to Appendix section B.2 for details of the derivation.

2.3.4 Nearest Neighbour Model

In the nearest-neighbor Ising spin model in one dimension, the original Hamiltonian reads

$$\mathcal{H} = (1-\lambda) \sum_{i=1}^N (-\gamma_i) \sigma_i^x - \lambda \left[\sum_{i=1}^N h_i \sigma_i^z + \sum_{i=1}^N J_{i,i+1} \sigma_i^z \sigma_{i+1}^z \right] \quad (2.65)$$

where we use periodic boundary conditions, i.e. $\sigma_{N+1}^z = \sigma_1^z$.

We again calculate all terms of the action operator $\mathcal{S} = \text{Tr}[G_\lambda^2] + \text{Tr}[G_\gamma^2]$ and with the ansatz for both gauge potentials

$$\mathcal{X} = \sum_{i=1}^N \alpha_i \sigma_i^y \quad (2.66)$$

$$\mathcal{Y} = \sum_{i=1}^N \beta_i \sigma_i^y \quad (2.67)$$

we receive for the optimal driving schedule

$$\alpha_i = -\frac{h_i \gamma_i}{2[\lambda^2 (J_{i,i+1}^2 + J_{i-1,i}^2) + h_i^2 \lambda^2 + \gamma_i^2 (1-\lambda)^2]} \quad (2.68)$$

$$(2.69)$$

$$\beta_i = \frac{(1-\lambda) \lambda h_i}{2[\lambda^2 h_i^2 + (1-\lambda)^2 \gamma_i^2 + \lambda^2 (J_{i,i+1}^2 + J_{i-1,i}^2)]} \quad (2.70)$$

Please find the detailed derivation in the appendix section B.3.

2.3.5 p -spin Model

In the p -spin model, the original Hamiltonian reads

$$\mathcal{H} = (1 - \lambda)\gamma \sum_{i=1}^N -\sigma_i^x - \lambda N \left(\frac{1}{N} \sum_{i=1}^N \sigma_i^z \right)^p \quad p = 1, 2, 3, \dots \quad (2.71)$$

Here, we consider the case $p = 3$.

$$\mathcal{H} = (1 - \lambda)\gamma \sum_{i=1}^N -\sigma_i^x - \lambda \frac{1}{N^2} \left(\sum_{i=1}^N \sigma_i^z \right)^3 \quad (2.72)$$

With the familiar minimization method we obtain

$$\alpha = -\frac{1}{2} \frac{\gamma N^2 (3N - 2)}{\lambda^2 (3N - 2)^2 + (1 - \lambda)^2 \gamma^2 N^4 + 18\lambda^2 (N - 1)(N - 2)} \quad (2.73)$$

$$\beta = \frac{1}{2} \frac{(1 - \lambda)\lambda N^2 (3N - 2)}{\lambda^2 (3N - 2)^2 + (1 - \lambda)^2 \gamma^2 N^4 + 18\lambda^2 (N - 1)(N - 2)} \quad (2.74)$$

The full derivation is outlined in Appendix section B.4.

The p -spin model received broader elaboration. The published work of our research collaboration with its detailed explanations and results is enclosed in the Appendix Chapter A.

2.3.6 Sherrington-Kirkpatrick Model

For the SK model, the original Hamiltonian reads

$$\mathcal{H} = (1 - \lambda) \sum_{i=1}^N (-\gamma_i) \sigma_i^x - \lambda \left[\sum_{i=1}^N h_i \sigma_i^z + \frac{1}{2} \sum_{i \neq j}^N J_{ij} \sigma_i^z \sigma_j^z \right] \quad (2.75)$$

Each spin has $(N - 1)$ interactions with all the other existing spins. In total we therefore count $\frac{N(N-1)}{2}$ distinct spin-pair interactions J_{ij} . The interactions in this model are drawn from a Gaussian distribution, with its mean value $[J_{ij}] = 0$ and its variance normalized by the number of spins $[(\Delta J_{ij})^2] = \frac{J^2}{N}$. This ensures that the thermodynamic limit is properly defined [34].

We again apply the same procedure as in the previous chapters to calculate α_i and β_i and obtain

$$\alpha_i = -\frac{1}{2} \frac{h_i \gamma_i}{\lambda^2 \sum_{j \neq i}^N J_{ij}^2 + h_i^2 \lambda^2 + \gamma_i^2 (1 - \lambda)^2} \quad (2.76)$$

$$\beta_i = \frac{1}{2} \frac{h_i (1 - \lambda) \lambda}{\lambda^2 \sum_{j \neq i}^N J_{ij}^2 + h_i^2 \lambda^2 + \gamma_i^2 (1 - \lambda)^2} \quad (2.77)$$

2.3.7 Coulomb glass model

For the Coulomb glass model, the original Hamiltonian reads

$$\mathcal{H} = (1 - \lambda) \sum_{i=1}^N (-\gamma_i) \sigma_i^x - \lambda \left[\sum_{i=1}^N h_i \sigma_i^z + \frac{1}{2} \sum_{i \neq j}^N \frac{J_{ij}}{|i-j|} \sigma_i^z \sigma_j^z \right] \quad (2.78)$$

with the driving parameters $\lambda(t)$ and $\gamma_i(t)$ and where we use periodic boundary conditions, i.e. $\sigma_{N+1}^z = \sigma_1^z$.

The interactions J_{ij} are again chosen from a Gaussian distribution. In this model the variance of the distribution is, however, not divided by the number of spins N , $(\Delta J_{ij})^2 = 1$. The interactions are divided by the spins distance - as one can see from the last sum of the Hamiltonian Eq.(2.78).

We again apply the same procedure as in the previous chapters to calculate α_i and β_i and obtain

$$\alpha_i = -\frac{1}{2} \frac{h_i \gamma_i}{\lambda^2 \sum_{j \neq i}^N \frac{J_{ij}^2}{|i-j|^2} + h_i^2 \lambda^2 + \gamma_i^2 (1 - \lambda)^2} \quad (2.79)$$

$$\beta_i = \frac{1}{2} \frac{h_i (1 - \lambda) \lambda}{\lambda^2 \sum_{j \neq i}^N \frac{J_{ij}^2}{|i-j|^2} + h_i^2 \lambda^2 + \gamma_i^2 (1 - \lambda)^2} \quad (2.80)$$

2.3.8 Two-dimensional spin glass

In the two-dimensional spin glass model, the original Hamiltonian reads

$$\mathcal{H} = (1 - \lambda) \sum_{i=1}^N (-\gamma_i) \sigma_i^x - \lambda \left[\sum_{i=1}^N h_i \sigma_i^z + \sum_{\langle ij \rangle} J_{ij} \sigma_i^z \sigma_j^z \right]. \quad (2.81)$$

We consider a square lattice with periodic boundaries in both directions.

We accomplish the desired driving functions for α_i and β_i with the discussed method and obtain

$$\alpha_i = -\frac{1}{2} \frac{h_i \gamma_i}{\lambda^2 \sum_{j \in i} J_{ij}^2 + h_i^2 \lambda^2 + \gamma_i^2 (1 - \lambda)^2} \quad (2.82)$$

$$\beta_i = \frac{1}{2} \frac{h_i (1 - \lambda) \lambda}{\lambda^2 \sum_{j \in i} J_{ij}^2 + h_i^2 \lambda^2 + \gamma_i^2 (1 - \lambda)^2} \quad (2.83)$$

where the index j runs over all four (horizontal and vertical) nearest neighbours of the spin i in the lattice.

2.4 Numerical results

This section comprises the results of the model applications. We will discuss and compare the introduced two parameter counter-diabatic driving $CD_{\lambda, \gamma}$ with the one parameter case CD_λ and the traditional quantum annealing QA .

$$CD_\lambda : \quad \mathcal{H}_{eff}^\lambda = (1 - \lambda) \mathcal{H}_{init} + \lambda \mathcal{H}_p + \dot{\lambda} \mathcal{A}_\lambda \quad (2.84)$$

$$CD_{\lambda, \gamma} : \quad \mathcal{H}_{eff}^{\lambda, \gamma} = (1 - \lambda) \mathcal{H}_{init}(\gamma) + \lambda \mathcal{H}_p + \dot{\lambda} \mathcal{A}_\lambda + \dot{\gamma} \mathcal{A}_\gamma \quad (2.85)$$

$$QA : \quad \mathcal{H}_{eff} = (1 - \lambda) \mathcal{H}_{init} + \lambda \mathcal{H}_p \quad (2.86)$$

We draw conclusions from two different measures:

1. The final fidelity of the systems state

$$F = |\langle \phi_{p,0} | \psi_{t=\tau} \rangle|^2 \quad (2.87)$$

determines the probability to find the state at the end of the annealing process $|\psi_{t=\tau}\rangle$ in the ground state of the problem Hamiltonian $|\phi_{p,0}\rangle$.

2. The residual energy of the final state

$$E_{res} = |\langle \psi_{t=\tau} | \mathcal{H}_p | \psi_{t=\tau} \rangle - \langle \mathcal{H}_{p,0} \rangle|. \quad (2.88)$$

It describes the distance between the obtained expected energy of the system and the true ground state energy of the problem Hamiltonian.

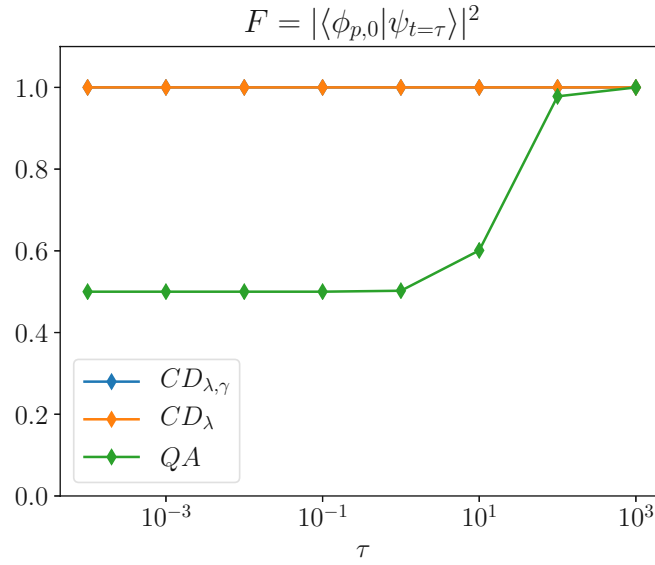


Figure 2.2: Final fidelities in the LZ Model of the three protocols for different annealing times τ . The curves for the one-parameter (orange) and two-parameter cases (blue) overlap on top of each other.

2.4.1 Landau-Zener formulation

The ansatz for the gauge potentials Eq.(2.36) is the most general possible for the one-body case our exact solutions. Therefore we always find the system in the desired final state, independent of the rapidness of the protocol.

Figure 2.2 shows the obtained results for both the one- and the two-parameter cases. The traditional quantum annealing does not suppress the dissipative forces. We can trace this fact by the final fidelities, which depend clearly on the speed of the driving protocol.

2.4.2 Two-spin model

From Figure 2.3 we clearly see that both investigated driving schedules show a significant improvement to the traditional quantum annealing. Within the range of annealing times $\tau \in [1, 10^3]$ the introduced driving results in almost 30% on average higher fidelities than its counter diabolic counterpart.

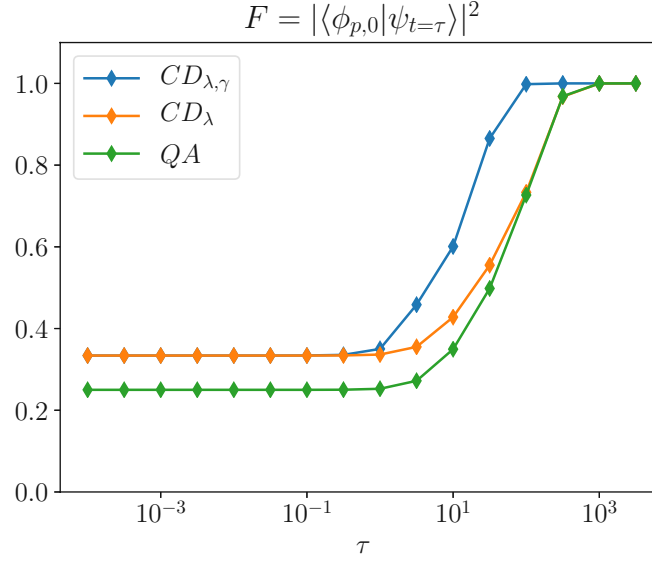


Figure 2.3: Final fidelities in the two-body system of the three protocols for different annealing time τ , with $\gamma_{const} = 0.1$, $h = 0.1$, $J = 1$

2.4.3 Nearest neighbour model

Figures 2.4 and 2.5 show the results for the increasing annealing time τ for different system sizes in the nearest neighbour model. The left panels of the figure depict a system with five spins, while on the right panels show the results for a ten-spin system. As hoped for, we again find a strong improvement over the two counterparts for annealing times $\tau \in [1, 10^3]$.

From Table 2.1 we recognize different aspects for the example duration of $\tau = 100$: The stability of the introduced scheme is highly remarkable. The increased number of spins results in a fidelity loss of only 10%, while the familiar counterpart suffers from a much higher loss of about 50%. We therefore find that the improvement ΔF grows with the number of spins, which is of course highly favourable.

	$CD_{\lambda, \gamma}$	CD_{λ}	ΔF
$N = 5$	0.93	0.44	+0.49
$N = 10$	0.82	0.21	+0.61

Table 2.1: Final groundstate fidelities of the introduced counter diabatic scheme and its counterpart for $\tau = 100$, $\Delta F = F_{CD_{\lambda, \gamma}} - F_{CD_{\lambda}}$, where $F_{CD_{\lambda, \gamma}}$ and $F_{CD_{\lambda}}$ denote the final groundstate fidelity for the two-parameter case and the one-parameter case, respectively.

$$F = |\langle \phi_{p,0} | \psi_{t=\tau} \rangle|^2$$

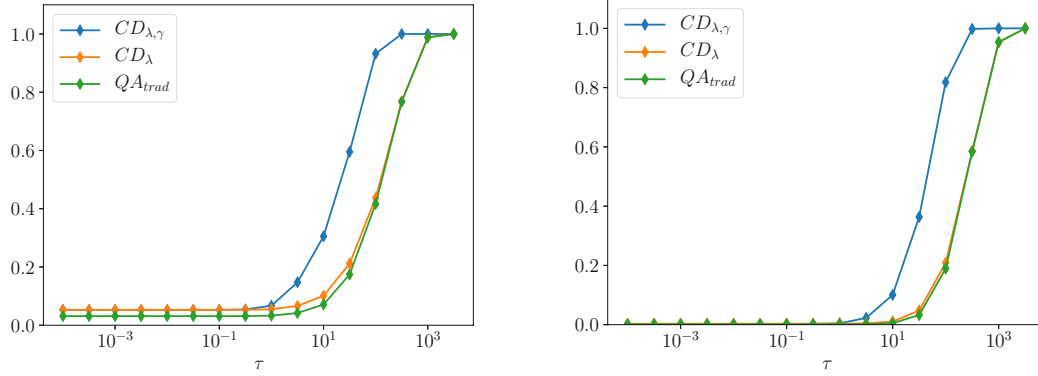


Figure 2.4: Time dependence of the final ground state fidelity for the one-dimensional nearest-neighbor model. Left: five spins. Right: ten spins, with $\gamma_{const} = 0.1$, $h = 0.1$, $J = 1$

$$E_{res} = |\langle \psi_{t=\tau} | \mathcal{H}_p | \psi_{t=\tau} \rangle - \langle \mathcal{H}_p | \phi_{p,0} \rangle|$$

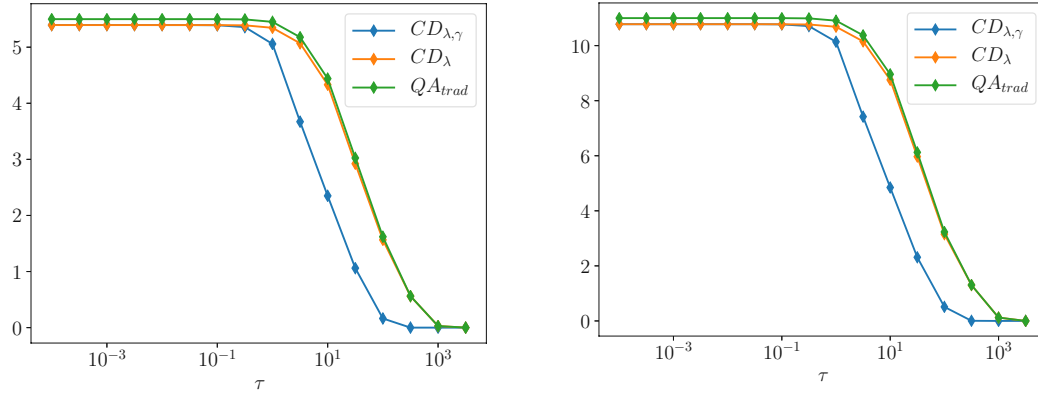


Figure 2.5: Time dependence of the residual energy for the one-dimensional nearest-neighbor model. Left: five spins. Right: ten spins, with $\gamma_{const} = 0.1$, $h = 0.1$, $J = 1$

2.4.4 p -spin model

The obtained numerical results for the p -spin model with $p = 3$ are outlined in this section.

Figure 2.6 depicts the familiar measures, the final ground state fidelity F in panels (a)-(c) and the residual energy ΔE in panels (d)-(f) as functions of annealing duration τ . We investigated the system sizes $N = 4$ in panels (a),(d), $N = 30$ in

panels (b),(e) and $N = 50$ in panels (c),(f).

For the traditional quantum annealing protocol, we see that the final state is far away from the ground state for short annealing time τ [green-shaded areas, where $F(\tau) \approx 1/2^N$] and reach the final ground state in the adiabatic regime [gray-shaded areas, where $F(\tau) > 0.99$] for very long annealing time.

For the two-parameter method we observe considerably higher final ground state fidelity and lower residual energy compared to traditional quantum annealing and one-parameter CD driving for long annealing time regime (yellow-shaded areas). This is important since the asymptotic adiabatic regime (gray-shaded areas) starts at later times for larger system sizes as seen in Figure 2.6(c). This means the two-parameter CD driven Hamiltonian reaches the adiabatic regime more quickly, thus performing much better (around an order of magnitude reduction in annealing time to reach the same values of fidelity and residual energy) compared to its traditional quantum annealing and single-parameter CD driving counterparts.

We can conclude that the present numerical results clearly indicate that our two-parameter method leads to significant advantages in the intermediate time region. This time region is important in practice because, first, the gray-shaded adiabatic region is often hard to reach for very large systems, and second, the short-time region, green shaded, has large residual energy and low fidelity.

The included publication on the p -spin model (Appendix Chapter A) comprises further details regarding the central measure *time-to-solution*.

2.4.5 Sherrington-Kirkpatrick model

As already described in the previous section, each spin in the Sherrington-Kirkpatrick model has $(N - 1)$ interactions with all the other existing spins. In total we therefore count $\frac{N(N-1)}{2}$ distinct spin-pair interactions J_{ij} . The interactions in this model are drawn from a Gaussian distribution, with its mean value $[J_{ij}] = 0$ and its variance normalized by the number of spins $[(\Delta J_{ij})^2] = \frac{J_{ij}^2}{N}$. This ensures that the thermodynamic limit is properly defined [34].

For each spin interaction we draw $(N - 1)$ random Gaussian distributed inter-

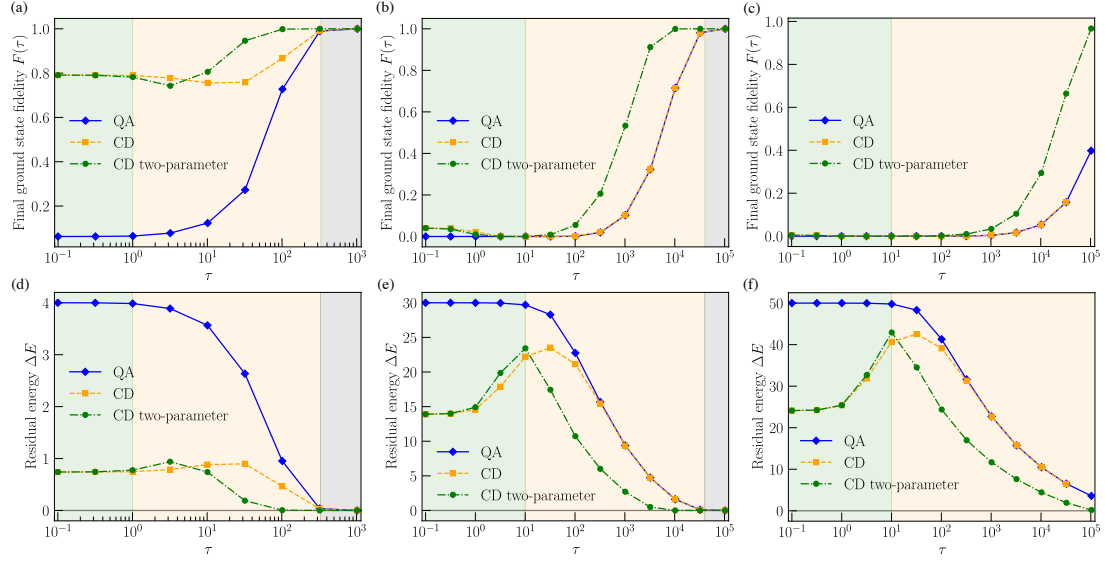


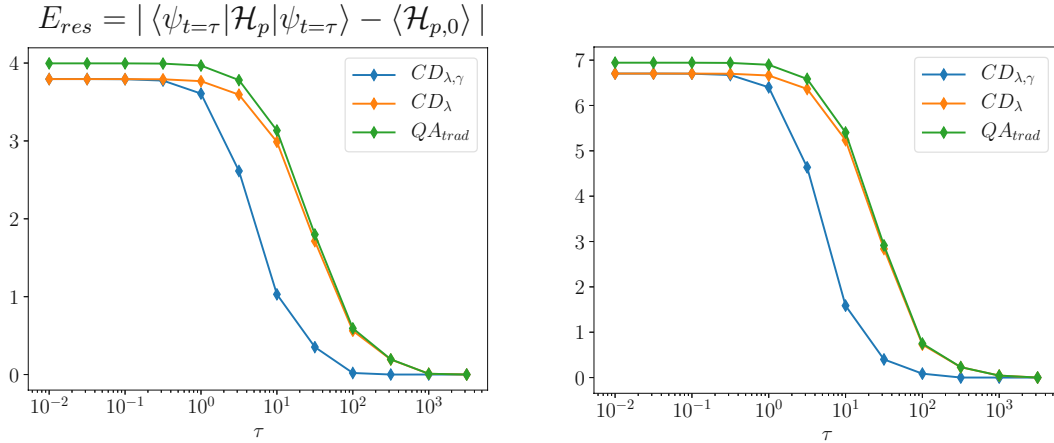
Figure 2.6: **Ground state fidelity and residual energy.** (a)-(c) Final ground state fidelity and (d)-(f) residual energy for (i) traditional quantum annealing (diamonds, blue solid line), (ii) single-parameter CD drive (squares, orange dashed line), and (iii) two-parameter CD drive (circles, green dash-dotted line) as functions of annealing time τ . The system sizes are $N = 4$ [panels (a),(d)], $N = 30$ [(b),(e)], and $N = 50$ [(c),(f)], where $\gamma_{\text{init}} = 0.1$ for all panels. Time ranges are color-coded as: Short-time regime (green-shaded areas) where the fidelity is approximately $1/2^N$ for traditional quantum annealing, long-time regime (yellow-shaded areas) where transient behavior is observed and the two-parameter CD drive shows a clear advantage, and adiabatic regime (gray-shaded areas) where $F(\tau) > 0.99$.

actions and store them in a $N \times (N - 1)$ matrix.

$$\mathbf{J} = \begin{pmatrix} \mathbf{J}_{12} & J_{13} & J_{14} & \dots & J_{1N} \\ \mathbf{J}_{21} & \mathbf{J}_{23} & J_{24} & \dots & J_{2N} \\ J_{31} & \mathbf{J}_{32} & J_{34} & \dots & J_{3N} \\ \vdots & \vdots & \vdots & \ddots & \vdots \\ J_{N1} & J_{N2} & J_{N3} & \dots & J_{N(N-1)} \end{pmatrix} \quad (2.89)$$

As of course the interaction between two spins is always the same $J_{ij} \equiv J_{ji}$, the entries in the matrix are then replaced as follows: $J_{21} = J_{12}$, $J_{32} = J_{23}$ \dots $J_{N(N-1)} = J_{(N-1)N}$.

The first measure we are interested in is again the residual energy. In Figure ?? we see again the comparison of a 5- and a 10-spin system. For $h = 0.1$ we detect a significant improvement for the $CD_{\lambda,\gamma}$ scheme to both counterparts in most of the annealing times



Time dependence of the residual energy for the Sherrington-Kirkpatrick model. Left: five spins. Right: ten spins, with $\gamma_{const} = 0.1$, $h = 0.1$, $J = 1$

Figure 2.7 shows the final groundstate fidelities over increasing annealing time τ for the field strength $h = 0.1$. The left panel depicts a system with 5 spins, while on the right panel we see the results for a 10-spin system. As hoped for, we again find a strong improvement of the introduced driving scheme to the two counterparts, especially for durations $\tau \in [1, 10^3]$.

From Table 2.2, we compare exact values for the example duration of $\tau = 100$: While increasing the number of spins results in a loss of 14% in the $CD_{\lambda,\gamma}$ case, we encounter a loss of about 38% in the familiar counterpart. We therefore find that the improvement ΔF grows with the number of spins in this very model.

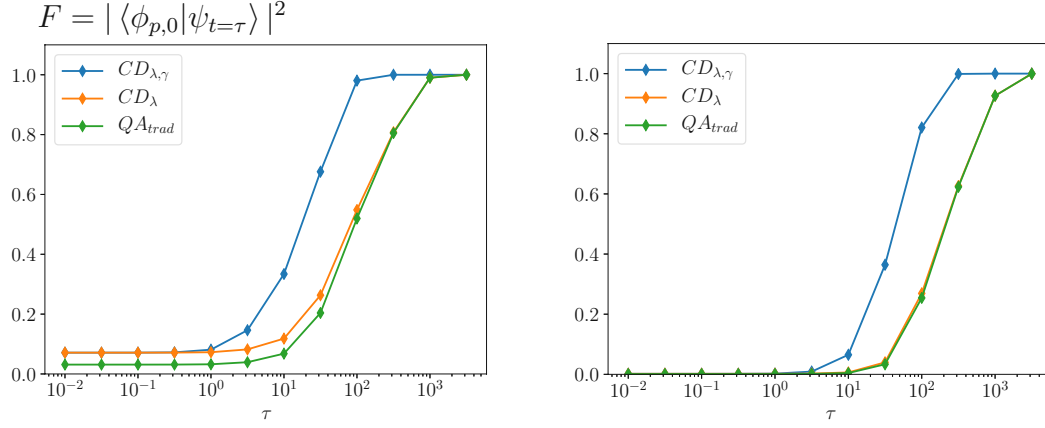


Figure 2.7: Time dependence of the final ground state fidelity for the Sherrington-Kirkpatrick model. Left: five spins. Right: ten spins, with $\gamma_{const} = 0.1$, $h = 0.1$, $J = 1$

	$CD_{\lambda,\gamma}$	CD_{λ}	ΔF
$N = 5$	0.96	0.63	+0.33
$N = 10$	0.82	0.25	+0.57

Table 2.2: Final groundstate fidelities of the introduced counter diabatic scheme and its counterpart for $\tau = 100$, $\Delta F = F_{CD_{\lambda,\gamma}} - F_{CD_{\lambda}}$

2.4.6 Coulomb glass model

In the Coulomb glass model we draw the interactions from a Gaussian distribution with mean zero and $(\Delta J_{ij})^2 = 1$ in the same manner as described in the last section. In this model the interactions-matrix J_{ij} is element-wise divided by $|i - j|$ matrix.

The results depicted in Figures 2.8 and 2.9 show similar promising behaviour as in the previous model. At durations $\tau \in [1, 10^3]$ the introduced scheme clearly stands out of the considered driving schemes - this accounts for the two system sizes $N = 5$ and $N = 10$.

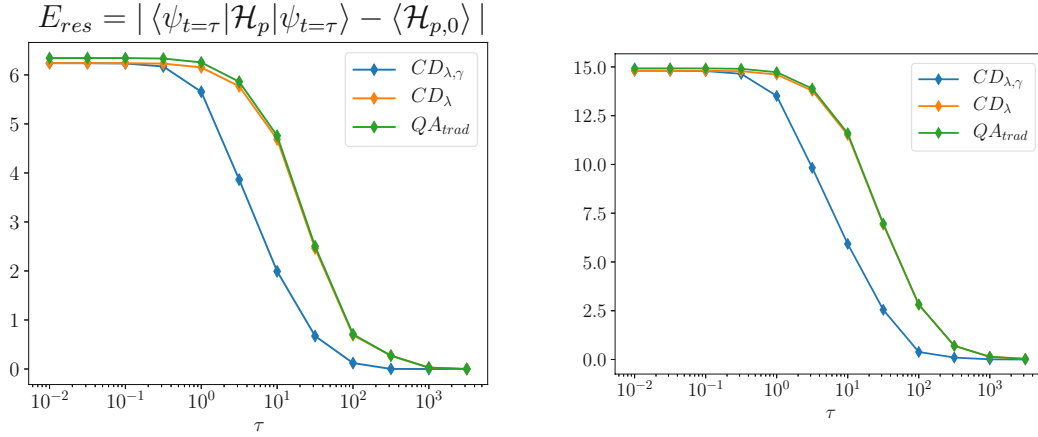


Figure 2.8: Time dependence of the final ground state fidelity for the Coulombglass model. Left: five spins. Right: ten spins, with $\gamma_{const} = 0.1$, $h = 0.1$, $J = 1$

The other performance measure, we are interested in, are the final ground state fidelities. Similar to the previous model the introduced scheme surpasses at durations $\tau \in [1, 10^3]$ its counterparts. This conclusion can also be drawn from the residual energies.

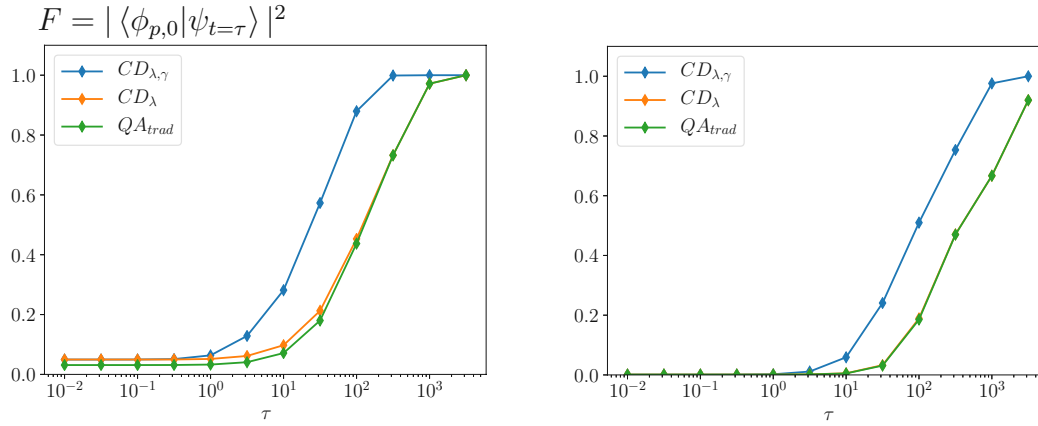


Figure 2.9: Time dependence of the residual energy for the Coulombglass model. Left: five spins. Right: ten spins, with $\gamma_{const} = 0.1$, $h = 0.1$, $J = 1$

From Table 2.3 we find that the improvement ΔF shrinks with the increase of spins, but results in a still quite high value of 32% for $N = 10$.

	$CD_{\lambda,\gamma}$	CD_{λ}	ΔF
$N = 5$	0.88	0.44	+0.44
$N = 10$	0.51	0.19	+0.32

Table 2.3: Final groundstate fidelities of the introduced counter diabatic scheme and its counterpart for $\tau = 100$, $\Delta F = F_{CD_{\lambda,\gamma}} - F_{CD_{\lambda}}$

2.4.7 Two-dimensional spin glass

The interactions J_{ij} are generated randomly by a Gaussian distribution with zero mean and a unit variance for each (ij) on the 2d square lattice. The true ground state of the problem Hamiltonian, where $h = 0$, as well as the interactions J_{ij} are obtained on the spin-glass server (<https://software.cs.uni-koeln.de/spinglass/>).

We investigated the behaviour of all three driving schemes on a 3×3 lattice.

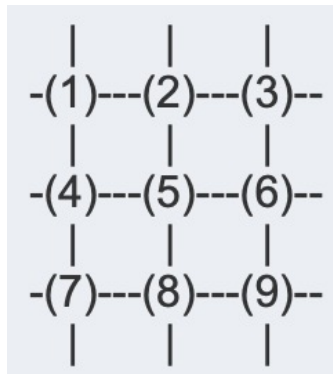


Figure 2.10: (3×3) lattice

A generated sample for example reads

i	j	J_{ij}
1	2	-1.16969
2	3	-1.54779
3	1	-0.78213
4	5	0.72646
5	6	1.03186
6	4	1.38889
7	8	-1.27895
8	9	0.10678
9	7	0.22161
1	4	-1.30251
2	5	-1.11524
3	6	-0.83041
4	7	-1.55248
5	8	0.19936
6	9	0.31503
7	1	0.41487
8	2	0.60799
9	3	0.00920

Table 2.4: Gaussian distributed sample for a 2D lattice with periodic boundaries in both directions

With the received ground state $|\phi_z\rangle = |\uparrow\downarrow\uparrow\downarrow\downarrow\uparrow\downarrow\downarrow\rangle$ we obtained the following final fidelities and final residual energies, Figure 2.11.

Thereby we detect the expected behaviour for all schemes: As there are two optimal states to the problem Hamiltonian, the final fidelity of the chosen optimal state $|\phi_z\rangle$ reaches its limit at 50% fidelity for long annealing times. From the course of the residual energy we trace that the system appears at its minimum energy at sufficiently long annealing times.

As $h = 0$, there is no difference between the traditional driving scheme QA_{trad} and the familiar counterdiabatic CD_λ , as the gauge potential $\mathcal{A}_\lambda = 0$. Even though the gauge potentials $\mathcal{A}_\lambda = 0$ and $\mathcal{A}_\gamma = 0$ as well, the driving scheme with the time dependent $\gamma(t)$ leads to a better performance.

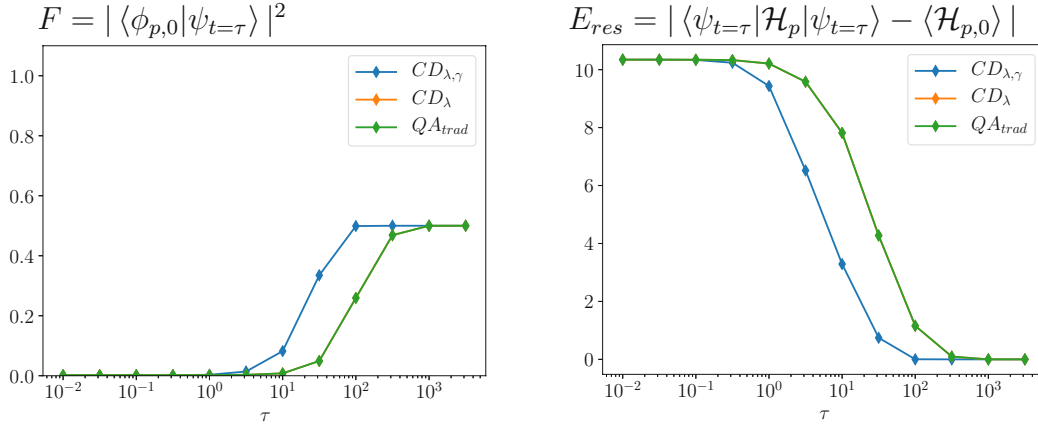


Figure 2.11: Time dependence of for the two-dimensional spin glass. Left: final ground state fidelity, Right: residual energy , with $h = 0$

In Figure 2.12 the results for $h = 0.5$ are shown. Here the gauge potentials come into effect. The introduced driving scheme represents again a clear improvement to its counterparts for annealing times $\tau \in [1, 10^3]$

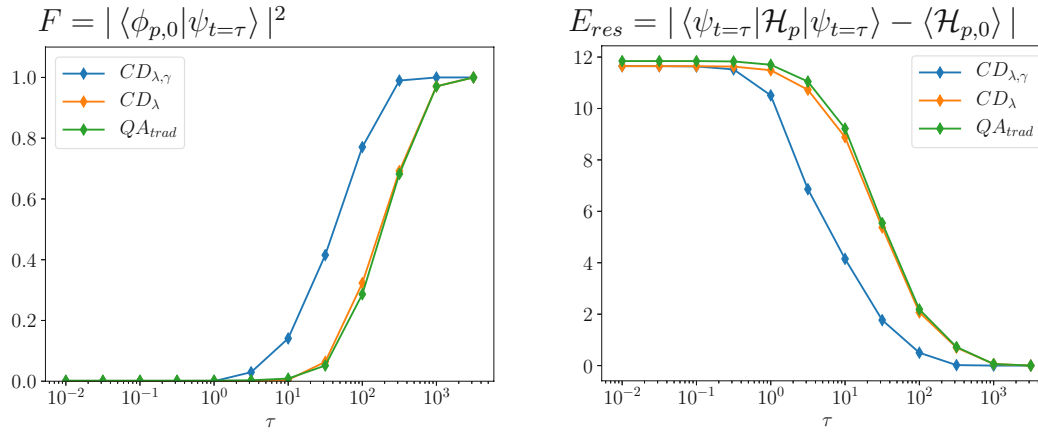


Figure 2.12: Time dependence of for the two-dimensional spin glass. Left: final ground state fidelity, Right: residual energy , with $h = 0.5$

Chapter 3

Conclusion and outlook

This work proposes and analyses a method to find an efficient counter diabatic term that outperforms its traditional quantum annealing and single-parameter method counterparts with respect to enhanced final ground state fidelity and reduced residual energy.

The method introduces a time-dependent transverse magnetic field strength $\gamma(t)$ to the initial system Hamiltonian, which naturally gives rise to a second gauge potential. This two-parameter counter-diabatic approach generalizes the existing method of single-parameter driving by expanding the driving control of the system and expanding the search space of parameters for an optimal control. The method is tested on various commonly used models. The results show that it significantly advances the annealing process in all investigated applications.

Additionally it was shown that the effective Hamiltonian can be expressed, after a rotation in spin space, in terms of the usual transverse field Ising model but with unconventional diabatic control of the magnetic field strengths. The latter may thus be implemented in current quantum annealing devices on various platforms considerably more easily than the traditional annealing control with imaginary terms.

Since $\gamma(t)$ is chosen more or less arbitrarily a future task is to find the optimal choice of the driving function. For this, it is especially interesting to investigate the dynamic behaviour of the eigen spectrum of the initial Hamiltonian when the transverse field is changed.

There exist other approaches to optimize the time dependence of coefficients in quantum annealing, e.g., from the viewpoint of optimal control theory and related ideas often under the context of the quantum approximate optimization algorithm [35–38]. Since the criteria of optimality are defined differently, a comparison in

terms of relevant physical quantities such as fidelity and residual energy reveals an interesting future topic to be studied.

Acknowledgements

Throughout the writing of this thesis I have received a great amount of support and assistance.

I would first like to thank my supervisor, Professor Hidetoshi Nishimori at Tokyo Institute of Technology, whose expertise was invaluable in formulating the research questions and methodology. His continuous feedback pushed me to sharpen my thinking and always gave the incentive to broaden my conceptual understanding. I would also like to thank my supervisor Professor Yuji Hasegawa from the Technical University of Vienna, for his consistent support throughout this master thesis project. I am especially grateful that due to the mutual consent of the Tokyo, Institute of Technology and the TU Vienna, I could conduct this research project despite the exceptional circumstances.


Further, I received great guidance from my colleague and supervisor Andreas Hartmann, Phd. He provided me with the tools and indispensable insights that I needed to choose the right direction to successfully complete my master thesis.

Finally, I would also like to thank my parents for their everlasting support and confidence in me and my abilities in the years of my studies.

Appendices

Appendix A

Publication: Two-parameter counter-diabatic driving in quantum annealing

Two-parameter counter-diabatic driving in quantum annealingLuise Prielinger,¹ Andreas Hartmann ,^{2,*} Yu Yamashiro ,^{3,4} Kohji Nishimura,⁴
Wolfgang Lechner,^{2,5} and Hidetoshi Nishimori ,^{6,7,8}¹Atominstytut, TU Wien, Stadionallee 2, 1020 Vienna, Austria²Institut für Theoretische Physik, Universität Innsbruck, Technikerstraße 21a, A-6020 Innsbruck, Austria³Department of Physics, Tokyo Institute of Technology, Nagatsuta-cho, Midori-ku, Yokohama 226-8503, Japan⁴Jij Inc., Bunkyo-ku, Tokyo 113-0031, Japan⁵Parity Quantum Computing GmbH, Rennweg 1, A-6020 Innsbruck, Austria⁶Institute of Innovative Research, Tokyo Institute of Technology, Nagatsuta-cho, Midori-ku, Yokohama 226-8503, Japan⁷Graduate School of Information Sciences, Tohoku University, Sendai 980-8579, Japan⁸RIKEN Interdisciplinary Theoretical and Mathematical Sciences Program (iTHEMS), Wako, Saitama 351-0198, Japan

(Received 12 November 2020; revised 22 January 2021; accepted 24 February 2021; published 9 March 2021)

We introduce a two-parameter approximate counter-diabatic term into the Hamiltonian of the transverse-field Ising model for quantum annealing to accelerate convergence to the solution, generalizing an existing single-parameter approach. The protocol is equivalent to unconventional diabatic control of the longitudinal and transverse fields in the transverse-field Ising model and thus makes it more feasible for experimental realization than an introduction of new terms such as nonstoquastic catalysts toward the same goal of performance enhancement. We test the idea for the p -spin model with $p = 3$, which has a first-order quantum phase transition, and show that our two-parameter approach leads to significantly larger ground-state fidelity and lower residual energy than those by traditional quantum annealing and by the single-parameter method. We also find a scaling advantage in terms of the time-to-solution as a function of the system size in a certain range of parameters as compared to the traditional methods in the sense that an exponential time complexity is reduced to another exponential complexity with a smaller coefficient. Although the present method may not always lead to a drastic exponential speedup in difficult optimization problems, it is useful because of its versatility and applicability for any problem after a simple algebraic manipulation, in contrast to some other powerful prescriptions for acceleration such as nonstoquastic catalysts in which one should carefully study in advance if it works in a given problem and should identify a proper way to meticulously control the system parameters to achieve the goal, which is generally highly nontrivial.

DOI: [10.1103/PhysRevResearch.3.013227](https://doi.org/10.1103/PhysRevResearch.3.013227)**I. INTRODUCTION**

Quantum annealing is a metaheuristic for combinatorial optimization problems [1–7] and has often been analyzed theoretically in the framework of adiabatic quantum computing [8–10]. A serious bottleneck in this approach originates in the exponential closing of the energy gap between the ground state and the first-excited state as a function of the system size, typically at a first-order quantum phase transition, by which the computation time explodes exponentially according to the adiabatic theorem of quantum mechanics (see, e.g., Ref. [10]). One of the promising candidates to circumvent this difficulty is diabatic quantum annealing [11], in which one ingeniously drives the system out of the ground state to avoid the problem

of closing the minimal energy gap and thus to reach the final ground state with high fidelity. There have been attempts to design protocols to control the system variables based on this idea [11], and shortcuts to adiabaticity [12–15] present strong candidates, providing a systematic way toward this goal.

Among these shortcuts-to-adiabaticity methods [16–22], counter-diabatic (CD) driving [21,23–27] is one of the most promising approaches. The underlying idea of CD driving is to speed up an originally adiabatic process by additionally applying a CD Hamiltonian (adiabatic gauge potential) that suppresses the transitions between the system eigenstates. However, for many-body quantum systems, finding the exact CD Hamiltonian requires *a priori* knowledge of these eigenstates at all times during the dynamics [17], which is practically unfeasible. Recently, Sels, Polkovnikov, and collaborators [25,26,28] have developed a variational approach where a simple and local, but approximate, CD Hamiltonian is introduced, which makes the formulation and realization much simpler not just theoretically but experimentally as well [27,29] (see, also, [30,31] for related developments). The price to pay is that the enhancement of performance is often limited.

*Corresponding author: andreas.hartmann@uibk.ac.at

Published by the American Physical Society under the terms of the [Creative Commons Attribution 4.0 International license](https://creativecommons.org/licenses/by/4.0/). Further distribution of this work must maintain attribution to the author(s) and the published article's title, journal citation, and DOI.

In the present contribution, we propose a method to identify an enhanced local approximate CD Hamiltonian. The latter entails a second adiabatic gauge potential that appears naturally due to the introduction of an additional time-dependent driving function of the Hamiltonian. We find its optimal coefficients by minimizing the operator distance between the exact and approximate CD Hamiltonians in order to maximize the performance of the latter. This approach generalizes the existing method of single-parameter local CD driving by expanding the search space into a second dimension. We test the idea for the p -spin model with $p = 3$ as the problem Hamiltonian, which is known to be a simple model, yet a hard problem to solve by traditional quantum annealing [32–37]. We demonstrate that our approximate two-parameter CD Hamiltonian leads to clearly enhanced final ground-state fidelity and reduced residual energy compared to traditional quantum annealing and the existing method of the approximate single-parameter CD Hamiltonian. We further show a scaling advantage of the method compared to its traditional counterparts in a certain parameter range in the sense that an exponential time complexity is reduced to another exponential complexity with a smaller coefficient. Our two-parameter CD Hamiltonian improves the ground-state fidelity and residual energy for both short and longer annealing times, which thus decreases the time-to-solution considerably. We note that the modified CD Hamiltonian used in this approach involves only local σ_i^y operators, where i is the site index, and can thus be rotated in the spin space at each site such that the result consists only of σ_i^x and σ_i^z in addition to the original transverse-field Ising Hamiltonian. This is simply the usual transverse-field Ising model, but with unconventional diabatic control of the transverse and longitudinal fields, making it feasible for experimental realization.

The paper is structured as follows. In Sec. II, we introduce the method of finding the two-parameter CD protocol and apply the formulation to the p -spin model. Numerical tests are presented in Sec. III for the p -spin model with $p = 3$, and Sec. IV discusses and concludes the paper.

II. METHOD

Quantum annealing is a metaheuristic that aims to solve combinatorial optimization problems. The basic idea is to find the lowest-energy eigenstate of a problem Hamiltonian \mathcal{H}_p —that encodes a combinatorial optimization problem that we want to solve as an Ising model [38]—by adiabatically transferring the easy-to-prepare ground state of the driver Hamiltonian,

$$\mathcal{H}_d = -\gamma \sum_{i=1}^N \sigma_i^x, \quad (1)$$

with γ the time-independent transverse magnetic field strength and N the number of sites (qubits) in the system, into the ground state of \mathcal{H}_p . The annealing schedule is often chosen as

$$\mathcal{H}_0(t) = [1 - \lambda(t)]\mathcal{H}_d + \lambda(t)\mathcal{H}_p, \quad (2)$$

where $\lambda(t)$ is a time-dependent driving function that fulfills the boundary conditions $\lambda(t = 0) = 0$ and $\lambda(t = \tau) = 1$, with

τ the total annealing time. Reaching the exact ground state of \mathcal{H}_p —which for most interesting optimization problems is written in the form of single- and multispin σ_i^z terms that describe high-order polynomial unconstrained binary optimization (PUBO) problems with k -local interactions—generally requires adiabaticity, and the time necessary to satisfy this condition grows exponentially as a function of N if the energy gap between the ground state and the first-excited state closes exponentially, which is the case in most of the interesting combinatorial optimization problems [10].

To overcome this bottleneck, one can implement a so-called counter-diabatic Hamiltonian $\mathcal{H}_{CD}(t)$ to suppress transitions between the system eigenstates. The full Hamiltonian then reads

$$\mathcal{H}(t) = \mathcal{H}_0(t) + \mathcal{H}_{CD}(t), \quad (3)$$

where $\mathcal{H}_{CD}(t) = \dot{\lambda}(t)\mathcal{A}_\lambda(t)$ is the additional counter-diabatic Hamiltonian, and $\mathcal{A}_\lambda(t) = i\hbar U^\dagger(t)\partial_\lambda U(t)$ with

$$U(t) = \mathcal{T} \exp \left[-\frac{i}{\hbar} \int_0^t \mathcal{H}_0(t') dt' \right] \quad (4)$$

is the exact time-dependent adiabatic gauge potential [25,26,28] with respect to the driving function $\lambda(t)$ of Eq. (2) and $\dot{\lambda}(t)$ its time derivative.

Finding the exact adiabatic gauge potential is a challenging task and generally requires *a priori* knowledge of the system eigenstates for the whole annealing time as can be seen from the above expression of $\mathcal{A}_\lambda(t)$ [17], which is impossible in practice. To overcome this difficulty, one can employ an approximate adiabatic gauge potential, denoted with a prime as $\mathcal{A}'_\lambda(t)$ (not to be confused with the derivative), which includes only local single-spin terms involving $\{\sigma_i^y\}_i$ and which adds a new degree of freedom to the system [25]. We note here that in the case of the original Hamiltonian $\mathcal{H}_0(t)$, given by Eq. (2), with driver Hamiltonian \mathcal{H}_d , given by Eq. (1), and problem Hamiltonian \mathcal{H}_p including σ^z terms, additional $\{\sigma_i^x\}_i$ and $\{\sigma_i^z\}_i$ operators do not yield further improvement (see Appendix B for the example of the Landau-Zener model for more details).

Following the variational principle of Ref. [25], one finds the best possible approximate adiabatic gauge potential by defining a Hermitian operator $G_\lambda(\mathcal{A}_\lambda) \equiv \partial_\lambda \mathcal{H}_0 + i[\mathcal{A}_\lambda, \mathcal{H}_0]$ and minimizing the operator distance

$$\mathcal{D}^2(\mathcal{A}'_\lambda) = \text{Tr} \{ [G_\lambda(\mathcal{A}_\lambda) - G_\lambda(\mathcal{A}'_\lambda)]^2 \} \quad (5)$$

between the exact, \mathcal{A}_λ , and approximate, \mathcal{A}'_λ , adiabatic gauge potentials with respect to the parameters in \mathcal{A}'_λ . This is equivalent to minimizing the action $\mathcal{S}(\mathcal{A}'_\lambda) = \text{Tr} [G_\lambda^2(\mathcal{A}'_\lambda)]$ with respect to its parameters, symbolically written as $\delta \mathcal{S}(\mathcal{A}'_\lambda) / \delta \mathcal{A}'_\lambda = 0$, as detailed in Refs. [25,26,28] and Appendix A. In this general approach, the driver \mathcal{H}_d and problem Hamiltonian \mathcal{H}_p are kept intact.

Now, we notice that the time-dependent coefficients of the two terms in the Hamiltonian $\mathcal{H}_0(t)$, given by Eq. (2), can be chosen independently—not necessarily in a single-parameter form as in Eq. (2)—as long as the initial Hamiltonian is \mathcal{H}_d and the final Hamiltonian is \mathcal{H}_p . We take advantage of this degree of freedom and choose to write these coefficients using

two time-dependent parameters $\lambda(t)$ and $\gamma(t)$ as

$$\mathcal{H}_0^{\lambda,\gamma}(t) = -[1 - \lambda(t)]\gamma(t) \sum_{i=1}^N \sigma_i^x + \lambda(t)\mathcal{H}_p, \quad (6)$$

where $\lambda(t)$ satisfies the same boundary conditions as before, $\lambda(0) = 0$ and $\lambda(\tau) = 1$, and $\gamma(t)$ is an arbitrary function satisfying $\gamma(0) \neq 0$ and which generalizes the form of γ in Eq. (1). Since we have an additional function $\gamma(t)$, it is natural to introduce a corresponding additional adiabatic gauge potential \mathcal{A}_γ . We therefore employ the approximate local two-parameter CD Hamiltonian,

$$\mathcal{H}_{\text{CD}}^{\lambda,\gamma}(t) = \dot{\lambda}(t)\mathcal{A}'_\lambda(t) + \dot{\gamma}(t)\mathcal{A}'_\gamma(t), \quad (7)$$

where $\mathcal{A}'_\gamma(t)$ is also a linear combination of σ_i^y but with a different coefficient than in $\mathcal{A}'_\lambda(t)$.

One may wonder if the same linear combination of σ_i^y operators as in $\mathcal{A}'_\lambda(t)$ with just a different coefficient would lead to different results. As we will see in the next section, it indeed leads to an improvement of the annealing performance in several measures, thanks to the enhanced space of search for variational optimization of the coefficients as functions of time. See, also, Appendix D.

As shown in Appendix A, finding the optimal coefficients in the two adiabatic gauge potentials \mathcal{A}'_λ and \mathcal{A}'_γ is equivalent to minimizing the two-parameter action,

$$\mathcal{S} = \text{Tr}[G_\lambda^2(\mathcal{A}'_\lambda)] + \text{Tr}[G_\gamma^2(\mathcal{A}'_\gamma)], \quad (8)$$

with respect to the parameters in the two adiabatic gauge potentials \mathcal{A}'_λ and \mathcal{A}'_γ , i.e.,

$$\frac{\delta \mathcal{S}}{\delta \mathcal{A}'_\lambda} = 0, \quad \frac{\delta \mathcal{S}}{\delta \mathcal{A}'_\gamma} = 0, \quad (9)$$

where $G_\gamma(\mathcal{A}'_\gamma) \equiv \partial_\gamma \mathcal{H}_0 + i[\mathcal{A}'_\gamma, \mathcal{H}_0]$ is the additional Hermitian operator with respect to $\gamma(t)$.

As we will see later, the introduction of an additional time dependence for the transverse magnetic field strength, $\gamma(t)$, and thus the emergence of the additional adiabatic gauge potential $\mathcal{A}'_\gamma(t)$ has significant consequences for local CD driving. The operator distance and thus the corresponding action, given by Eq. (8), can be algebraically determined for a given set of two functions $\lambda(t)$ and $\gamma(t)$. A detailed derivation of Eqs. (7) and (8) can be found in Appendix A and its application on the easy single-body Landau-Zener model in Appendix B.

Although it is desirable to find the best possible functional forms of $\lambda(t)$ and $\gamma(t)$, this poses an additional complex step of functional optimization, about which we do not have a clear principle to rely upon. Indeed, existing studies adopt simple functions satisfying boundary conditions without elaborating on further optimization of functional forms [25,26,28]. We follow this tradition and work with simple conventional forms of those functions, as illustrated in the next section, and delegate the optimization of those functions to a future project. See Appendix D for additional information.

p-spin model

Our method can be applied to any problem Hamiltonian \mathcal{H}_p . In the present paper, we test our approach by using the

p-spin model with $p = 3$ as the problem Hamiltonian since it is a hard problem for traditional quantum annealing due to a first-order quantum phase transition, though the final ground state is trivially known to be ferromagnetic [32–36]. Another advantage of the *p*-spin model is that the total spin quantum number is conserved, which can also be stated as that the Hamiltonian is invariant under an arbitrary permutation of site indices. This fact makes it possible to study very large system sizes numerically by restricting ourselves to the subspace of a fixed spin quantum number corresponding to the ground state, as we shall see in the next section.

The total Hamiltonian of interest reads

$$\mathcal{H}_0^{\lambda,\gamma}(t) = -[1 - \lambda(t)]\gamma(t) \sum_{i=1}^N \sigma_i^x - \lambda(t)N \left(\frac{1}{N} \sum_{i=1}^N \sigma_i^z \right)^3. \quad (10)$$

This Hamiltonian fulfills the commutation relation

$$[\mathcal{H}_0^{\lambda,\gamma}(t), \mathbf{S}_{\text{total}}^2] = 0, \quad (11)$$

where $\mathbf{S}_{\text{total}} = (S_{\text{total}}^x, S_{\text{total}}^y, S_{\text{total}}^z)$ is the total spin quantum number with $S_{\text{total}}^x = (1/2) \sum_{i=1}^N \sigma_i^x$, and similarly for the *y* and *z* components. Since the initial condition is that the ground state of \mathcal{H}_d of Eq. (1) is an eigenstate of $\mathbf{S}_{\text{total}}^2$ with largest eigenvalue, we can restrict our numerical computations to the space of this eigenvalue, which greatly reduces the dimension of the Hilbert space to be explored numerically from exponential to linear in *N*.

Throughout this work, we will use the driving functions

$$\lambda(t) = \sin^2 \left[\frac{\pi}{2} \sin^2 \left(\frac{\pi t}{2\tau} \right) \right], \quad \gamma(t) = \gamma_{\text{init}} + \lambda(t), \quad (12)$$

where we have chosen the function $\lambda(t)$ following Ref. [25]. The above form of $\gamma(t)$ is chosen arbitrarily and its deeper investigation is a future task as mentioned before. We note here that $\gamma(t)$ can generally take a most generic form as long as $\gamma(t) \neq 0$ and does not necessarily need to include $\lambda(t)$. We have checked numerically that small variations of the value of γ_{init} do not lead to noticeable changes of the results.

Since any local adiabatic gauge potential is a linear combination of σ_i^y (cf. Appendix B), we write, for the latter,

$$\mathcal{A}'_\lambda = \sum_{i=1}^N \alpha \sigma_i^y, \quad \mathcal{A}'_\gamma = \sum_{i=1}^N \beta \sigma_i^y. \quad (13)$$

We choose α and β to be site independent, reflecting the permutation symmetry of the *p*-spin Hamiltonian of Eq. (10). These coefficients can generally be chosen to depend on the site index *i* for problems without such symmetries.

Minimizing the corresponding action \mathcal{S} , given by Eq. (8), with respect to the coefficients α and β , as detailed in Appendix C, leads to their optimal algebraic solutions and thus the CD Hamiltonian, given by Eq. (7), as

$$\begin{aligned} \mathcal{H}_{\text{CD}}^{\lambda,\gamma}(t) &= \sum_{i=1}^N (\dot{\lambda}\alpha + \dot{\gamma}\beta) \sigma_i^y, \\ \alpha &= -\kappa\gamma, \quad \beta = \kappa(1 - \lambda)\lambda, \\ \kappa &= \frac{1}{2} \frac{N^2(3N - 2)}{(1 - \lambda)^2\gamma^2 N^4 + \lambda^2(27N^2 - 66N + 40)}. \end{aligned} \quad (14)$$

It is noticed that κ is proportional to $1/N$ for large N and thus the CD Hamiltonian $\mathcal{H}_{\text{CD}}^{\lambda,\gamma}(t)$ becomes small for very large N [39]. We therefore expect that the effect of the adiabatic gauge potentials is seen most prominently for relatively small to moderate N . This also means that as long as the p -spin model is concerned, the present method does not lead to a drastic scaling advantage that reduces the asymptotic computational complexity from exponential to polynomial in the limit of very large N , although significant improvements will be observed numerically even for moderately large N , as we will see in the next section.

The corresponding full Hamiltonian then reads

$$\mathcal{H}^{\lambda,\gamma}(t) = \mathcal{H}_0^{\lambda,\gamma}(t) + \sum_{i=1}^N (\dot{\lambda}\alpha + \dot{\gamma}\beta)\sigma_i^y, \quad (15)$$

with the solutions α and β , given by Eq. (14), and $\dot{\lambda}$ and $\dot{\gamma}$ the time derivatives of Eq. (12).

To facilitate experimental implementation, we eliminate the σ_i^y terms by rotating this full Hamiltonian around the z axis in spin space, i.e., applying the unitary gauge transformation

$$U_g(t) = \exp\left[i\frac{\theta(t)}{2}\sum_i\sigma_i^z\right] \quad (16)$$

over the angle $\theta(t) = \arctan(Y/X)$, with $X = -(1-\lambda)\gamma$ and $Y = \dot{\lambda}\alpha + \dot{\gamma}\beta$. The resulting effective Hamiltonian in the laboratory frame then has the form

$$\begin{aligned} \mathcal{H}_{\text{eff}}^{\lambda,\gamma}(t) = & \sum_{i=1}^N \sqrt{X^2 + Y^2}\sigma_i^x - \lambda(t)\frac{6}{N^2} \sum_{i<j<k}^N \sigma_i^z\sigma_j^z\sigma_k^z \\ & - \sum_{i=1}^N \left[\frac{1}{2} \frac{XY - Y\dot{X}}{X^2 + Y^2} + \lambda(t)\frac{3N-2}{N^2} \right] \sigma_i^z \end{aligned} \quad (17)$$

(see Appendix C and Ref. [25] for additional details). This Hamiltonian consists only of σ_i^x and σ_i^z terms, which makes it more feasible for experimental realization than Eq. (15) with σ_i^y .

III. NUMERICAL VERIFICATION

We next present numerical results of our method for the p -spin model with $p = 3$. To this end, we compute the final ground-state fidelity $F(\tau) = |\langle\psi(\tau)|\phi_0\rangle|^2$, with $|\psi(\tau)\rangle$ and $|\phi_0\rangle$ the states at the end of annealing and the true ground state of the problem Hamiltonian, respectively, and residual energy $\Delta E = E(\tau) - E_0$, with $E(\tau)$ and E_0 being the energy at the end of annealing and the true ground-state energy, respectively. We compare three protocols: (i) traditional quantum annealing with the original Hamiltonian [$\mathcal{H}_0^{\lambda,\gamma}(t)$, Eq. (10)], (ii) the existing method with single-parameter CD Hamiltonian [Eq. (17) with $\gamma(t) = \gamma_{\text{init}}$ and thus $\beta = 0$], and (iii) two-parameter CD Hamiltonian [$\mathcal{H}_{\text{eff}}^{\lambda,\gamma}(t)$, Eq. (17)]. We test a wide range of annealing times τ from 10^{-1} to 10^5 and different system sizes up to $N = 100$ by exploiting the spin symmetry of the problem.

We numerically solved the Schrödinger equation for the Hamiltonian dynamics and computed the fidelity, residual energy, and the time-to-solution, which is a measure of the

effective annealing time to reach the solution of the optimization problem with probability p_r [40], i.e.,

$$\text{TTS}(\tau) = \begin{cases} \tau \frac{\ln(1-p_r)}{\ln[1-F(\tau)]} & \text{for } F(\tau) < 1 \\ \tau & \text{for } F(\tau) = 1, \end{cases} \quad (18)$$

where we have set $p_r = 0.99$ as the success probability threshold. For our numerical computations, we used QUTIP 4.5 [41].

A. Dependence on annealing time

Figure 1 depicts the final ground-state fidelity $F(\tau)$ [Figs. 1(a)–1(c)] and residual energy ΔE [Figs. 1(d)–1(f)] as functions of annealing time τ for system sizes $N = 4$ [Figs. 1(a) and 1(d)], $N = 30$ [Figs. 1(b) and 1(e)], and $N = 50$ [Figs. 1(c) and 1(f)].

For the original Hamiltonian without the CD term [$\mathcal{H}_0(t)$, Eq. (10); diamond with blue solid line in the figure], we see that the final state is far away from the ground state for short annealing time τ [green-shaded areas, where $F(\tau) \approx 1/2^N$ for $\mathcal{H}_0(t)$] and reach the final ground state in the adiabatic regime [gray-shaded areas, where $F(\tau) > 0.99$] for very long annealing time.

The existing method of a single-parameter CD driven Hamiltonian [Eq. (14) with $\gamma(t) = \gamma_{\text{init}}$ and thus $\beta = 0$; square, orange dashed line] reaches a considerably higher final ground-state fidelity and lower residual energy, respectively, especially for short annealing time (green-shaded areas), yet approaches their original counterpart for longer annealing time (yellow-shaded areas) due to the fact that $\dot{\lambda} \propto 1/\tau$ [cf. Eq. (12)]. Consequently, the counter-diabatic Hamiltonian $\mathcal{H}_{\text{CD}}^{\lambda,\gamma}(t)$ naturally converges towards zero for longer annealing time, in particular in the adiabatic limit (gray-shaded areas), and thus does not yield any further speedup.

On the other hand, for the two-parameter CD driven Hamiltonian [$\mathcal{H}_{\text{CD}}^{\lambda,\gamma}(t)$, Eq. (17), where $\gamma(t) = \gamma_{\text{init}} + \lambda(t)$; circle, green dash-dotted line], it is observed that we reach considerably higher final ground-state fidelity and lower residual energy compared to traditional quantum annealing (QA) and single-parameter CD driving for the long annealing time regime (yellow-shaded areas). This is important since the asymptotic adiabatic regime (gray-shaded areas) starts at later times for larger system sizes, as seen in Fig. 1(c), meaning that the system performance in the long-, but not yet adiabatic, time regime (yellow-shaded areas) becomes more and more vital for larger systems. In other words, for the two-parameter CD driven Hamiltonian, we come closer to the adiabatic regime more quickly, thus performing much better (around an order of magnitude reduction in annealing time to reach the same values of fidelity and residual energy) compared to its traditional quantum annealing and single-parameter CD driving counterparts. Although the last term in Eq. (15) with $\dot{\gamma}\beta$ may superficially seem not to add a new element to the single-parameter method just with $\dot{\lambda}\alpha$, the present numerical results clearly indicate that our two-parameter method leads to significant advantages in the intermediate-time region (yellow-shaded region in Fig. 1). This time region is important in practice because, first, the gray-shaded adiabatic region is often hard to reach for very large systems, and, second, the

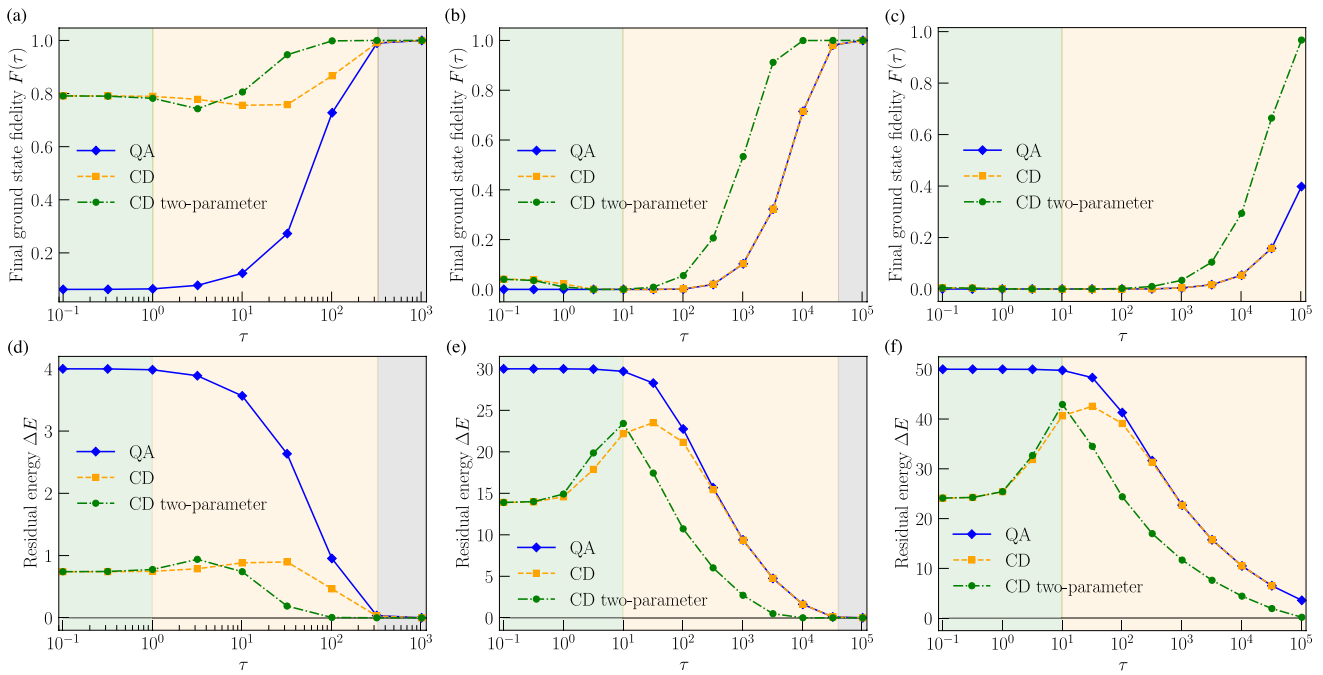


FIG. 1. Ground-state fidelity and residual energy. (a)–(c) Final ground-state fidelity and (d)–(f) residual energy for (i) traditional quantum annealing (diamonds, blue solid line), (ii) single-parameter CD drive (squares, orange dashed line), and (iii) two-parameter CD drive (circles, green dash-dotted line) as functions of annealing time τ . The system sizes are (a),(d) $N = 4$, (b),(e) $N = 30$, and (c),(f) $N = 50$, where $\gamma_{\text{init}} = 0.1$ for all panels. Time ranges are color coded as follows: short-time regime (green-shaded areas) where the fidelity is approximately $1/2^N$ for traditional quantum annealing, long-time regime (yellow-shaded areas) where transient behavior is observed and the two-parameter CD drive shows a clear advantage, and adiabatic regime (gray-shaded areas) where $F(\tau) > 0.99$.

green-shaded short-time region has large residual energy and low fidelity.

B. Time-to-solution

We further studied the time-to-solution, a central measure of annealing time necessary to reach the solution of the optimization problem of interest with a certain high success probability, for different system sizes N . Figures 2(a) and 2(b) depict the time-to-solution $\text{TTS}(\tau)$, given by Eq. (18), for fixed system sizes $N = 20$ and $N = 100$, respectively. It is observed that the minimal time-to-solution is located at the shortest annealing time that we studied, i.e., $\tau = 10^{-1}$, except for the case of traditional quantum annealing. We did not study even shorter time ranges because the time derivative of $\lambda(t)$, given by Eq. (12), becomes anomalous for very small τ and also experimental implementation may be difficult for too short annealing time. We further found a local minimum of $\text{TTS}(\tau)$ at a longer time, $\tau \approx 10^3$.

Figure 2(c) depicts the system size dependence of the minimal time-to-solution at the shortest annealing time that we studied, $\tau = 10^{-1}$. We see that the existing single-parameter CD method and our two-parameter method have a scaling advantage over traditional quantum annealing in the sense that the slope is smaller, i.e., a smaller constant in the exponent. Figure 2(d) depicts the time-to-solution at the local minimum $\tau \approx 10^3$ as a function of the system size. Our two-parameter approach has the same scaling behavior (the same slope) as the other two methods, but depicts a constant speedup of the order of around 10. The same scaling behavior for large N

is not very surprising because the adiabatic gauge potentials \mathcal{A}'_x and \mathcal{A}'_y are proportional to $1/N$ and will consequently disappear for increasing system sizes. We notice here that this asymptotic vanishing of the adiabatic gauge potentials is a special property of the p -spin model, and the advantage of the present method is expected to remain finite for large system size and large annealing time in other models, for which we have preliminary analytical and numerical evidence. The comparison of Figs. 2(c) and 2(d) reveals that it is more advantageous to repeat very short annealing processes many times than to run a single long annealing, at least in the present problem.

Our preliminary data for a few other problem Hamiltonians indicate the possibility that the absolute minimum at the shortest annealing time may be a finite-size effect and seems to vanish for large system sizes and, in particular, in the thermodynamic limit. If this proves to be true, the p -spin model is peculiar in the sense that finite-size effects persist even for system sizes as large as $N = 100$. Whether or not this behavior is shared by other problem Hamiltonians is an interesting future topic of research.

C. Behavior of coefficients

Figure 3(a) depicts the time dependence of the coefficient of each term of the full Hamiltonian $\mathcal{H}_{\text{eff}}^{\lambda,\gamma}(t)$, given by Eq. (17), in the rotated frame, i.e.,

$$\mathcal{H}_x(t) = \sum_{i=1}^N \sqrt{X^2 + Y^2} \sigma_i^x, \quad (19)$$

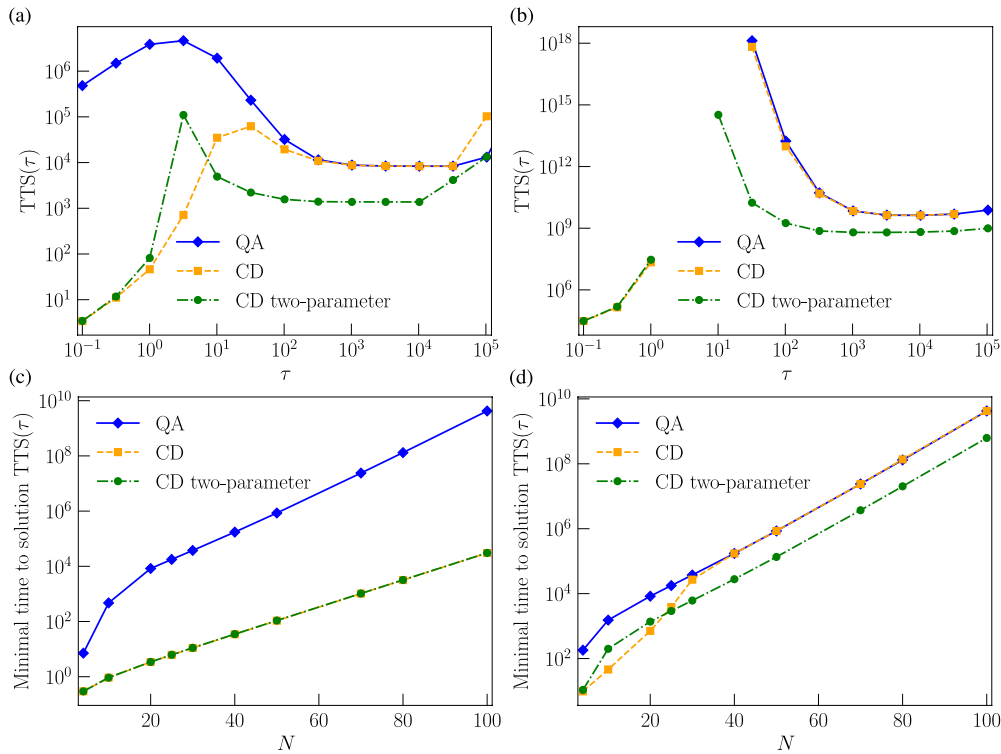


FIG. 2. Time-to-solution. Time-to-solution $TTS(\tau)$ for (i) traditional quantum annealing (diamonds, blue solid line), (ii) single-parameter CD drive (squares, orange dashed line), and (iii) two-parameter CD drive (circles, green dash-dotted line) for (a) $N = 20$ and (b) $N = 100$. For the latter, the data between $\tau = 1$ to about 10 are not shown because the values are too large to achieve reasonable numerical precision. Minimal time-to-solution for (c) short-time region ($\tau \lesssim 1$) and (d) long-time region ($\tau \gtrsim 10$). Other parameters are the same as in Fig. 1.

$$\mathcal{H}_{zzz}(t) = -\lambda(t) \frac{6}{N^2} \sum_{i < j < k} \sigma_i^z \sigma_j^z \sigma_k^z, \quad (20)$$

$$\mathcal{H}_z(t) = -\sum_{i=1}^N \left[\frac{1}{2} \frac{X\dot{Y} - \dot{X}Y}{X^2 + Y^2} + \lambda(t) \frac{3N-2}{N^2} \right] \sigma_i^z, \quad (21)$$

for annealing time $\tau = 10$, system size $N = 30$, and other parameters as in Fig. 1. Figure 3(b) depicts the coefficients of the adiabatic gauge potentials $\mathcal{A}'_\lambda(t)$ and $\mathcal{A}'_Y(t)$ and the corresponding coefficients $\alpha(t)$ and $\beta(t)$, given by Eq. (14), in the inset. The maximal corresponding strengths of the additional magnetic field in the y direction in the original frame [Fig. 3(b)] and in the rotated frame [reflected in the coefficients of $\mathcal{H}_x(t)$ and $\mathcal{H}_z(t)$ in Fig. 3(a)] are not (overwhelmingly) larger than the original parameters in $\mathcal{H}_{zzz}(t)$ for this annealing time regime, which makes this approach attractive for experimental realization.

D. Energy spectrum of two-parameter CD drive

It is useful to see how the wave function is spread over the instantaneous eigenstates of the rotated full Hamiltonian, given by Eq. (17), during the present two-parameter CD drive in the laboratory frame.

Figure 4 depicts the occupation probability of each instantaneous eigenstate, expressed by the thickness of the red lines, for a system size $N = 30$ and annealing time $\tau = 300$, corresponding to Figs. 1(b) and 1(e), where the two-parameter

CD drive shows a clear advantage over traditional quantum annealing and the existing method of single-parameter CD driving. We observe that Figs. 4(a) and 4(b) share a very similar eigenspectrum, and the wave function is spread over many excited states after $t/\tau \approx 0.3$ via a cascade of avoided level crossings. In contrast, in the two-parameter CD case [Fig. 4(c)] the structure of the eigenspectrum has significantly changed and the system is driven downward in the spectrum around $t/\tau \approx 0.3$, which results in the high occupation probabilities in low-energy eigenstates in the end of the annealing process. We emphasize that such an ingenious protocol has emerged naturally from the two-parameter variational approach to suppress undesirable diabatic transitions observed in Figs. 4(a) and 4(b).

IV. DISCUSSION AND CONCLUSION

We have proposed and tested a method to find an efficient local CD Hamiltonian that outperforms its traditional quantum annealing and single-parameter approximate CD counterparts with respect to enhanced final ground-state fidelity and reduced residual energy as well as time-to-solution. The method introduces an additional term in the adiabatic gauge potential by taking advantage of the degree of freedom of choosing a time-dependent transverse magnetic field strength. This two-parameter local CD approach generalizes the existing method of single-parameter CD driving by expanding the search space of optimal parameters by introducing a second controllable driving function $\gamma(t)$. The

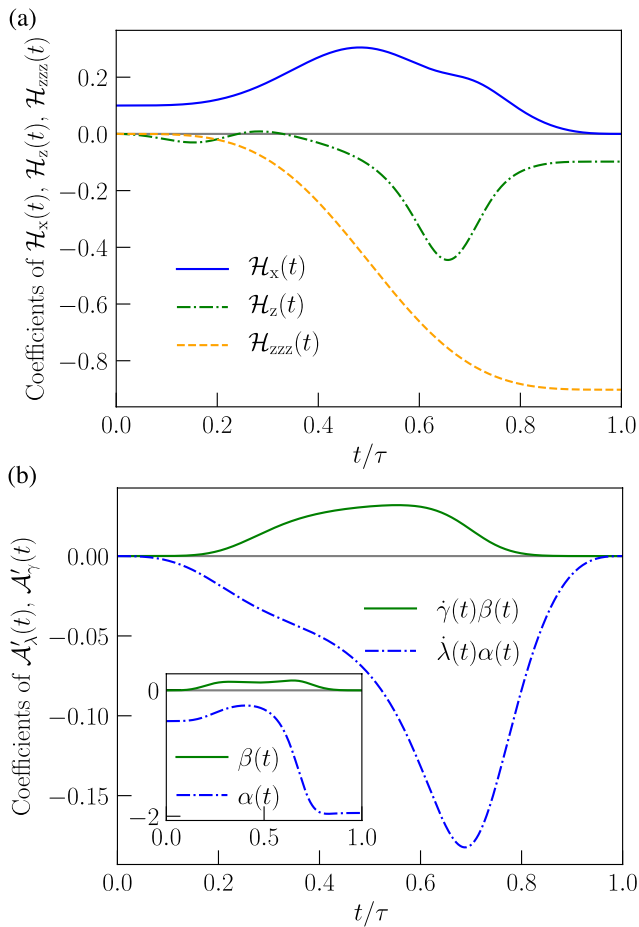


FIG. 3. Coefficients of two-parameter CD Hamiltonian. (a) Time dependence of coefficients of terms of the Hamiltonian as described in the text, $\mathcal{H}_x(t)$ (upper blue solid line), $\mathcal{H}_z(t)$ (middle green dash-dotted line), and $\mathcal{H}_{zzz}(t)$ (lower orange dashed line), the last one being scaled by N to fairly compare coefficients of extensive operator terms. (b) Time dependence of the coefficients of the adiabatic gauge potentials $\mathcal{A}_x'(t)$ (lower blue dash-dotted line) and $\mathcal{A}_y'(t)$ (upper green solid line). Inset depicts the corresponding coefficients $\alpha(t)$ and $\beta(t)$ under the two-parameter CD drive with $\gamma(t) = 0.1 + \lambda(t)$, annealing time $\tau = 10$, and system size $N = 30$. Other parameters are the same as in Fig. 1.

corresponding CD Hamiltonian in this approach is local and can be expressed, after a rotation in spin space, just in terms of the usual transverse-field Ising model but with unconventional diabatic control of the magnetic field strengths. For the goal of performance improvement, the latter may thus be implemented in current quantum annealing devices on various platforms considerably more easily than other approaches, which introduce more involved terms into the Hamiltonian such as two-body $\sigma_i^x \sigma_j^x$ interactions.

We have tested the idea using the p -spin model with $p = 3$ because it is possible to simulate the Schrödinger dynamics numerically for very large system sizes for this model due to its special symmetry of conserved total quantum spin number. We have derived the algebraic expression of the two-parameter CD Hamiltonian and numerically demonstrated a considerable increase in final ground-state fidelity and reduc-

tion in residual energy as well as time-to-solution compared to traditional quantum annealing and the single-parameter CD Hamiltonian approach. We further demonstrated a scaling advantage of time-to-solution of the approximate single- and two-parameter CD methods in the short-time region, and a constant speedup of the two-parameter method in the long-time region. The division of annealing processes in short-time and long-time regions has important numerical and operational consequences. Whereas the time-to-solution in the short-time region depicts a global minimum, the experimental realization of the strongly increasing additional magnet fields in this time region constitutes a severe hindrance for practical purposes. The local minimum of time-to-solution in the long-time region serves as a promising regime for experimental implementation since the additional magnetic fields are not (considerably) larger than their original analogs. The lack of scaling advantage in the long-time region may originate in the $1/N$ scaling of the coefficients of the CD Hamiltonian for the p -spin model, which is a special property of this many-body mean-field-like problem. We may expect an even better scaling behavior in many other problems where those coefficients of the CD Hamiltonian generally stay finite in the large- N limit. Even when a clear scaling advantage is not achieved, the present method becomes useful at least for a quantitative improvement as exemplified in the p -spin model. In particular, our method may be realized in an improvement of existing annealing devices by a better control of system parameters of the transverse-field Ising model only. We note that the method can also be applied in the case of additional random longitudinal magnetic fields where site-dependent optimal algebraic solutions for the coefficients of the adiabatic gauge potentials can be easily found. As a consequence, it does not need further additional terms to be realized experimentally and is versatile to be applicable to any problem, in contrast to other approaches such as nonstochastic catalysts [33–36] and inhomogeneous field driving [37,42,43], in which one should determine in advance if the idea works in a given problem and, if it does, should find a proper way to meticulously control the system parameters, which is in general highly nontrivial for a generic optimization problem.

We have also illustrated how the two-parameter CD Hamiltonian resolves the problem of excitation to higher-energy states by showing the modification of the energy eigenspectrum that eliminates a cascade of avoided level crossings toward higher-energy states. It is an interesting future problem to identify problems in which this mechanism leads to a clear scaling advantage even for very large system sizes. Such examples may well exist because of the special disadvantageous property of the p -spin model as described above, i.e., that the coefficients of the CD Hamiltonian tends to vanish for larger system size.

We note that there exist other approaches to optimize the time dependence of coefficients in quantum annealing, e.g., from the viewpoint of optimal control theory and related ideas often under the context of the quantum approximate optimization algorithm [29,44–46] (see, also, Ref. [47] for a related idea of inverse engineering). It is not clear *a priori* whether or not our two-parameter CD Hamiltonian is better in comparison with these approaches since the criteria of optimality are different. The comparison in terms of relevant physical

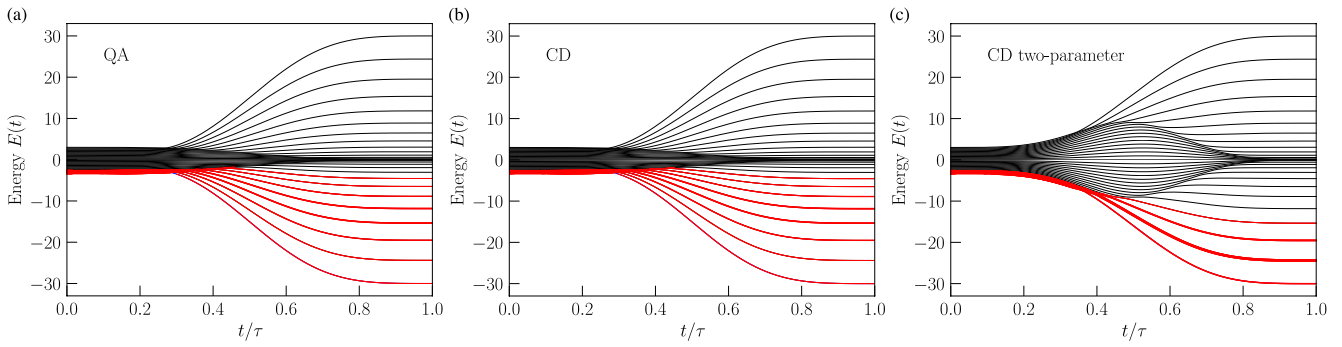


FIG. 4. Energy spectrum. Instantaneous energy spectrum $E(t)$ for (a) traditional quantum annealing, (b) single-parameter CD driving, and (c) two-parameter CD driving for system size $N = 30$, annealing time $\tau = 300$, and $\gamma_{\text{mit}} = 0.1$. Thickness of red curves indicates the occupation probability of each eigenstate in the dynamical processes of the three annealing protocols. Higher excited states have a negligibly small occupation probability and thus the corresponding very thin red lines cannot be seen.

quantities such as fidelity, residual energy, and the time-to-solution will be the best way to measure the performance of different protocols. It can happen that one is better than the other in some problems and the reverse in other problems, which reveals an interesting future topic to be studied.

ACKNOWLEDGMENTS

We thank Kazutaka Tahakashi for useful comments. This work was supported by the Austrian Science Fund (FWF) through a START grant under Project No. Y1067-N27 and the SFB BeyondC Project No. F7108-N38, the Hauser-Raspe Foundation, and the European Union's Horizon 2020 research and innovation program under Grant Agreement No. 817482. This material is based upon work supported by the Defense Advanced Research Projects Agency (DARPA) under Contract No. HR001120C0068. Any opinions, findings, and conclusions or recommendations expressed in this material are those of the author(s) and do not necessarily reflect the views of DARPA. The research is also based upon work partially supported by the Office of the Director of National Intelligence (ODNI), Intelligence Advanced Research Projects Activity (IARPA), and the Defense Advanced Research Projects Agency (DARPA), via the U.S. Army Research Office Contract No. W911NF-17-C-0050. The views and conclusions contained herein are those of the authors and should not be interpreted as necessarily representing the official policies or endorsements, either expressed or implied, of the ODNI, IARPA, DARPA, or the U.S. Government. The U.S. Government is authorized to reproduce and distribute reprints for Governmental purposes notwithstanding any copyright annotation thereon.

APPENDIX A: DERIVATION OF ADIABATIC GAUGE POTENTIALS

In this Appendix, we derive the two adiabatic gauge potentials \mathcal{A}_λ and \mathcal{A}_γ by considering a quantum state $|\psi\rangle$ evolving under the time-dependent Hamiltonian $\mathcal{H}_0^{\lambda,\gamma}(t)$.

The effective Schrödinger equation $i\partial_t|\psi\rangle = \mathcal{H}_0^{\lambda,\gamma}|\psi\rangle$ in the moving frame by applying the unitary transformation $U = U(\lambda, \gamma)$ with $|\psi(t)\rangle = U^\dagger|\psi\rangle$, and thus $|\psi\rangle = U|\psi(t)\rangle$,

is written as

$$\begin{aligned} i\partial_t[U|\psi(t)\rangle] &= \mathcal{H}_0^{\lambda,\gamma}[U|\psi(t)\rangle], \\ i(\partial_\lambda U \dot{\lambda} + \partial_\gamma U \dot{\gamma})|\psi(t)\rangle + iU\partial_t|\psi(t)\rangle &= \mathcal{H}_0^{\lambda,\gamma}U|\psi(t)\rangle. \end{aligned} \quad (\text{A1})$$

If we apply U^\dagger from the left, we have

$$\begin{aligned} i(U^\dagger\partial_\lambda U \dot{\lambda} + U^\dagger\partial_\gamma U \dot{\gamma})|\psi(t)\rangle + iU^\dagger U\partial_t|\psi(t)\rangle \\ = U^\dagger\mathcal{H}_0^{\lambda,\gamma}U|\psi(t)\rangle, \end{aligned} \quad (\text{A2})$$

and, consequently,

$$i\partial_t|\psi(t)\rangle = \tilde{\mathcal{H}}_0^{\lambda,\gamma}|\psi(t)\rangle - i(U^\dagger\partial_\lambda U \dot{\lambda} + U^\dagger\partial_\gamma U \dot{\gamma})|\psi(t)\rangle, \quad (\text{A3})$$

which we write as

$$i\partial_t|\psi(t)\rangle = \tilde{\mathcal{H}}_0^{\lambda,\gamma}|\psi(t)\rangle - (\dot{\lambda}\tilde{\mathcal{A}}_\lambda + \dot{\gamma}\tilde{\mathcal{A}}_\gamma)|\psi(t)\rangle, \quad (\text{A4})$$

where $\tilde{\mathcal{H}}_0^{\lambda,\gamma}(\lambda, \gamma) = U^\dagger\mathcal{H}_0^{\lambda,\gamma}U$ is diagonal in its instantaneous eigenbasis, and $\tilde{\mathcal{A}}_\lambda = iU^\dagger\partial_\lambda U$ and $\tilde{\mathcal{A}}_\gamma = iU^\dagger\partial_\gamma U$ are the corresponding adiabatic gauge potentials in the moving frame with respect to the two time-dependent driving parameters $\lambda(t)$ and $\gamma(t)$, respectively.

The counter-diabatic Hamiltonian with respect to these two adiabatic gauge potentials that suppresses any transitions between the eigenstates back in the laboratory frame can consequently be written as

$$\mathcal{H}_{\text{CD}}^{\lambda,\gamma}(t) = \dot{\lambda}(t)\mathcal{A}_\lambda(t) + \dot{\gamma}(t)\mathcal{A}_\gamma(t). \quad (\text{A5})$$

It is straightforward to verify that the two adiabatic gauge potentials fulfill the relations

$$[\mathcal{A}_\lambda, \mathcal{H}_0^{\lambda,\gamma}] = i\partial_\lambda\mathcal{H}_0^{\lambda,\gamma} + i\mathcal{M}_\lambda, \quad [\mathcal{A}_\gamma, \mathcal{H}_0^{\lambda,\gamma}] = i\partial_\gamma\mathcal{H}_0^{\lambda,\gamma} + i\mathcal{M}_\gamma, \quad (\text{A6})$$

where the operators $\mathcal{M}_\lambda = -\sum_n|n\rangle\langle n|\partial_\lambda\mathcal{H}_0^{\lambda,\gamma}|n\rangle\langle n|$ and $\mathcal{M}_\gamma = -\sum_n|n\rangle\langle n|\partial_\gamma\mathcal{H}_0^{\lambda,\gamma}|n\rangle\langle n|$ are diagonal in the instantaneous eigenbasis $|n(\lambda, \gamma)\rangle$. As $[\mathcal{H}_0^{\lambda,\gamma}, i\mathcal{M}_\lambda] = [\mathcal{H}_0^{\lambda,\gamma}, i\mathcal{M}_\gamma] = 0$ and thus commute, we can rewrite the conditions, given by Eq. (A6), as

$$\begin{aligned} [\mathcal{H}_0^{\lambda,\gamma}, [\mathcal{A}_\lambda, \mathcal{H}_0^{\lambda,\gamma}] - i\partial_\lambda\mathcal{H}_0^{\lambda,\gamma}] &= 0, \\ [\mathcal{H}_0^{\lambda,\gamma}, [\mathcal{A}_\gamma, \mathcal{H}_0^{\lambda,\gamma}] - i\partial_\gamma\mathcal{H}_0^{\lambda,\gamma}] &= 0. \end{aligned} \quad (\text{A7})$$

The exact solution for the adiabatic gauge potentials \mathcal{A}_λ and \mathcal{A}_γ generally requires *a priori* knowledge of the system eigenstates, i.e., \mathcal{M}_λ and \mathcal{M}_γ , during the whole annealing time through $|n\rangle = |n[\lambda(t), \gamma(t)]\rangle$. To generate the latter, \mathcal{A}_λ and \mathcal{A}_γ have complicated many-body interacting terms of all combinations of the operators σ_i^x , σ_i^y , and σ_i^z up to complicated nonlocal N -spin terms (cf. Ref. [49] in the case of quantum criticality).

To circumvent this difficulty, we follow Ref. [25] and define the Hermitian operators $G_\lambda(\mathcal{A}'_\lambda) \equiv \partial_\lambda \mathcal{H}_0^{\lambda,\gamma} + i[\mathcal{A}'_\lambda, \mathcal{H}_0^{\lambda,\gamma}]$ and $G_\gamma(\mathcal{A}'_\gamma) \equiv \partial_\gamma \mathcal{H}_0^{\lambda,\gamma} + i[\mathcal{A}'_\gamma, \mathcal{H}_0^{\lambda,\gamma}]$ and insert a suitable Ansatz \mathcal{A}'_λ and \mathcal{A}'_γ , respectively, to approximately solve Eqs. (A7). Notice that inserting the exact solutions into the Hermitian operators by multiplying Eqs. (A6) with the imaginary number i and solving for the generalized forces \mathcal{M}_λ and \mathcal{M}_γ leads to the expressions $G_\lambda(\mathcal{A}_\lambda) = -\mathcal{M}_\lambda$ and $G_\gamma(\mathcal{A}_\gamma) = -\mathcal{M}_\gamma$.

We aim to approximate the exact solutions for the adiabatic gauge potentials as faithfully as possible. To measure the distance between our approximate (\mathcal{A}'_λ and \mathcal{A}'_γ) and exact (\mathcal{A}_λ and \mathcal{A}_γ) adiabatic gauge potentials, it is convenient to introduce the operator distance as the Frobenius norm. The two-parameter operator distance can be written as

$$\begin{aligned} D^2 &= \text{Tr}[(G_\lambda(\mathcal{A}'_\lambda) + \mathcal{M}_\lambda)^2] + \text{Tr}[(G_\gamma(\mathcal{A}'_\gamma) + \mathcal{M}_\gamma)^2] \\ &= \text{Tr}[G_\lambda^2(\mathcal{A}'_\lambda)] + \text{Tr}[G_\gamma^2(\mathcal{A}'_\gamma)] - \text{Tr}[\mathcal{M}_\lambda^2] - \text{Tr}[\mathcal{M}_\gamma^2], \end{aligned} \quad (\text{A8})$$

where we use the fact that $\mathcal{H}_0^{\lambda,\gamma}$ commutes with \mathcal{M}_λ and \mathcal{M}_γ , respectively, and $\text{Tr}[\mathcal{M}_\lambda \partial_\lambda \mathcal{H}_0^{\lambda,\gamma}] = -\text{Tr}[\mathcal{M}_\lambda^2]$ and $\text{Tr}[\mathcal{M}_\gamma \partial_\gamma \mathcal{H}_0^{\lambda,\gamma}] = -\text{Tr}[\mathcal{M}_\gamma^2]$. As the generalized forces \mathcal{M}_λ and \mathcal{M}_γ do not depend on \mathcal{A}'_λ and \mathcal{A}'_γ , we can minimize the two-parameter operator distance, given by Eq. (A8), by minimizing the two-parameter action,

$$\mathcal{S} = \text{Tr}[G_\lambda^2(\mathcal{A}'_\lambda)] + \text{Tr}[G_\gamma^2(\mathcal{A}'_\gamma)], \quad (\text{A9})$$

with respect to the parameters of our Ansätze for the adiabatic gauge potentials, \mathcal{A}'_λ and \mathcal{A}'_γ , symbolically written as $\{\delta\mathcal{S}/\delta\mathcal{A}'_\lambda = 0, \delta\mathcal{S}/\delta\mathcal{A}'_\gamma = 0\}$.

APPENDIX B: LANDAU-ZENER MODEL

In this Appendix, we illustrate the method of our two-parameter CD drive for the Landau-Zener model. Its original Hamiltonian reads

$$\mathcal{H}_{\text{LZ},0}^{\lambda,\gamma}(t) = -[1 - \lambda(t)]\gamma(t)\sigma^x - \lambda(t)h\sigma^z, \quad (\text{B1})$$

where the driving functions are

$$\begin{aligned} \lambda(t) &= \sin^2 \left[\frac{\pi}{2} \sin^2 \left(\frac{\pi t}{2\tau} \right) \right], \\ \gamma(t) &= \gamma_{\text{init}} + \lambda(t). \end{aligned} \quad (\text{B2})$$

We have followed Ref. [25] in choosing the functional form of $\lambda(t)$ and have arbitrarily chosen the form of $\gamma(t)$. We now employ the Ansätze $\mathcal{A}'_\lambda \equiv \alpha\sigma^y$ and $\mathcal{A}'_\gamma \equiv \beta\sigma^y$ for the adiabatic gauge potentials with respect to λ and γ , respectively, and calculate the two Hermitian operators $G_\lambda(\mathcal{A}'_\lambda) = \partial_\lambda \mathcal{H}_{\text{LZ},0}^{\lambda,\gamma} + i[\mathcal{A}'_\lambda, \mathcal{H}_{\text{LZ},0}^{\lambda,\gamma}]$ and $G_\gamma(\mathcal{A}'_\gamma) = \partial_\gamma \mathcal{H}_{\text{LZ},0}^{\lambda,\gamma} + i[\mathcal{A}'_\gamma, \mathcal{H}_{\text{LZ},0}^{\lambda,\gamma}]$ and then minimize the corresponding

two-parameter action \mathcal{S} , given by Eq. (A9), with respect to the coefficients α and β . The Hermitian operators then turn out to be

$$\begin{aligned} G_\lambda(\mathcal{A}'_\lambda) &= (\gamma + 2\lambda h\alpha)\sigma^x - [h + 2(1 - \lambda)\gamma\alpha]\sigma^z, \\ G_\gamma(\mathcal{A}'_\gamma) &= [2\lambda h\beta - (1 - \lambda)]\sigma^x - 2(1 - \lambda)\gamma\beta\sigma^z. \end{aligned} \quad (\text{B3})$$

Pauli matrices are traceless and thus calculating the trace of the square of the Hermitian operators is equivalent to adding up squares of the coefficients in front of every Pauli matrix. Therefore, the action \mathcal{S} , given by Eq. (A9), reads

$$\begin{aligned} \mathcal{S} &= (\gamma + 2\lambda h\alpha)^2 + [h + 2(1 - \lambda)\gamma\alpha]^2 \\ &+ [2\lambda h\beta - (1 - \lambda)]^2 + 4(1 - \lambda)^2\gamma^2\beta^2. \end{aligned} \quad (\text{B4})$$

By calculating the derivatives of this action with respect to α and β , i.e., solving the system of equations $\{\delta\mathcal{S}/\delta\alpha = 0, \delta\mathcal{S}/\delta\beta = 0\}$, we obtain the optimal solution for the CD Hamiltonian $\mathcal{H}_{\text{LZ,CD}}^{\lambda,\gamma}(t) = (\dot{\lambda}\alpha + \dot{\gamma}\beta)\sigma^y$, given by Eq. (7) from the main text, as

$$\begin{aligned} \alpha &= -\frac{1}{2} \frac{h\gamma(t)}{\lambda^2(t)h^2 + \gamma^2(t)[1 - \lambda(t)]^2}, \\ \beta &= \frac{1}{2} \frac{[1 - \lambda(t)]\lambda(t)h}{\lambda^2(t)h^2 + \gamma^2(t)[1 - \lambda(t)]^2}. \end{aligned} \quad (\text{B5})$$

It turns out that this solution reduces to the exact CD term (cf. Ref. [20]) when $\gamma(t)$ is constant—as $\dot{\gamma}(t)$ then becomes zero and, consequently, we are left with the solution for α in Eq. (B5) with $\gamma(t) = \gamma$ alone, i.e., $\beta = 0$.

We can gauge away the imaginary σ^y term by applying the unitary gauge transformation $U_g(t) = \exp[i\theta(t)\sigma^z/2] = \cos[\theta(t)/2]\mathbb{1} + i\sin[\theta(t)/2]\sigma^z$ to the full Hamiltonian $\mathcal{H}_{\text{LZ}}^{\lambda,\gamma}(t) = \mathcal{H}_{\text{LZ},0}^{\lambda,\gamma}(t) + \mathcal{H}_{\text{LZ,CD}}^{\lambda,\gamma}(t)$ according to

$$\mathcal{H}_{\text{LZ,eff}}^{\lambda,\gamma}(t) = U_g \mathcal{H}_{\text{LZ}}^{\lambda,\gamma}(t) U_g^\dagger + i(\partial_t U_g) U_g^\dagger. \quad (\text{B6})$$

Here, the second term evaluates to $i(\partial_t U_g) U_g^\dagger = -(\dot{\theta}/2)\sigma^z$ with the right angle $\theta = \arctan(Y/X)$ along with $X = -[1 - \lambda(t)]\gamma(t)$ and $Y = \dot{\lambda}(t)\alpha(t) + \dot{\gamma}(t)\beta(t)$, and where we set $\hbar = 1$. The effective full Hamiltonian in the rotated frame then reads

$$\mathcal{H}_{\text{LZ,eff}}^{\lambda,\gamma}(t) = \sqrt{X^2 + Y^2}\sigma^x - \left[\frac{1}{2} \frac{\dot{Y}X - \dot{X}Y}{X^2 + Y^2} + h\lambda(t) \right] \sigma^z, \quad (\text{B7})$$

where the term involving time derivatives of X and Y stems from the corresponding derivatives of U_g and $\dot{\theta}$.

Figure 5 depicts the coefficients of the rotated driver and problem Hamiltonian, i.e.,

$$\begin{aligned} \mathcal{H}_{\text{LZ,x}}^{\lambda,\gamma}(t) &= \sqrt{X^2 + Y^2}\sigma^x, \\ \mathcal{H}_{\text{LZ,z}}^{\lambda,\gamma}(t) &= -\left[\frac{\dot{Y}X - \dot{X}Y}{2(X^2 + Y^2)} + h\lambda(t) \right] \sigma^z, \end{aligned} \quad (\text{B8})$$

with $\gamma(t) = \gamma_{\text{init}} + \lambda(t)$ and annealing time $\tau = 1$. The coefficients are quite nonmonotonic and become rather large at intermediate times.

We, finally, note that an introduction of σ^x and σ^z in the approximate adiabatic gauge potential, in addition to σ^y , i.e., employing the Ansätze $\mathcal{A}'_\lambda = \alpha^x\sigma^x + \alpha^y\sigma^y + \alpha^z\sigma^z$ and $\mathcal{A}'_\gamma = \beta^x\sigma^x + \beta^y\sigma^y + \beta^z\sigma^z$, leads to vanishing coefficients

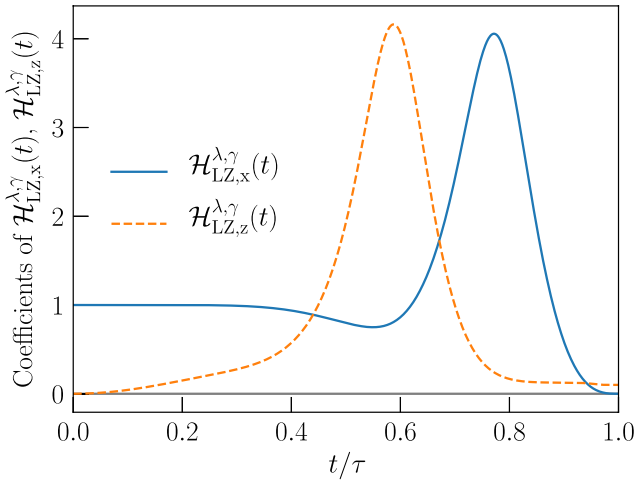


FIG. 5. Coefficient of two-parameter CD drive. Coefficients of the driver Hamiltonian, i.e., $\mathcal{H}_{LZ,x}^{\lambda,\gamma}(t)$ (blue solid line) and problem Hamiltonian $\mathcal{H}_{LZ,z}^{\lambda,\gamma}(t)$ (orange dashed line), as described in Eq. (B8) for two-parameter CD driving during annealing of $\tau = 1$. Other parameter: $h = 0.1$.

α^x and α^z as well as β^x and β^z . This can directly be seen by calculating the corresponding Hermitian operators $G(\mathcal{A}_\lambda)$ and $G(\mathcal{A}_\gamma)$, which entail additional $2[(1-\lambda)\gamma\alpha^z - \lambda h\alpha^x]\sigma^y$ and $2[(1-\lambda)\gamma\beta^z - \lambda h\beta^x]\sigma^y$ terms. The resulting action S , given by Eq. (A9), thus comprises additional $(\alpha^x)^2$, $(\alpha^z)^2$, and $\alpha^x\alpha^z$ as well as $(\beta^x)^2$, $(\beta^z)^2$, and $\beta^x\beta^z$ terms which, after taking the square and building the derivative with respect to α^x and α^z as well as β^x and β^z , become zero. This justifies the framework to use only σ^y in the approximate adiabatic gauge potential. The same can be observed in more generic cases with interactions in the cost function, i.e., the Ising model.

APPENDIX C: p -SPIN MODEL

In this Appendix, we derive the solutions of the optimal two-parameter CD Hamiltonian, $\mathcal{H}_{CD}^{\lambda,\gamma}(t) = \sum_{i=1}^N (\lambda\alpha + \gamma\beta)\sigma_i^y$, given by Eq. (14) from the main text, for the p -spin model with $p = 3$ and original Hamiltonian $\mathcal{H}_0(t)$, given by Eq. (10), with driving functions $\lambda(t)$ and $\gamma(t)$, given by Eq. (12). For the latter, we can rewrite the original Hamiltonian into the form

$$\mathcal{H}_0^{\lambda,\gamma}(t) = -[1 - \lambda(t)] \sum_{i=1}^N \gamma(t) \sigma_i^x - \lambda(t) \frac{1}{N^2} \left[6 \sum_{i<j<k} \sigma_i^z \sigma_j^z \sigma_k^z + (3N-2) \sum_{i=1}^N \sigma_i^z \right]. \quad (C1)$$

For this many-body case, we employ the *Ansätze* $\mathcal{A}'_\lambda \equiv \sum_{i=1}^N \alpha \sigma_i^y$ and $\mathcal{A}'_\gamma \equiv \sum_{i=1}^N \beta \sigma_i^y$ for the corresponding adiabatic gauge potentials. Calculating the Hermitian operators $G_\lambda(\mathcal{A}'_\lambda)$ and $G_\gamma(\mathcal{A}'_\gamma)$ requires the commutators

$$\begin{aligned} i[\mathcal{A}'_\lambda, \mathcal{H}_0^{\lambda,\gamma}] &= \sum_{i=1}^N \frac{2\lambda(3N-2)}{N^2} \alpha \sigma_i^x - 2(1-\lambda)\alpha\gamma\sigma_i^z + \frac{12\lambda}{N^2} \sum_{i<j<k} \alpha (\sigma_i^x \sigma_j^z \sigma_k^z + \sigma_i^z \sigma_j^x \sigma_k^z + \sigma_i^z \sigma_j^z \sigma_k^x), \\ i[\mathcal{A}'_\gamma, \mathcal{H}_0^{\lambda,\gamma}] &= \sum_{i=1}^N \frac{2\lambda(3N-2)}{N^2} \beta \sigma_i^x - 2(1-\lambda)\beta\gamma\sigma_i^z + \frac{12\lambda}{N^2} \sum_{i<j<k} \beta (\sigma_i^x \sigma_j^z \sigma_k^z + \sigma_i^z \sigma_j^x \sigma_k^z + \sigma_i^z \sigma_j^z \sigma_k^x). \end{aligned} \quad (C2)$$

Adding the two partial derivatives $\partial_\lambda \mathcal{H}_0^{\lambda,\gamma}$ and $\partial_\gamma \mathcal{H}_0^{\lambda,\gamma}$, respectively, leads to the Hermitian operators

$$\begin{aligned} G_\lambda(\mathcal{A}'_\lambda) &= \sum_{i=1}^N \left[\gamma + \frac{2\alpha\lambda(3N-2)}{N^2} \right] \sigma_i^x - \frac{6}{N^2} \sum_{i<j<k} \sigma_i^z \sigma_j^z \sigma_k^z - \sum_{i=1}^N \left[\frac{3N-2}{N^2} + 2\alpha(1-\lambda)\gamma \right] \sigma_i^z \\ &\quad + \frac{12\lambda}{N^2} \sum_{i<j<k} \alpha (\sigma_i^x \sigma_j^z \sigma_k^z + \sigma_i^z \sigma_j^x \sigma_k^z + \sigma_i^z \sigma_j^z \sigma_k^x), \\ G_\gamma(\mathcal{A}'_\gamma) &= \sum_{i=1}^N \left[\frac{2\beta\lambda(3N-2)}{N^2} - (1-\lambda) \right] \sigma_i^x - \sum_{i=1}^N \left[\frac{3N-2}{N^2} + 2\beta(1-\lambda)\gamma \right] \sigma_i^z - \frac{6}{N^2} \sum_{i<j<k} \sigma_i^z \sigma_j^z \sigma_k^z \\ &\quad + \frac{12\lambda}{N^2} \sum_{i<j<k} \beta (\sigma_i^x \sigma_j^z \sigma_k^z + \sigma_i^z \sigma_j^x \sigma_k^z + \sigma_i^z \sigma_j^z \sigma_k^x). \end{aligned} \quad (C3)$$

Consequently, the action $S = \text{Tr}[G_\lambda^2(\mathcal{A}'_\lambda)] + \text{Tr}[G_\gamma^2(\mathcal{A}'_\gamma)]$, given by Eq. (A9), can be written as

$$\begin{aligned} \frac{S}{N} &= \sum_{i=1}^N \left[\gamma + \frac{2\alpha\lambda(3N-2)}{N^2} \right]^2 + \left[\frac{3N-2}{N^2} + 2\alpha(1-\lambda)\gamma \right]^2 + \frac{72\lambda^2}{N^4} (N-1)(N-2)\alpha^2 \\ &\quad + \sum_{i=1}^N \left[\frac{2\beta\lambda(3N-2)}{N^2} - (1-\lambda) \right]^2 + \left[\frac{3N-2}{N^2} + 2\beta(1-\lambda)\gamma \right]^2 + \frac{72\lambda^2}{N^4} (N-1)(N-2)\beta^2 - \frac{12(N-1)(N-2)}{N^2}, \end{aligned} \quad (C4)$$

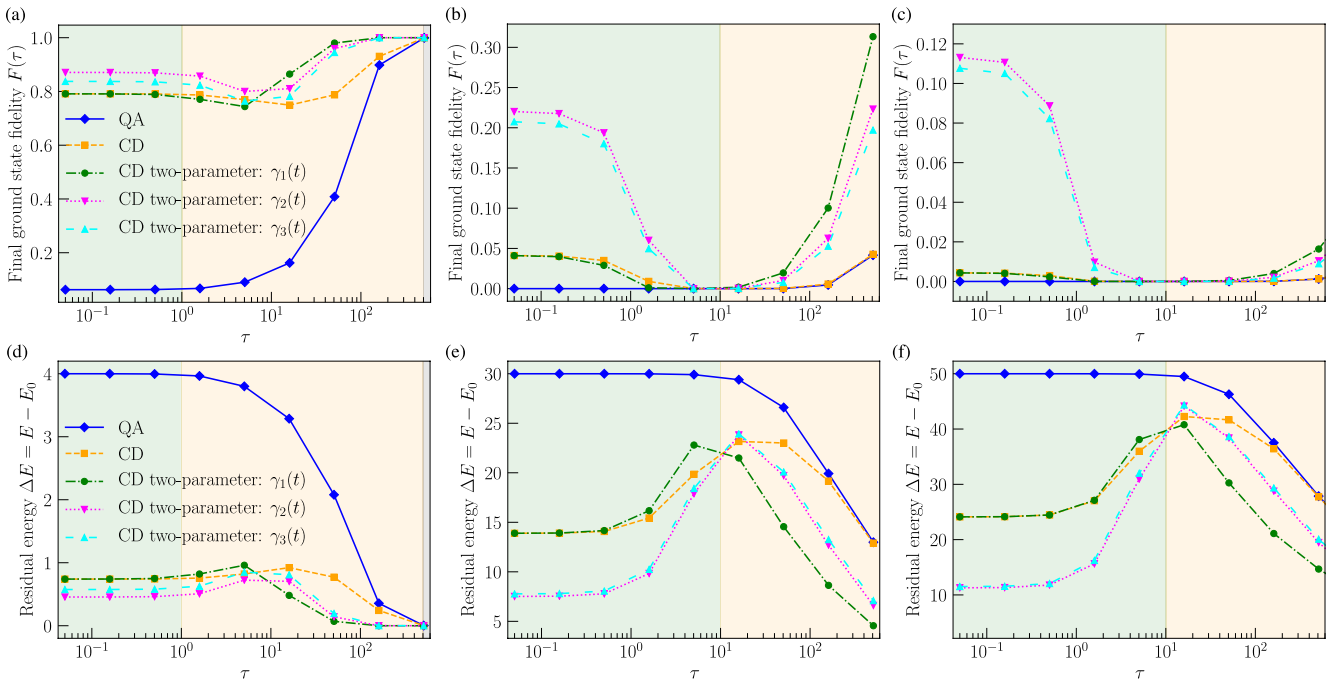


FIG. 6. Ground-state fidelity and residual energy. (a)–(c) Final ground-state fidelity and (d)–(f) residual energy for (i) traditional quantum annealing (diamonds, blue solid line), (ii) single-parameter CD drive (squares, orange dashed line), and (iii) two-parameter CD drive with driving functions $\gamma_1(t)$, given by Eq. (D2) (circles, green dash-dotted line), $\gamma_2(t)$, given by Eq. (D3) (down triangles, magenta dotted line), and $\gamma_3(t)$, given by Eq. (D4) (up triangles, cyan widely dashed line), as functions of annealing time τ . The system sizes are (a),(d) $N = 4$, (b),(e) $N = 30$, and (c),(f) $N = 50$, where $\gamma_{\text{init}} = 1$ for all panels. Time ranges are color coded as follows: short-time regime (green-shaded areas) where the fidelity is approximately $1/2^N$ for traditional quantum annealing, long-time regime (yellow-shaded areas) where transient behavior is observed and the two-parameter CD drive shows a clear advantage, and adiabatic regime (gray-shaded areas) where $F(\tau) > 0.99$.

and minimizing this action with respect to each coefficient α and β leads to the solutions, given by Eq. (14), from the text.

To bring the full Hamiltonian $\mathcal{H}^{\lambda,\gamma}(t) = \mathcal{H}_0^{\lambda,\gamma}(t) + \mathcal{H}_{\text{CD}}^{\lambda,\gamma}(t)$ with $\mathcal{H}_{\text{CD}}^{\lambda,\gamma}(t)$ from Eq. (14) in an experimentally more feasible form, we can gauge away the imaginary single-body σ_i^y terms by applying the unitary gauge transformation $U_g[\theta(t)] = \exp[i\theta(t)/2 \sum_{i=1}^N \sigma_i^z]$, given by Eq. (16), for convenience written as $U_g = \prod_{j=1}^N [\cos(\theta/2)\mathbb{1} + i \sin(\theta/2)\sigma_j^z]$. The effective, i.e., rotated, full Hamiltonian in the laboratory frame then reads

$$\mathcal{H}_{\text{eff}}^{\lambda,\gamma}(t) = U_g \mathcal{H}^{\lambda,\gamma}(t) U_g^\dagger - \sum_{i=1}^N \frac{\dot{\theta}}{2} \sigma_i^z, \quad (\text{C5})$$

which can straightforwardly be derived by multiplying both sides of the time-dependent Schrödinger equation $i\partial_t \psi = H\psi$ in the original frame with the unitary transformation U_g , given by Eq. (16), employing the relation $\tilde{\psi} = U_g \psi$ and expressing the dynamics in the moving frame. Analogously to Appendix B, the rotational right angle is $\theta = \arctan(Y/X)$ with $Y = \lambda\alpha + \dot{\gamma}\beta$ and $X = -(1 - \lambda)\gamma$. For the first term of Eq. (C5), we use that $U_g \sigma_i^x U_g^\dagger = \cos\theta \sigma_i^x - \sin\theta \sigma_i^y$, $U_g \sigma_i^y U_g^\dagger = \sin\theta \sigma_i^x + \cos\theta \sigma_i^y$, and $U_g \sigma_i^z U_g^\dagger = \sigma_i^z$, as well as the trigonometrical relations $\sin\theta = Y/\sqrt{X^2 + Y^2}$ and $\cos\theta = X/\sqrt{X^2 + Y^2}$. The first term then evaluates to $\sqrt{X^2 + Y^2} \sigma_i^x$ and, together with the second term and $\dot{\theta} = (\dot{Y}X - \dot{X}Y)/(X^2 + Y^2)$, describe the expression of the effective Hamiltonian, given by Eq. (17), from the text.

APPENDIX D: DIFFERENT DRIVING FUNCTIONS $\gamma_i(t)$

The numerical results of the two-parameter CD approach with particular choice of the driving function $\gamma(t)$, given by Eq. (12), revealed a considerable enhancement in the reached final ground-state fidelity and residual energy. We are thus interested in whether this enhancement stems from this particular choice of driving functions or constitutes a general feature due to the expansion of the search space for the optimal parameters α and β , given by Eq. (14). Although it is difficult to systematically explore the best possible functional forms, we nevertheless tried a few different cases to confirm that our conclusion remains unchanged qualitatively. To this end, we compare the numerical performance of this two-parameter CD method for three different forms of the driving function, i.e.,

$$\lambda(t) = \sin^3\left(\frac{\pi t}{2\tau}\right), \quad (\text{D1})$$

$$\gamma_1(t) = \gamma_{\text{init}} - \lambda(t), \quad (\text{D2})$$

$$\gamma_2(t) = \cos^3\left(\frac{\pi t}{2\tau}\right), \quad (\text{D3})$$

$$\gamma_3(t) = 1 - \sin^3\left(\frac{\pi t}{2\tau}\right), \quad (\text{D4})$$

where, in contrast to the case of Fig. 1, we set the initial value of $\gamma(t)$ to $\gamma_{\text{init}} = 1$. The corresponding numerical results are depicted in Fig. 6 with the same other parameters as in Fig. 1. They reveal that the full Hamiltonians with two-parameter CD driving and all three driving functions

considerably outperform the traditional quantum annealing and existing one-parameter counterparts. Interestingly, the two newly added driving functions $\gamma_2(t)$ and $\gamma_3(t)$, which have considerably different forms than the one originally used in Fig. 1, even considerably outperform the latter for short sweep durations (green-shaded area), though the function $\gamma_1(t)$, which is similar to the one in the main text, works best in the intermediate-time region (yellow-shaded area). This

is a promising result as the two-parameter approach provides a systematic enhancement for a variety of driving functions due to the expanded search space in two dimensions. These results motivate more systematic analytical and numerical investigations of driving functions that yield the maximal reached final ground-state fidelities and—as mentioned in the main text—constitute an interesting topic for future research.

- [1] T. Kadowaki and H. Nishimori, Quantum annealing in the transverse Ising model, *Phys. Rev. E* **58**, 5355 (1998).
- [2] J. Brooke, D. Bitko, T. F. Rosenbaum, and G. Aeppli, Quantum annealing of a disordered magnet, *Science* **284**, 779 (1999).
- [3] G. E. Santoro, R. Martoňák, E. Tosatti, and R. Car, Theory of quantum annealing of an Ising spin glass, *Science* **295**, 2427 (2002).
- [4] G. E. Santoro and E. Tosatti, Optimization using quantum mechanics: Quantum annealing through adiabatic evolution, *J. Phys. A* **39**, R393 (2006).
- [5] A. Das and B. K. Chakrabarti, Colloquium: Quantum annealing and analog quantum computation, *Rev. Mod. Phys.* **80**, 1061 (2008).
- [6] S. Morita and H. Nishimori, Mathematical foundation of quantum annealing, *J. Math. Phys.* **49**, 125210 (2008).
- [7] P. Hauke, H. G. Katzgraber, W. Lechner, H. Nishimori, and W. D. Oliver, Perspectives of quantum annealing: Methods and implementations, *Rep. Prog. Phys.* **83**, 054401 (2020).
- [8] E. Farhi, J. Goldstone, S. Gutmann, and M. Sipser, Quantum computation by adiabatic evolution, [arXiv:quant-ph/0001106](https://arxiv.org/abs/quant-ph/0001106).
- [9] E. Farhi, J. Goldstone, S. Gutmann, J. Lapan, A. Lundgren, and D. Preda, A quantum adiabatic evolution algorithm applied to random instances of an NP-complete problem, *Science* **292**, 472 (2001).
- [10] T. Albash and D. A. Lidar, Adiabatic quantum computation, *Rev. Mod. Phys.* **90**, 015002 (2018).
- [11] E. J. Crosson and D. A. Lidar, Prospects for quantum enhancement with diabatic quantum annealing, [arXiv:2008.09913](https://arxiv.org/abs/2008.09913).
- [12] E. Torrontegui, S. Ibáñez, S. Martínez-Garaot, M. Modugno, A. del Campo, D. Guéry-Odelin, A. Ruschhaupt, X. Chen, and J. G. Muga, in *Advances in Atomic, Molecular, and Optical Physics*, Vol. 62, edited by E. Arimondo, P. R. Berman, and C. C. Lin (Academic Press, Cambridge, Massachusetts, 2013), pp. 117–169.
- [13] A. del Campo and K. Sengupta, Controlling quantum critical dynamics of isolated systems, *Eur. Phys. J. Spec. Top.* **224**, 189 (2015).
- [14] A. del Campo and K. Kim, Focus on shortcuts to adiabaticity, *New J. Phys.* **21**, 050201 (2019).
- [15] D. Guéry-Odelin, A. Ruschhaupt, A. Kiely, E. Torrontegui, S. Martínez-Garaot, and J. G. Muga, Shortcuts to adiabaticity: Concepts, methods, and applications, *Rev. Mod. Phys.* **91**, 045001 (2019).
- [16] M. Demirplak and S. A. Rice, Adiabatic population transfer with control fields, *J. Phys. Chem. A* **107**, 9937 (2003).
- [17] M. V. Berry, Transitionless quantum driving, *J. Phys. A Math. Theor.* **42**, 365303 (2009).
- [18] X. Chen, A. Ruschhaupt, S. Schmidt, A. del Campo, D. Guéry-Odelin, and J. G. Muga, Fast Optimal Frictionless atom Cooling in Harmonic Traps: Shortcut to Adiabaticity, *Phys. Rev. Lett.* **104**, 063002 (2010).
- [19] X. Chen, E. Torrontegui, and J. G. Muga, Lewis-Riesenfeld invariants and transitionless quantum driving, *Phys. Rev. A* **83**, 062116 (2011).
- [20] K. Takahashi, Transitionless quantum driving for spin systems, *Phys. Rev. E* **87**, 062117 (2013).
- [21] C. Jarzynski, Generating shortcuts to adiabaticity in quantum and classical dynamics, *Phys. Rev. A* **88**, 040101(R) (2013).
- [22] K. Takahashi, Hamiltonian engineering for adiabatic quantum computation: Lessons from shortcuts to adiabaticity, *J. Phys. Soc. Jpn.* **88**, 061002 (2019).
- [23] A. del Campo, Shortcuts to Adiabaticity by Counterdiabatic Driving, *Phys. Rev. Lett.* **111**, 100502 (2013).
- [24] B. Damski, Counterdiabatic driving of the quantum Ising model, *J. Stat. Mech. Theor. Expt.* (2014) P12019.
- [25] D. Sels and A. Polkovnikov, Minimizing irreversible losses in quantum systems by local counterdiabatic driving, *Proc. Natl. Acad. Sci.* **114**, E3909 (2017).
- [26] P. W. Claeys, M. Pandey, D. Sels, and A. Polkovnikov, Floquet-Engineering Counterdiabatic Protocols in Quantum Many-Body Systems, *Phys. Rev. Lett.* **123**, 090602 (2019).
- [27] A. Hartmann and W. Lechner, Rapid counter-diabatic sweeps in lattice gauge adiabatic quantum computing, *New J. Phys.* **21**, 043025 (2019).
- [28] M. Kolodrubetz, D. Sels, P. Mehta, and A. Polkovnikov, Geometry and nonadiabatic response in quantum and classical systems, *Phys. Rep.* **697**, 1 (2017).
- [29] H. Zhou, Y. Ji, X. Nie, X. Yang, X. Chen, J. Bian, and X. Peng, Experimental Realization of Shortcuts to Adiabaticity in a Nonintegrable Spin Chain by Local Counterdiabatic Driving, *Phys. Rev. Appl.* **13**, 044059 (2020).
- [30] G. Passarelli, V. Cataudella, R. Fazio, and P. Lucignano, Counterdiabatic driving in the quantum annealing of the p -spin model: A variational approach, *Phys. Rev. Res.* **2**, 013283 (2020).
- [31] N. N. Hegade, K. Paul, Y. Ding, M. Sanz, F. Albarrán-Arriagada, E. Solano, and X. Chen, Shortcuts to Adiabaticity in Digitized Adiabatic Quantum Computing, *Phys. Rev. Appl.* **15**, 024038 (2021).
- [32] T. Jörg, F. Krzakala, J. Kurchan, A. C. Maggs, and J. Pujos, Energy gaps in quantum first-order mean-field-like transitions: The problems that quantum annealing cannot solve, *Europhys. Lett.* **89**, 40004 (2010).

- [33] Y. Seki and H. Nishimori, Quantum annealing with antiferromagnetic fluctuations, *Phys. Rev. E* **85**, 051112 (2012).
- [34] B. Seoane and H. Nishimori, Many-body transverse interactions in the quantum annealing of the p -spin ferromagnet, *J. Phys. A Math. Theor.* **45**, 435301 (2012).
- [35] Y. Seki and H. Nishimori, Quantum annealing with antiferromagnetic transverse interactions for the Hopfield model, *J. Phys. A Math. Theor.* **48**, 335301 (2015).
- [36] H. Nishimori and K. Takada, Exponential enhancement of the efficiency of quantum annealing by non-stoquastic Hamiltonians, *Front. ICT* **4**, 2 (2017).
- [37] A. Hartmann and W. Lechner, Quantum phase transition with inhomogeneous driving in the Lechner-Hauke-Zoller model, *Phys. Rev. A* **100**, 032110 (2019).
- [38] A. Lucas, Ising formulations of many NP problems, *Front. Phys.* **2**, 5 (2014).
- [39] It is known that in the p -spin model, the thermodynamic limit $N \rightarrow \infty$ is equivalent to the classical limit and a correction of $O(1/N)$ is equivalent to a quantum correction of the order of $O(\hbar)$ [48]. Thus the present adiabatic gauge potential may be regarded as representing delicate quantum effects in the p -spin model.
- [40] T. Albash and D. A. Lidar, Demonstration of a Scaling Advantage for a Quantum Annealer over Simulated Annealing, *Phys. Rev. X* **8**, 031016 (2018).
- [41] J. R. Johansson, P. D. Nation, and F. Nori, QUTIP 2: A PYTHON framework for the dynamics of open quantum systems, *Comput. Phys. Commun.* **184**, 1234 (2013).
- [42] Y. Susa, Y. Yamashiro, M. Yamamoto, and H. Nishimori, Exponential speedup of quantum annealing by inhomogeneous driving of the transverse field, *J. Phys. Soc. Jpn.* **87**, 023002 (2018).
- [43] Y. Susa, Y. Yamashiro, M. Yamamoto, I. Hen, D. A. Lidar, and H. Nishimori, Quantum annealing of the p -spin model under inhomogeneous transverse field driving, *Phys. Rev. A* **98**, 042326 (2018).
- [44] Z.-C. Yang, A. Rahmani, A. Shabani, H. Neven, and C. Chamon, Optimizing Variational Quantum Algorithms Using Pontryagin's Minimum Principle, *Phys. Rev. X* **7**, 021027 (2017).
- [45] G. B. Mbeng, R. Fazio, and G. Santoro, Quantum Annealing: A journey through Digitalization, Control, and hybrid Quantum Variational schemes, [arXiv:1906.08948](https://arxiv.org/abs/1906.08948).
- [46] L. T. Brady, C. L. Baldwin, A. Bapat, Y. Kharkov, and A. V. Gorshkov, Optimal Protocols in Quantum Annealing and QAOA Problems, *Phys. Rev. Lett.* **126**, 070505 (2021).
- [47] K. Takahashi, Shortcuts to adiabaticity for quantum annealing, *Phys. Rev. A* **95**, 012309 (2017).
- [48] M. Ohkuwa and H. Nishimori, Exact expression of the energy gap at first-order quantum phase transitions of the fully connected p -body transverse-field Ising model with transverse interactions, *J. Phys. Soc. Jpn.* **86**, 114004 (2017).
- [49] A. del Campo, M. M. Rams, and W. H. Zurek, Assisted Finite-Rate Adiabatic Passage Across a Quantum Critical Point: Exact Solution for the Quantum Ising Model, *Phys. Rev. Lett.* **109**, 115703 (2012).

Appendix B

Method Application

B.1 Landau-Zener Model

We follow the steps of section 2.1 and form the trace of the hermitian operators squares

$$G_\lambda(\mathcal{X}) = \partial_\lambda \mathcal{H} + i[\mathcal{X}, \mathcal{H}] \quad (\text{B.1})$$

$$= \gamma\sigma^x - h\sigma^z + i(1-\lambda)(-\gamma)\alpha[\sigma^y, \sigma^x] - i\lambda h\alpha[\sigma^y, \sigma^z] \quad (\text{B.2})$$

$$= \gamma\sigma^x - h\sigma^z + i(1-\lambda)(-\gamma)\alpha(-2i\sigma^z) - i\lambda h\alpha 2i\sigma^x \quad (\text{B.3})$$

$$= \gamma\sigma^x - h\sigma^z - 2(1-\lambda)\gamma\alpha\sigma^z + 2\lambda h\alpha\sigma^x \quad (\text{B.4})$$

$$= (\gamma + 2\lambda h\alpha)\sigma^x - (h + 2(1-\lambda)\gamma\alpha)\sigma^z \quad (\text{B.5})$$

$$\text{Tr}[G_\lambda^2] = (\gamma + 2\lambda h\alpha)^2 + (h + 2(1-\lambda)\gamma\alpha)^2 \quad (\text{B.6})$$

$$= \gamma^2 + 4\lambda h\alpha\gamma + 4\lambda^2 h^2 \alpha^2 + h^2 + 4h(1-\lambda)\gamma\alpha + 4(1-\lambda)^2 \gamma^2 \alpha^2 \quad (\text{B.7})$$

$$= \gamma^2 + 4\lambda^2 h^2 \alpha^2 + h^2 + 4h\gamma\alpha + 4(1-\lambda)^2 \gamma^2 \alpha^2 \quad (\text{B.8})$$

$$G_\gamma(\mathcal{Y}) = \partial_\gamma \mathcal{H} + i[\mathcal{Y}, \mathcal{H}] \quad (\text{B.9})$$

$$= -(1-\lambda)\sigma^x - 2(1-\lambda)\gamma\beta\sigma^z + 2\lambda h\beta\sigma^x \quad (\text{B.10})$$

$$= (2\lambda h\beta - (1-\lambda))\sigma^x - 2(1-\lambda)\gamma\beta\sigma^z \quad (\text{B.11})$$

$$\text{Tr}[G_\gamma^2] = (2\lambda h\beta - (1-\lambda))^2 + 4(1-\lambda)^2 \gamma^2 \beta^2 \quad (\text{B.12})$$

$$= 4\lambda^2 h^2 \beta^2 - 4(1-\lambda)\lambda h\beta + (1-\lambda)^2 + 4(1-\lambda)^2 \gamma^2 \beta^2 \quad (\text{B.13})$$

$$(\text{B.14})$$

$$(\text{B.15})$$

and minimize the action operator

$$\frac{\partial \mathcal{S}}{\partial \alpha} = 8\lambda^2 h^2 \alpha + 4h\gamma + 8(1-\lambda)^2 \gamma^2 \alpha \quad (\text{B.19})$$

$$= (2\lambda^2 h^2 + 2(1-\lambda)^2 \gamma^2) \alpha + h\gamma \stackrel{!}{=} 0 \quad (\text{B.20})$$

$$(\text{B.21})$$

$$\frac{\partial \mathcal{S}}{\partial \beta} = 8\lambda^2 h^2 \beta - 4(1-\lambda)\lambda h + 8(1-\lambda)^2 \gamma^2 \beta \quad (\text{B.22})$$

$$= (2\lambda^2 h^2 + 2(1-\lambda)^2 \gamma^2) \beta - (1-\lambda)\lambda h \stackrel{!}{=} 0 \quad (\text{B.23})$$

to receive the final results for the driving parameters

$$\alpha = -\frac{1}{2} \frac{h\gamma}{\lambda^2 h^2 + (1-\lambda)^2 \gamma^2} \quad (\text{B.24})$$

$$\beta = \frac{1}{2} \frac{(1-\lambda)\lambda h}{\lambda^2 h^2 + (1-\lambda)^2 \gamma^2} \quad (\text{B.25})$$

B.2 2 Spin Model

We minimize the familiar action operator $\mathcal{S} = \text{Tr}[G_\lambda^2] + \text{Tr}[G_\gamma^2]$ with respect to the two gauge potentials

$$\mathcal{X} = \sum_{i=1}^2 \alpha_i \sigma_i^y \quad (\text{B.26})$$

$$\mathcal{Y} = \sum_{i=1}^2 \beta_i \sigma_i^y \quad (\text{B.27})$$

inserting both ansätze into the hermitian operator

$$G_\lambda(\mathcal{X}) = \partial_\lambda \mathcal{H} + i[\mathcal{X}, \mathcal{H}] \quad (\text{B.28})$$

$$= \sum_{i=1}^2 \gamma_i \sigma_i^x - \sum_{i=1}^2 h_i \sigma_i^z - J \sigma_1^z \sigma_2^z - 2(1-\lambda) \sum_{i=1}^2 \alpha_i \gamma_i \sigma_i^z \quad (\text{B.29})$$

$$+ 2\lambda \sum_{i=1}^2 \alpha_i h_i \sigma_i^x + 2\lambda \sum_{i=1}^2 \alpha_i J \sigma_1^x \sigma_2^z \quad (\text{B.30})$$

$$= \sum_{i=1}^2 (\gamma_i + 2\lambda \alpha_i h_i) \sigma_i^x - \sum_{i=1}^2 (2(1-\lambda) \alpha_i \gamma_i + h_i) \sigma_i^z \quad (\text{B.31})$$

$$- J \sigma_1^z \sigma_2^z + 2\lambda \sum_{i=1}^2 \alpha_i J \sigma_1^x \sigma_2^z \quad (\text{B.32})$$

$$\text{Tr}[G_\lambda^2] = \sum_{i=1}^2 (\gamma_i + 2\lambda\alpha_i h_i)^2 + \sum_{i=1}^2 (2(1-\lambda)\alpha_i \gamma_i + h_i)^2 + J^2 + 4\lambda^2 \sum_{i=1}^2 \alpha_i^2 J^2 \quad (\text{B.33})$$

$$= J^2 + \sum_{i=1}^2 \gamma_i^2 + 4\gamma_i \lambda \alpha_i h_i + 4\lambda^2 \alpha_i^2 h_i^2 + 4(1-\lambda)^2 \alpha_i^2 \gamma_i^2 \quad (\text{B.34})$$

$$+ 4(1-\lambda)\alpha_i \gamma_i h_i + h_i^2 + 4\lambda^2 \alpha_i^2 J^2 \quad (\text{B.35})$$

and minimizing the action

$$\frac{\partial \text{Tr}[G_\lambda^2]}{\partial \alpha_i} = \gamma_i \lambda h_i + 2\lambda^2 h_i^2 \alpha_i + 2(1-\lambda)^2 \gamma_i^2 \alpha_i + (1-\lambda)\gamma_i h_i + 2\lambda^2 J^2 \alpha_i \stackrel{!}{=} 0 \quad (\text{B.36})$$

we receive our result

$$\alpha_i = -\frac{1}{2} \frac{\gamma_i h_i}{\lambda^2 h_i^2 + (1-\lambda)^2 \gamma_i^2 + \lambda^2 J^2} \quad (\text{B.37})$$

Going through the same steps with the $G_\gamma(\mathcal{Y})$ operator yields

$$\beta_i = \frac{1}{2} \frac{(1-\lambda)\lambda h_i}{\lambda^2 h_i^2 + (1-\lambda)^2 \gamma_i^2 + \lambda^2 J^2} \quad (\text{B.38})$$

B.3 Nearest Neighbour Model

We follow the familiar action optimization and find

$$\text{Tr}[G_\lambda^2] = \sum_{i=1}^N J_{i,i+1}^2 + 4\lambda^2 \sum_{i=1}^N \alpha_i^2 (J_{i,i+1}^2 + J_{i-1,i}^2) \quad (\text{B.39})$$

$$+ \sum_{i=1}^N (\gamma_i + 2\alpha_i h_i \lambda)^2 + \sum_{i=1}^N (h_i + 2\alpha_i \gamma_i (1-\lambda))^2 \quad (\text{B.40})$$

further we derive the terms $\text{Tr}[G_{\gamma_i}^2]$

$$G_{\gamma_i} = \partial_{\gamma_i} \mathcal{H} + i[\mathcal{Y}_i, \mathcal{H}] \quad (\text{B.41})$$

$$(\text{B.42})$$

$$\partial_{\gamma_i} \mathcal{H} = -(1 - \lambda) \sigma_i^x \quad (\text{B.43})$$

$$[\mathcal{Y}_i, \mathcal{H}] = -(1 - \lambda) \left[\sum_{i=1}^N \beta_i \sigma_i^y, \sum_{i=1}^N \gamma_i \sigma_i^x \right] \quad (\text{B.44})$$

$$- \lambda \left(\left[\sum_{i=1}^N \beta_i \sigma_i^y, \sum_{i=1}^N h_i \sigma_i^z \right] + \left[\sum_{i=1}^N \beta_i \sigma_i^y, \sum_{j=1}^N J_{j,j+1} \sigma_j^z \sigma_{j+1}^z \right] \right) \quad (\text{B.45})$$

$$(\text{B.46})$$

$$= -2(1 - \lambda) \sum_{i=1}^N \gamma_i \beta_i \sigma_i^z \quad (\text{B.47})$$

$$+ 2\lambda \left(\sum_{i=1}^N h_i \beta_i \sigma_i^x + \sum_{i=1}^N \beta_i J_{i,i+1} \sigma_i^x \sigma_{i+1}^z + \beta_{i+1} J_{i,i+1} \sigma_i^z \sigma_{i+1}^x \right) \quad (\text{B.48})$$

$$(\text{B.49})$$

$$G_{\gamma_i} = -(1 - \lambda) \sigma_i^x - 2(1 - \lambda) \sum_{i=1}^N \gamma_i \beta_i \sigma_i^z \quad (\text{B.50})$$

$$+ 2\lambda \left(\sum_{i=1}^N h_i \beta_i \sigma_i^x + \sum_{i=1}^N \beta_i J_{i,i+1} \sigma_i^x \sigma_{i+1}^z + \beta_{i+1} J_{i,i+1} \sigma_i^z \sigma_{i+1}^x \right) \quad (\text{B.51})$$

$$= \sum_{i=1}^N [2\lambda h_i \beta_i - (1 - \lambda)] \sigma_i^x - 2(1 - \lambda) \sum_{i=1}^N \gamma_i \beta_i \sigma_i^z \quad (\text{B.52})$$

$$+ 2\lambda \left(\sum_{i=1}^N h_i \beta_i \sigma_i^x + \sum_{i=1}^N \beta_i J_{i,i+1} \sigma_i^x \sigma_{i+1}^z + \beta_{i+1} J_{i,i+1} \sigma_i^z \sigma_{i+1}^x \right) \quad (\text{B.53})$$

$$(\text{B.54})$$

$$\text{Tr}[G_{\gamma_i}^2] = \sum_{i=1}^N (2\lambda h_i \beta_i - (1 - \lambda))^2 + 4(1 - \lambda)^2 \sum_{i=1}^N \gamma_i^2 \beta_i^2 \quad (\text{B.55})$$

$$+ 4\lambda^2 \sum_{i=1}^N \beta_i^2 (J_{i,i+1}^2 + J_{i-1,i}^2) \quad (\text{B.56})$$

Inserting B.39 - B.40 and B.55 - B.56 into the action $\mathcal{S} = Tr[G_\lambda^2] + Tr[G_{\gamma_i}^2]$ gives

$$\mathcal{S} = \sum_{i=1}^N (2\lambda h_i \beta_i - (1 - \lambda))^2 + 4(1 - \lambda)^2 \sum_{i=1}^N \gamma_i^2 \beta_i^2 + 4\lambda^2 \sum_{i=1}^N \beta_i^2 (J_{i,i+1}^2 + J_{i-1,i}^2) \quad (\text{B.57})$$

$$+ \sum_{i=1}^N J_{i,i+1}^2 + 4\lambda^2 \sum_{i=1}^N \alpha_i^2 (J_{i,i+1}^2 + J_{i-1,i}^2) + \sum_{i=1}^N (\gamma_i + 2\alpha_i h_i \lambda)^2 + \sum_{i=1}^N (h_i + 2\alpha_i \gamma_i (1 - \lambda))^2 \quad (\text{B.58})$$

$$\frac{\partial \mathcal{S}}{\partial \alpha_i} = 8\lambda^2 \alpha_i (J_{i,i+1}^2 + J_{i-1,i}^2) + 4(\gamma_i + 2\alpha_i h_i \lambda) h_i \lambda + 4(h_i + 2\alpha_i \gamma_i (1 - \lambda)) \gamma_i (1 - \lambda) \quad (\text{B.59})$$

$$= 8\lambda^2 \alpha_i (J_{i,i+1}^2 + J_{i-1,i}^2) + 4\gamma_i h_i \lambda + 8\alpha_i h_i^2 \lambda^2 + 4\gamma_i (1 - \lambda) + 8\alpha_i \gamma_i^2 (1 - \lambda)^2 \quad (\text{B.60})$$

$$= [2\lambda^2 (J_{i,i+1}^2 + J_{i-1,i}^2) + 2h_i^2 \lambda^2 + 2\gamma_i^2 (1 - \lambda)^2] \alpha_i + \gamma_i h_i \lambda + h_i \gamma_i (1 - \lambda) \quad (\text{B.61})$$

$$= [2\lambda^2 (J_{i,i+1}^2 + J_{i-1,i}^2) + 2h_i^2 \lambda^2 + 2\gamma_i^2 (1 - \lambda)^2] \alpha_i + h_i \gamma_i \stackrel{!}{=} 0 \quad (\text{B.62})$$

$$\Rightarrow \alpha_i = - \frac{h_i \gamma_i}{2[\lambda^2 (J_{i,i+1}^2 + J_{i-1,i}^2) + h_i^2 \lambda^2 + \gamma_i^2 (1 - \lambda)^2]} \quad (\text{B.63})$$

$$\Rightarrow \alpha_i = - \frac{h_i \gamma_i}{2[\lambda^2 (J_{i,i+1}^2 + J_{i-1,i}^2) + h_i^2 \lambda^2 + \gamma_i^2 (1 - \lambda)^2]} \quad (\text{B.64})$$

$$\Rightarrow \alpha_i = - \frac{h_i \gamma_i}{2[\lambda^2 (J_{i,i+1}^2 + J_{i-1,i}^2) + h_i^2 \lambda^2 + \gamma_i^2 (1 - \lambda)^2]} \quad (\text{B.65})$$

$$\frac{\partial \mathcal{S}}{\partial \beta_i} = 2[2\lambda h_i \beta_i - (1 - \lambda)] 2\lambda h_i + 8(1 - \lambda)^2 \gamma_i^2 \beta_i + 8\lambda^2 \beta_i (J_{i,i+1}^2 + J_{i-1,i}^2) \quad (\text{B.66})$$

$$= 8\lambda^2 h_i^2 \beta_i - 4(1 - \lambda) \lambda h_i + 8(1 - \lambda)^2 \gamma_i^2 \beta_i + 8\lambda^2 \beta_i (J_{i,i+1}^2 + J_{i-1,i}^2) \quad (\text{B.67})$$

$$= 2\beta_i [\lambda^2 h_i^2 + (1 - \lambda)^2 \gamma_i^2 + \lambda^2 (J_{i,i+1}^2 + J_{i-1,i}^2)] - (1 - \lambda) \lambda h_i \quad (\text{B.68})$$

$$\Rightarrow \beta_i = \frac{(1 - \lambda) \lambda h_i}{2[\lambda^2 h_i^2 + (1 - \lambda)^2 \gamma_i^2 + \lambda^2 (J_{i,i+1}^2 + J_{i-1,i}^2)]} \quad (\text{B.69})$$

$$\Rightarrow \beta_i = \frac{(1 - \lambda) \lambda h_i}{2[\lambda^2 h_i^2 + (1 - \lambda)^2 \gamma_i^2 + \lambda^2 (J_{i,i+1}^2 + J_{i-1,i}^2)]} \quad (\text{B.70})$$

B.4 p-spin Model

Here, we consider the case $p = 3$.

$$\mathcal{H}(\lambda(t), \gamma(t)) = (1 - \lambda(t))\gamma(t) \sum_{i=1}^N -\sigma_i^x - \lambda(t) \frac{1}{N^2} \left(\sum_{i=1}^N \sigma_i^z \right)^3 \quad (\text{B.71})$$

$$\mathcal{H}(\lambda(t), \gamma(t)) = (1 - \lambda(t))\gamma(t) \sum_{i=1}^N -\sigma_i^x - \lambda(t) \frac{1}{N^2} \left(3! \sum_{i<j<k} \sigma_i^z \sigma_j^z \sigma_k^z + (3N - 2) \sum_{i=1}^N \sigma_i^z \right) \quad (\text{B.72})$$

We minimize the distance operator $\mathcal{S} = \text{Tr}[G_\lambda^2] + \text{Tr}[G_\gamma^2]$ with respect to the two gauge potentials $\mathcal{X} = \sum_{i=1}^N \alpha_i \sigma_i^y$ and $\mathcal{Y} = \sum_{i=1}^N \beta_i \sigma_i^y$.

$$\frac{\partial \mathcal{S}}{\partial \alpha_i} \stackrel{!}{=} 0 \quad (\text{B.73})$$

$$\frac{\partial \mathcal{S}}{\partial \beta_i} \stackrel{!}{=} 0 \quad (\text{B.74})$$

First, we calculate the Hermitian Operators $G_\lambda(\mathcal{X})$ and $G_\gamma(\mathcal{Y})$

$$G_\lambda(\mathcal{X}) = \partial_\lambda \mathcal{H} + i[\mathcal{X}, \mathcal{H}] \quad (\text{B.75})$$

$$= \gamma \sum_{i=1}^N \sigma_i^x - \frac{1}{N^2} \left(6 \sum_{i<j<k} \sigma_i^z \sigma_j^z \sigma_k^z + (3N - 2) \sum_{i=1}^N \sigma_i^z \right) \quad (\text{B.76})$$

$$+ i \left[\sum_{i=1}^N \alpha_i \sigma_i^y, \mathcal{H} \right] \quad (\text{B.77})$$

For the last term (138) we write

$$\left[\sum_{i=1}^N \alpha_i \sigma_i^y, \sum_{i=1}^N -\sigma_i^x \right] = 2i \sum_{i=1}^N \alpha_i \sigma_i^z \quad (\text{B.78})$$

$$\left[\sum_{i=1}^N \alpha_i \sigma_i^y, \sum_{i=1}^N \sigma_i^z \right] = 2i \sum_{i=1}^N \alpha_i \sigma_i^x \quad (\text{B.79})$$

$$\left[\sum_{i=1}^N \alpha_i \sigma_i^y, 6 \sum_{l<j<k} \sigma_l^z \sigma_j^z \sigma_k^z \right] = 6 \sum_{l<j<k} \left[\sum_{i=1}^N \alpha_i \sigma_i^y, \sigma_l^z \sigma_j^z \sigma_k^z \right] \quad (\text{B.80})$$

$$= 6 \sum_{l<j<k} \sigma_l^z \sigma_j^z \left[\sum_{i=1}^N \alpha_i \sigma_i^y, \sigma_k^z \right] \quad (\text{B.81})$$

$$+ \sigma_l^z \left[\sum_{i=1}^N \alpha_i \sigma_i^y, \sigma_j^z \right] \sigma_k^z + \left[\sum_{i=1}^N \alpha_i \sigma_i^y, \sigma_l^z \right] \sigma_j^z \sigma_k^z \quad (\text{B.82})$$

$$= 2i \cdot 6 \sum_{l<j<k} \sigma_l^z \sigma_j^z \alpha_k \sigma_k^x + \sigma_l^z \alpha_j \sigma_j^x \sigma_k^z + \alpha_l \sigma_l^x \sigma_j^z \sigma_k^z \quad (\text{B.83})$$

$$= 2i \cdot 6 \sum_{l<j<k} \sigma_l^z (\sigma_j^z \alpha_k \sigma_k^x + \alpha_j \sigma_j^x \sigma_k^z) + \alpha_l \sigma_l^x \sigma_j^z \sigma_k^z \quad (\text{B.84})$$

$$(\text{B.85})$$

and obtain

$$i\alpha \left[\sum_{i=1}^N \sigma_i^y, \mathcal{H} \right] = -2(1-\lambda)\gamma \sum_i \alpha_i \sigma_i^z + \frac{2\lambda(3N-2)}{N^2} \alpha_i \sigma_i^x \quad (\text{B.86})$$

$$+ \frac{12\lambda}{N^2} \sum_{l<j<k} \sigma_l^z (\sigma_j^z \alpha_k \sigma_k^x + \alpha_j \sigma_j^x \sigma_k^z) + \alpha_l \sigma_l^x \sigma_j^z \sigma_k^z \quad (\text{B.87})$$

$$(\text{B.88})$$

Therefore the Hermitian operator G_λ reads

$$G_\lambda(\mathcal{X}) = \partial_\lambda \mathcal{H} + i[\mathcal{X}, \mathcal{H}] \quad (\text{B.89})$$

$$= \gamma \sum_{i=1}^N \sigma_i^x - \frac{1}{N^2} \left(6 \sum_{i<j<k} \sigma_i^z \sigma_j^z \sigma_k^z + (3N-2) \sum_{i=1}^N \sigma_i^z \right) \quad (\text{B.90})$$

$$- 2(1-\lambda)\gamma \sum_i \alpha_i \sigma_i^z + \frac{2\lambda(3N-2)}{N^2} \alpha_i \sigma_i^x \quad (\text{B.91})$$

$$+ \frac{12\lambda}{N^2} \sum_{l<j<k} \sigma_l^z (\sigma_j^z \alpha_k \sigma_k^x + \alpha_j \sigma_j^x \sigma_k^z) + \alpha_l \sigma_l^x \sigma_j^z \sigma_k^z \quad (\text{B.92})$$

$$(\text{B.93})$$

$$= \sum_{i=1}^N \left(\gamma + \frac{2\alpha_i \lambda (3N-2)}{N^2} \right) \sigma_i^x \quad (\text{B.94})$$

$$- \frac{6}{N^2} \sum_{i<j<k=1}^N \sigma_i^z \sigma_j^z \sigma_k^z - \sum_{i=1}^N \left(\frac{(3N-2)}{N^2} + 2\alpha_i(1-\lambda)\gamma \right) \sigma_i^z \quad (\text{B.95})$$

$$+ \frac{12\lambda}{N^2} \sum_{l<j<k} \sigma_l^z (\sigma_j^z \alpha_k \sigma_k^x + \alpha_j \sigma_j^x \sigma_k^z) + \alpha_l \sigma_l^x \sigma_j^z \sigma_k^z \quad (\text{B.96})$$

We take the trace norm of the square of the Hermitian operator G_λ . For this purpose, consider the last term (157) in more detail:

N=3:

$$G_\lambda(\mathcal{X})^2 = \dots + \frac{144\lambda^2}{3^4} \underbrace{\left(\sum_{l<j<k}^3 \sigma_l^z (\sigma_j^z \alpha_k \sigma_k^x + \alpha_j \sigma_j^x \sigma_k^z) + \alpha_l \sigma_l^x \sigma_j^z \sigma_k^z \right)^2}_{(\sigma_1^z)^2(\sigma_2^z \alpha_3 \sigma_3^x + \alpha_2 \sigma_2^x \sigma_3^z)^2 + \dots + (\alpha_1 \sigma_1^x \sigma_2^z \sigma_3^z)^2} \quad (\text{B.97})$$

$$\text{Tr}[G_\lambda(\mathcal{X})^2] = \dots + \frac{144\lambda^2}{3^4} (\alpha_3^2 + \alpha_2^2 + \alpha_1^2) \quad (\text{B.98})$$

N=4:

$$G_\lambda(\mathcal{X})^2 = \dots + \frac{144\lambda^2}{4^4} \left(\underbrace{\sum_{l<j<k}^4 \sigma_l^z (\sigma_j^z \alpha_k \sigma_k^x + \alpha_j \sigma_j^x \sigma_k^z) + \alpha_l \sigma_l^x \sigma_j^z \sigma_k^z}_{\begin{aligned} &(\sigma_1^z)^2 (\sigma_2^z \alpha_3 \sigma_3^x + \alpha_2 \sigma_2^x \sigma_3^z)^2 + \dots + (\alpha_1 \sigma_1^x \sigma_2^z \sigma_3^z)^2 \\ &+ (\sigma_1^z)^2 (\sigma_2^z \alpha_4 \sigma_4^x + \alpha_2 \sigma_2^x \sigma_4^z)^2 + \dots + (\alpha_1 \sigma_1^x \sigma_2^z \sigma_4^z)^2 \\ &+ (\sigma_1^z)^2 (\sigma_3^z \alpha_4 \sigma_4^x + \alpha_3 \sigma_3^x \sigma_4^z)^2 + \dots + (\alpha_1 \sigma_1^x \sigma_3^z \sigma_4^z)^2 \\ &+ (\sigma_2^z)^2 (\sigma_3^z \alpha_4 \sigma_4^x + \alpha_3 \sigma_3^x \sigma_4^z)^2 + \dots + (\alpha_2 \sigma_2^x \sigma_3^z \sigma_4^z)^2 \end{aligned}} \right)^2 \quad (\text{B.99})$$

$$\text{Tr}[G_\lambda(\mathcal{X})^2] = \dots + \frac{144\lambda^2}{4^4} (\alpha_3^2 + \alpha_2^2 + \alpha_1^2 + \alpha_4^2 + \alpha_2^2 + \alpha_1^2 + \alpha_4^2 + \alpha_3^2 + \alpha_1^2 + \alpha_4^2 + \alpha_3^2 + \alpha_2^2) \quad (\text{B.100})$$

$$\dots + \frac{144\lambda^2}{4^4} (3\alpha_1^2 + 3\alpha_2^2 + 3\alpha_3^2 + 3\alpha_4^2) \quad (\text{B.101})$$

$$\dots + \frac{144\lambda^2}{4^4} 3(\alpha_1^2 + \alpha_2^2 + \alpha_3^2 + \alpha_4^2) \quad (\text{B.102})$$

N=5:

$$\text{Tr}[G_\lambda(\mathcal{X})^2] = \dots + \frac{144\lambda^2}{5^4} 6(\alpha_1^2 + \alpha_2^2 + \alpha_3^2 + \alpha_4^2 + \alpha_5^2) \quad (\text{B.103})$$

This behaviour can therefore be generalized as

$$\text{Tr}[G_\lambda(\mathcal{X})^2] = \dots + \frac{144\lambda^2}{N^4} \frac{(N-1)(N-2)}{2} \sum_{i=1}^N \alpha_i^2 \quad (\text{B.104})$$

We can now turn our attention to the complete G_λ -Operator. Since most of the terms vanish with the trace, we are left with

$$\text{Tr}[G_\lambda(\mathcal{X})^2] = \left(\gamma + \frac{2\alpha_i\lambda(3N-2)}{N^2} \right)^2 + \left(\frac{(3N-2)}{N^2} + 2\alpha_i(1-\lambda)\gamma \right)^2 \quad (\text{B.105})$$

$$- \frac{6(N-1)(N-2)}{N^2} + \frac{144\lambda^2}{N^4} \frac{(N-1)(N-2)}{2} \sum_{i=1}^N \alpha_i^2 \quad (\text{B.106})$$

$$(\text{B.107})$$

$$= \gamma^2 + 4 \frac{\gamma\alpha_i\lambda(3N-2)}{N^2} + \frac{4\alpha_i^2\lambda^2(3N-2)^2}{N^4} \quad (\text{B.108})$$

$$+ \frac{(3N-2)^2}{N^4} + 4 \frac{\alpha(1-\lambda)\gamma(3N-2)}{N^2} + 4\alpha^2(1-\lambda)^2\gamma^2 \quad (\text{B.109})$$

$$+ \frac{144\alpha_i^2\lambda^2}{N^4} \frac{(N-1)(N-2)}{2} \sum_{i=1}^N \alpha_i - \frac{6(N-1)(N-2)}{N^2} \quad (\text{B.110})$$

$$(\text{B.111})$$

$$= \gamma^2 + 4 \frac{\alpha_i\gamma(3N-2)}{N^2} + \frac{4\alpha_i^2\lambda^2(3N-2)^2}{N^4} - \frac{6(N-1)(N-2)}{N^2} \quad (\text{B.112})$$

$$+ \frac{(3N-2)^2}{N^4} + 4\alpha_i^2(1-\lambda)^2\gamma^2 + \frac{144\lambda^2}{N^4} \frac{(N-1)(N-2)}{2} \sum_{i=1}^N \alpha_i^2 \quad (\text{B.113})$$

Minimization with respect to α_i reads

$$\frac{\partial \text{Tr}[G_\lambda(\mathcal{X})^2]}{\partial \alpha_i} = 4 \frac{\gamma(3N-2)}{N^2} + \frac{8\alpha_i\lambda^2(3N-2)^2}{N^4} \quad (\text{B.114})$$

$$+ 8\alpha_i(1-\lambda)^2\gamma^2 + \frac{144\alpha_i\lambda^2}{N^4} (N-1)(N-2) \stackrel{!}{=} 0 \quad (\text{B.115})$$

$$(\text{B.116})$$

$$= \gamma(3N-2)N^2 + 2\alpha_i\lambda^2(3N-2)^2 \quad (\text{B.117})$$

$$+ 2\alpha_i(1-\lambda)^2\gamma^2 N^4 + 36\alpha_i\lambda^2(N-1)(N-2) \stackrel{!}{=} 0 \quad (\text{B.118})$$

Thus,

$$\alpha_i = -\frac{1}{2} \frac{\gamma N^2 (3N-2)}{\lambda^2 (3N-2)^2 + (1-\lambda)^2 \gamma^2 N^4 + 18\lambda^2 (N-1)(N-2)} \quad (\text{B.119})$$

We receive the optimal driving scheme for β_i in the analogous manner

$$G_\gamma(\mathcal{X}) = \partial_\gamma \mathcal{H} + i[\mathcal{Y}, \mathcal{H}] \quad (\text{B.120})$$

$$= (1 - \lambda) \sum_{i=1}^N -\sigma_i^x \quad (\text{B.121})$$

$$- 2(1 - \lambda)\gamma \sum_i \beta_i \sigma_i^z + \frac{2\lambda(3N - 2)}{N^2} \beta_i \sigma_i^x \quad (\text{B.122})$$

$$+ \frac{12\lambda}{N^2} \sum_{l < j < k} \sigma_l^z (\sigma_j^z \beta_k \sigma_k^x + \beta_j \sigma_j^x \sigma_k^z) + \beta_l \sigma_l^x \sigma_j^z \sigma_k^z \quad (\text{B.123})$$

Again we take the trace of the square of the Hermitian operator

$$\text{Tr}[G_\gamma(\mathcal{X})^2] = \left(\frac{2\beta_i \lambda(3N - 2)}{N^2} - (1 - \lambda) \right)^2 + 4\beta_i^2 (1 - \lambda)^2 \gamma^2 \quad (\text{B.124})$$

$$+ \frac{144\lambda^2 (N - 1)(N - 2)}{N^4} \sum_i \beta_i^2 \quad (\text{B.125})$$

and minimize with respect to β

$$\frac{\partial \text{Tr}[G_\gamma(\mathcal{X})^2]}{\partial \beta} = \frac{8\beta_i \lambda^2 (3N - 2)^2}{N^4} - 4(1 - \lambda) \frac{\lambda(3N - 2)}{N^2} + 8\beta_i (1 - \lambda)^2 \gamma^2 \quad (\text{B.126})$$

$$+ \frac{144\beta_i \lambda^2}{N^4} (N - 1)(N - 2) \stackrel{!}{=} 0 \quad (\text{B.127})$$

$$(\text{B.128})$$

$$= 2\beta_i \lambda^2 (3N - 2)^2 - (1 - \lambda) N^2 \lambda (3N - 2) + 2\beta_i (1 - \lambda)^2 \gamma^2 N^4 \quad (\text{B.129})$$

$$+ 36\beta_i \lambda^2 (N - 1)(N - 2) \stackrel{!}{=} 0 \quad (\text{B.130})$$

We finally obtain

$$\beta_i = \frac{1}{2} \frac{(1 - \lambda) \lambda N^2 (3N - 2)}{\lambda^2 (3N - 2)^2 + (1 - \lambda)^2 \gamma^2 N^4 + 18\lambda^2 (N - 1)(N - 2)} \quad (\text{B.131})$$

Bibliography

- [1] R. P. Feynman, “Simulating physics with computers,” *International Journal of Theoretical Physics*, vol. 21, no. 6, pp. 467–488, 1982. [Online]. Available: <https://doi.org/10.1007/BF02650179>
- [2] “Quantum computational networks,” *Proceedings of the Royal Society of London. A. Mathematical and Physical Sciences*, vol. 425, no. 1868, pp. 73–90, 1989. [Online]. Available: <https://royalsocietypublishing.org/doi/abs/10.1098/rspa.1989.0099>
- [3] A. Messiah, *Quantum mechanics*. Amsterdam, The Netherlands: North-Holland, 1961, no. vol. 2. [Online]. Available: <https://books.google.at/books?id=BIOJswEACAAJ>
- [4] A. Lucas, “Ising formulations of many np problems,” *Front. Phys.*, vol. 2, p. 5, 2014. [Online]. Available: <https://www.frontiersin.org/article/10.3389/fphy.2014.00005>
- [5] B. Apolloni, N. Cesa-Bianchi, and D. De Falco, *A Numerical Implementation of "quantum Annealing"*, ser. Dipartimento di Scienze dell’ Informazione: Rapporto interno. Univ., Forschungszentrum BiBoS Bielefeld-Bochum Stochastik, 1988. [Online]. Available: <https://books.google.at/books?id=tWHmvgEACAAJ>
- [6] S. Kirkpatrick, C. D. Gelatt, and M. P. Vecchi, “Optimization by simulated annealing,” *Science*, vol. 220, no. 4598, pp. 671–680, 1983. [Online]. Available: <https://science.sciencemag.org/content/220/4598/671>
- [7] H. Nishimori. Quantum annealing by hidetoshi nishimori. [Online]. Available: http://www.qa.iir.titech.ac.jp/~nishimori/QA/q-annealing_e.html
- [8] M. Demirplak and S. A. Rice, “Adiabatic population transfer with control fields,” *The Journal of Physical Chemistry A*, vol. 107, no. 46, pp. 9937–9945, 2003. [Online]. Available: <https://doi.org/10.1021/jp030708a>

- [9] T. Kadowaki and H. Nishimori, “Quantum annealing in the transverse ising model,” *Phys. Rev. E*, vol. 58, pp. 5355–5363, Nov 1998. [Online]. Available: <https://link.aps.org/doi/10.1103/PhysRevE.58.5355>
- [10] A. Finnila, M. Gomez, C. Sebenik, C. Stenson, and J. Doll, “Quantum annealing: A new method for minimizing multidimensional functions,” *Chemical physics letters*, vol. 219, no. 5-6, pp. 343–348, 1994.
- [11] G. E. Santoro, R. Martoňák, E. Tosatti, and R. Car, “Theory of quantum annealing of an ising spin glass,” *Science*, vol. 295, no. 5564, pp. 2427–2430, 2002.
- [12] G. E. Santoro and E. Tosatti, “Optimization using quantum mechanics: quantum annealing through adiabatic evolution,” *Journal of Physics A: Mathematical and General*, vol. 39, no. 36, p. R393, 2006.
- [13] S. Boixo, T. F. Rønnow, S. V. Isakov, Z. Wang, D. Wecker, D. A. Lidar, J. M. Martinis, and M. Troyer, “Evidence for quantum annealing with more than one hundred qubits,” *Nature Physics*, vol. 10, no. 3, p. 218, 2014.
- [14] A. Lucas, “Ising formulations of many np problems,” *Frontiers in Physics*, vol. 2, p. 5, 2014.
- [15] S. Knysh, “Zero-temperature quantum annealing bottlenecks in the spin-glass phase,” *Nature Communications*, vol. 7, no. 1, p. 12370, 2016. [Online]. Available: <https://doi.org/10.1038/ncomms12370>
- [16] M. Keck, S. Montangero, G. E. Santoro, R. Fazio, and D. Rossini, “Dissipation in adiabatic quantum computers: lessons from an exactly solvable model,” *New Journal of Physics*, vol. 19, no. 11, p. 113029, nov 2017. [Online]. Available: <https://doi.org/10.1088%2F1367-2630%2Faa8cef>
- [17] T. Albash and D. A. Lidar, “Adiabatic quantum computation,” *Rev. Mod. Phys.*, vol. 90, p. 015002, Jan 2018. [Online]. Available: <https://link.aps.org/doi/10.1103/RevModPhys.90.015002>
- [18] A. Pearson, A. Mishra, I. Hen, and D. A. Lidar, “Analog errors in quantum annealing: doom and hope,” *npj Quantum Information*, vol. 5, no. 1, p. 107, 2019. [Online]. Available: <https://doi.org/10.1038/s41534-019-0210-7>
- [19] P. Hauke, H. G. Katzgraber, W. Lechner, H. Nishimori, and W. D. Oliver, “Perspectives of quantum annealing: Methods and implementations,” *Reports on Progress in Physics*, 2020. [Online]. Available: <http://iopscience.iop.org/10.1088/1361-6633/ab85b8>

- [20] S. Geman and D. Geman, “Stochastic relaxation, gibbs distributions, and the bayesian restoration of images,” *IEEE Transactions on Pattern Analysis and Machine Intelligence*, vol. PAMI-6, no. 6, pp. 721–741, 1984.
- [21] G. Rigolin, G. Ortiz, and V. H. Ponce, “Beyond the quantum adiabatic approximation: Adiabatic perturbation theory,” *Phys. Rev. A*, vol. 78, p. 052508, Nov 2008. [Online]. Available: <https://link.aps.org/doi/10.1103/PhysRevA.78.052508>
- [22] K.-P. Marzlin and B. C. Sanders, “Inconsistency in the application of the adiabatic theorem,” *Phys. Rev. Lett.*, vol. 93, p. 160408, Oct 2004. [Online]. Available: <https://link.aps.org/doi/10.1103/PhysRevLett.93.160408>
- [23] D. M. Tong, K. Singh, L. C. Kwek, and C. H. Oh, “Quantitative conditions do not guarantee the validity of the adiabatic approximation,” *Phys. Rev. Lett.*, vol. 95, p. 110407, Sep 2005. [Online]. Available: <https://link.aps.org/doi/10.1103/PhysRevLett.95.110407>
- [24]
- [25] R. MacKenzie, A. Morin-Duchesne, H. Paquette, and J. Pinel, “Validity of the adiabatic approximation in quantum mechanics,” *Phys. Rev. A*, vol. 76, p. 044102, Oct 2007. [Online]. Available: <https://link.aps.org/doi/10.1103/PhysRevA.76.044102>
- [26] D. M. Tong, K. Singh, L. C. Kwek, and C. H. Oh, “Sufficiency criterion for the validity of the adiabatic approximation,” *Phys. Rev. Lett.*, vol. 98, p. 150402, Apr 2007. [Online]. Available: <https://link.aps.org/doi/10.1103/PhysRevLett.98.150402>
- [27] M. V. Berry, “Quantal phase factors accompanying adiabatic changes,” *Proceedings of the Royal Society of London. A. Mathematical and Physical Sciences*, vol. 392, no. 1802, pp. 45–57, 1984. [Online]. Available: <https://royalsocietypublishing.org/doi/abs/10.1098/rspa.1984.0023>
- [28] —, “Transitionless quantum driving,” *Journal of Physics A: Mathematical and Theoretical*, vol. 42, no. 36, p. 365303, 2009.
- [29] C. Jarzynski, “Generating shortcuts to adiabaticity in quantum and classical dynamics,” *Phys. Rev. A*, vol. 88, p. 040101, Oct 2013. [Online]. Available: <https://link.aps.org/doi/10.1103/PhysRevA.88.040101>
- [30] D. Sels and A. Polkovnikov, “Minimizing irreversible losses in quantum systems by local counterdiabatic driving,” *Proc. Natl. Acad. Sci.*, vol. 114, p.

- 3909, 2017. [Online]. Available: <http://www.pnas.org/content/early/2017/04/26/1619826114>
- [31] C. Jarzynski, “Generating shortcuts to adiabaticity in quantum and classical dynamics,” *Physical Review A*, vol. 88, no. 4, p. 040101, 2013.
- [32] M. Kolodrubetz, D. Sels, P. Mehta, and A. Polkovnikov, “Geometry and non-adiabatic response in quantum and classical systems,” *Physics Reports*, vol. 697, pp. 1 – 87, 2017, geometry and non-adiabatic response in quantum and classical systems. [Online]. Available: <http://www.sciencedirect.com/science/article/pii/S0370157317301989>
- [33] D. Sels and A. Polkovnikov, “Minimizing irreversible losses in quantum systems by local counterdiabatic driving,” *Proceedings of the National Academy of Sciences*, vol. 114, no. 20, pp. E3909–E3916, 2017. [Online]. Available: <https://www.pnas.org/content/114/20/E3909>
- [34] H. Nishimori, “Statistical physics of spin glasses and information processing : An introduction,” 2001. [Online]. Available: <https://ci.nii.ac.jp/naid/10019464487/en/>
- [35] H. Zhou, Y. Ji, X. Nie, X. Yang, X. Chen, J. Bian, and X. Peng, “Experimental realization of shortcuts to adiabaticity in a nonintegrable spin chain by local counterdiabatic driving,” *Phys. Rev. Applied*, vol. 13, p. 044059, Apr 2020. [Online]. Available: <https://link.aps.org/doi/10.1103/PhysRevApplied.13.044059>
- [36] G. B. Mbeng, R. Fazio, and G. Santoro, “Quantum annealing: a journey through digitalization, control, and hybrid quantum variational schemes,” 2019.
- [37] Z.-C. Yang, A. Rahmani, A. Shabani, H. Neven, and C. Chamon, “Optimizing variational quantum algorithms using pontryagin’s minimum principle,” *Phys. Rev. X*, vol. 7, p. 021027, May 2017. [Online]. Available: <https://link.aps.org/doi/10.1103/PhysRevX.7.021027>
- [38] L. T. Brady, C. L. Baldwin, A. Bapat, Y. Kharkov, and A. V. Gorshkov, “Optimal protocols in quantum annealing and qaoa problems,” 2020.